United States
Department of
Agriculture

Forest Service

Forest
Products
Laboratory

General
Technical
Report
FPL–GTR–218

Nanocelluloses: Potential Materials for Advanced Forest Products

Proceedings of Nanotechnology in Wood Composites Symposium

Zhiyong Cai
Kristina Oksman Niska

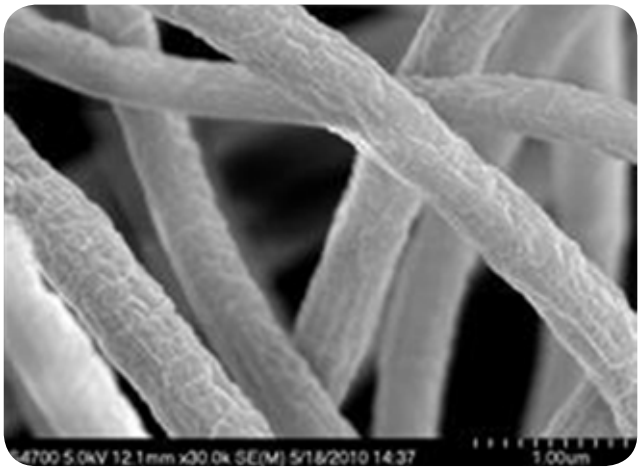

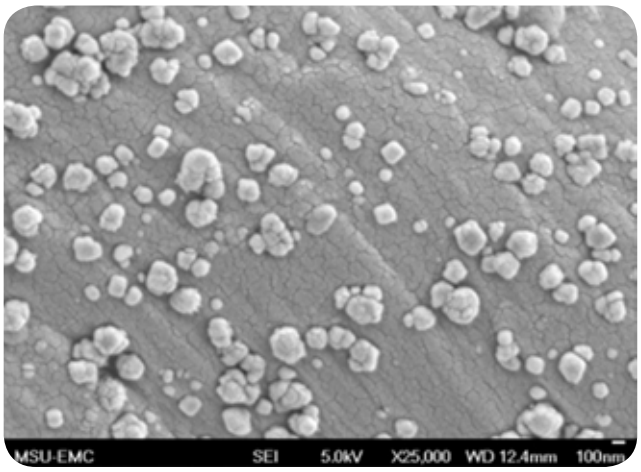

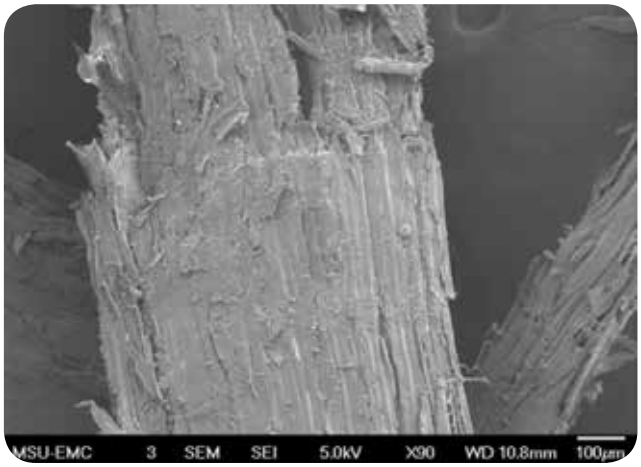

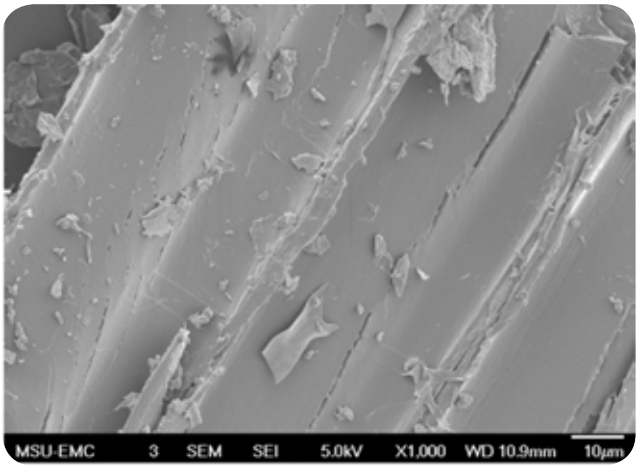

Abstract

This report provides a summary of technical papers presented at the Nanotechnology in Wood Composites Symposium held at the USDA Forest Products Laboratory in Madison, Wisconsin, May 18, 2011. Papers in this report included the oral presentations and posters that explore the adaptability and applicability of using nanocellulose as a potential resource to create value-added commodities and innovative bio-based composites. Presenters from around the world reviewed nanotechnology applications in developing and improving forest products in the past, present, and future. A variety of nanomaterials are obtained from wood, including nanofibrils, nanocrystals, lignin particles, and extractives. Most research efforts focus on developing continuous, high-performance composite reinforcement from cellulose nanofibrils; improving performance and value-added features of existing wood-based composites; developing coatings and additives for improved durability of wood composites; and developing films and membranes with tailored mechanical and barrier properties, sensing capabilities, and biodegradability.

Keywords: nanocellulose, nanofibril, nanocrystal, biocomposite, wood product

September 2012

Cai, Zhiyong; Oksman Niska, Kristina. 2012. Nanocelluloses: Potential materials for advanced forest products—Proceedings of nanotechnology in wood composites symposium. General Technical Report FPL-GTR-218. Madison, WI: U.S. Department of Agriculture, Forest Service, Forest Products Laboratory. 76 p.

A limited number of free copies of this publication are available to the public from the Forest Products Laboratory, One Gifford Pinchot Drive, Madison, WI 53726–2398. This publication is also available online at www.fpl.fs.fed.us. Laboratory publications are sent to hundreds of libraries in the United States and elsewhere.

The Forest Products Laboratory is maintained in cooperation with the University of Wisconsin.

The use of trade or firm names in this publication is for reader information and does not imply endorsement by the United States Department of Agriculture (USDA) of any product or service.

The USDA prohibits discrimination in all its programs and activities on the basis of race, color, national origin, age, disability, and where applicable, sex, marital status, familial status, parental status, religion, sexual orientation, genetic information, political beliefs, reprisal, or because all or a part of an individual's income is derived from any public assistance program. (Not all prohibited bases apply to all programs.) Persons with disabilities who require alternative means for communication of program information (Braille, large print, audiotape, etc.) should contact USDA's TARGET Center at (202) 720–2600 (voice and TDD). To file a complaint of discrimination, write to USDA, Director, Office of Civil Rights, 1400 Independence Avenue, S.W., Washington, D.C. 20250–9410, or call (800) 795–3272 (voice) or (202) 720–6382 (TDD). USDA is an equal opportunity provider and employer.

Acknowledgments

We acknowledge the contributions of symposium participants and especially recognize the extraordinary effort of the following individuals in organizing the meeting: Craig M. Clemons, Research Materials Engineer, USDA Forest Products Laboratory; Nicole M. Stark, Research Chemical Engineer, USDA Forest Products Laboratory; Julie Lang, Conference Coordinator, Forest Products Society; and, Stefan Bergmann, Executive Vice President, Forest Products Society.

Contents

Executive Summary 1

Presenters 1

Nanotechnology Applications in Forest Products—Past, Present, and Future 3

Transparent Polymer Composites Reinforced by Nanocrystalline Cellulose 5

Enhancing Durability of Wood-Based Composites with Nanotechnology 8

Artificial Ligaments/Tendons Based on Cellulose Nanofibers 13

Nanocellulose/Conducting Polymer Nanocomposite Films Based on Bacterial Cellulose 18

Eucalyptus Micro and Nanofibres for Reinforcement of Polymeric Nanocomposites 22

Impact Properties and Characteristic Impact Resistance Model of Cellulose Nanofibril-Filled Polypropylene Composites 25

Synthesis of Hybrid Porous Cellulose/Metal Nanocomposites 45

An Investigation into the Mechanical Behaviour of Surface-Modified Fibrillated Cellulose Reinforced Composites 50

Production and Characterization of Nano-Structured Carbons from Pine Chips 54

An Investigation of Fabrication Thermal Insulation Wood-Based Composite Using Nanotechnology 64

Mechanical and Thermal Properties of Microcrystalline Cellulose/Nanoclay/Polypropylene 70

Nanocelluloses: Potential Materials for Advanced Forest Products

Proceedings of Nanotechnology in Wood Composites Symposium

Zhiyong Cai, Supervisory Research Materials Engineer
Forest Products Laboratory, Madison, Wisconsin

Kristina Oksman Niska, Professor
Lulea University of Technology, Luleå, Sweden

Executive Summary

Nanotechnology has enormous promise to bring about fundamental changes and significant benefit to the forest products industry. Cellulose is the most abundant and inexhaustible natural polymer, with an annual production in the biosphere of about 90 billion tons. Use of nano-dimensional cellulose in nanocomposites will allow the production of much higher performance materials to replace nonrenewable metal and plastics, with widespread application in the forest products and other industries. This report compiles technical papers presented at the Nanotechnology in Wood Composites Symposium held at the USDA Forest Products Laboratory in Madison, Wisconsin, on May 18, 2011. The objective of this symposium was to provide information recognizing that the values of wood and bio-based materials at the nanoscale are virtually untapped and have huge potential for the economy. Wood-derived nanomaterials will offer new revenue streams with high-value-added products. Presenters from the world reviewed nanotechnology applications in developing and improving forest products in the past, present, and future. Future needs and challenges for applying nanotechnology in forest products require the ability to develop chemical and mechanical methodologies for converting nano-fibrillated cellulose into user-friendly forms and pilot-plant scale-up and industrial collaboration to refine and demonstrate the technology.

Presenters

1. Keynote Address: Nanotechnology Applications in Forest Products—Past, Present, and Future

   Douglas J. Gardner, University of Maine

2. Transparent Polymer Composites Reinforced by Nanocrystalline Cellulose

   James Snyder, U.S. Army Research Laboratory, Weapons and Materials Research Directorate, Aberdeen Proving Ground, Maryland; Hong Dong, U.S. Army Research Laboratory, Weapons and Materials Research Directorate, Aberdeen Proving Ground, Maryland; Joshua Steele, U.S. Army Research Laboratory, Weapons and Materials Research Directorate, Aberdeen Proving Ground, Maryland; Ken Strawhecker, U.S. Army Research Laboratory, Weapons and Materials Research Directorate, Aberdeen Proving Ground, Maryland; Joshua Orlicki, U.S. Army Research Laboratory, Weapons and Materials Research Directorate, Aberdeen Proving Ground, Maryland; Richard Reiner, USDA Forest Service, Forest Products Laboratory, Madison, Wisconsin; Alan Rudie, USDA Forest Service, Forest Products Laboratory, Madison, Wisconsin

3. Enhancing Durability of Wood-Based Composites with Nanotechnology

   Carol A. Clausen, USDA Forest Service, Forest Products Laboratory, Madison, Wisconsin

4. Artificial Ligaments/Tendons Based on Cellulose Nanofibers

   Aji P. Mathew, Department of Engineering Materials and Mathematics, Division of Manufacturing and Design of Wood and Bionanocomposites, University of Technology, Luleå, Sweden; Kristiina Oksman, Department of Engineering Materials and Mathematics, Division of Manufacturing and Design of Wood and Bionanocomposites, University of Technology, Luleå, Sweden

5. Nanocellulose/Conducting Polymer Nanocomposite Films Based on Bacterial Cellulose

   Byoung-Ho Lee, Laboratory of Adhesion & Bio-Composites, Program in Environmental Materials Science, Seoul National University, Seoul, Republic of Korea; Hyun-Ji Lee, Laboratory of Adhesion & Bio-Composites, Program in Environmental Materials Science, Seoul National University, Seoul, Republic of Korea; Taekjun Chung, Laboratory of Adhesion & Bio-Composites, Program in Environmental Materials Science, Seoul National University, Seoul, Republic of Korea; Hyun-Joong Kim, Laboratory of Adhesion & Bio-Composites, Program in Environmental Materials

Science, Seoul National University, Seoul, Republic of Korea and Research Team for Biomass-based Biomaterials, Research Institute for Agriculture and Life Sciences, Seoul, Republic of Korea

6. Eucalyptus Micro and Nanofibres for Reinforcement of Polymeric Nanocomposites

   G.H.D. Tonoli, Department of Forest Science, Universidade Federal de Lavras, Lavras, Brazil; L.A. Caixeta, Laboratório Nacional de Nanotecnologia para o Agronegócio (LNNA), Embrapa Instrumentação Agropecuária, São Carlos, Brazil; J.M. Marconcini, Laboratório Nacional de Nanotecnologia para o Agronegócio (LNNA), Embrapa Instrumentação Agropecuária, São Carlos, Brazil; A.C. Corrêa, Laboratório Nacional de Nanotecnologia para o Agronegócio (LNNA), Embrapa Instrumentação Agropecuária, São Carlos, Brazil; M.A. Pereira-da-Silva, Instituto de Física de São Carlos, Universidade de São Paulo, São Carlos, Brazil; L.M. Mendes, Department of Forest Science, Universidade Federal de Lavras, Lavras, Brazil; Luiz H. Capparelli Mattoso, Laboratório Nacional de Nanotecnologia para o Agronegócio (LNNA), Embrapa Instrumentação Agropecuária, São Carlos, Brazil

7. Impact Properties and Characteristic Impact Resistance Model of Cellulose Nanofibril-Filled Polypropylene Composites

   Han-Seung Yang, AEWC—Advanced Structures and Composites Center and Forest Bioproducts Research Institute (FBRI), University of Maine, Orono, Maine; Douglas J. Gardner, AEWC—Advanced Structures and Composites Center, University of Maine, Orono, Maine; Jacques W. Nader, AEWC—Advanced Structures and Composites Center, University of Maine, Orono, Maine

8. Synthesis of Hybrid Porous Cellulose/Metal Nanocomposites

   Tao Wang, Center for Nano Science and Technology and Department of Electrical Engineering, University of Notre Dame, Notre Dame, Indiana; Zhiyong Cai, USDA Forest Service, Forest Products Laboratory, Madison, Wisconsin; Abhijit Biswas, Center for Nano Science and Technology, Department of Electrical Engineering, University of Notre Dame, Notre Dame, Indiana; Lei Liu, Advanced Diagnostics and Therapeutics, Department of Electrical Engineering, University of Notre Dame, Notre Dame, Indiana

9. An Investigation into the Mechanical Behaviour of Surface-Modified Fibrillated Cellulose Reinforced Composites

   M.Sc. Bulota M., Aalto University, School of Chemical Technology, Department of Forest Products Technology, Espoo, Finland; M.Sc. Hänninen T., Aalto University, School of Chemical Technology, Department of Forest Products Technology, Espoo, Finland; Dr. Jääskeläinen A.-S., Aalto University, School of Chemical Technology, Department of Forest Products Technology, Espoo, Finland; Dr. Kontturi E., Aalto University, School of Chemical Technology, Department of Forest Products Technology, Espoo, Finland; Professor Hughes M., Aalto University, School of Chemical Technology, Department of Forest Products Technology, Espoo, Finland

10. Production and Characterization of Nano-Structured Carbons from Pine Chips

    Qiangu Yan, Department of Agricultural & Biological Engineering, Mississippi State University, Mississippi; Hossein Toghiani, Dave C. Swalm School of Chemical Engineering, Mississippi State University, Mississippi; Zhiyong Cai, USDA Forest Service, Forest Products Laboratory, Madison, Wisconsin; Fei Yu, Department of Agricultural & Biological Engineering, Mississippi State University, Mississippi; Jilei Zhang, Forest Products Laboratory, Mississippi State University, Mississippi

11. An Investigation of Fabrication Thermal Insulation Wood-Based Composite Using Nanotechnology

    Reza Zahedsheijani, Department of Wood and Paper Science & Technology, Faculty of Natural Resources, University of Tehran, Karaj, Iran; Mohammad Layeghi, Department of Wood and Paper Science & Technology, Faculty of Natural Resources, University of Tehran, Karaj, Iran; Hosein Yousefi, Department of Wood and Paper Science & Technology, Faculty of Natural Resources, University of Tehran, Karaj, Iran; Mehdi Faezipour, Department of Wood and Paper Science & Technology, Faculty of Natural Resources, University of Tehran, Karaj, Iran

12. Mechanical and Thermal Properties of Microcrystalline Cellulose/Nanoclay/Polypropylene

    Amir Nourbakhsh, Department of Wood and Paper Science, Research Institute of Forests and Rangelands (RIFR), Tehran, Iran; Alireza Ashori, Department of Chemical Technologies, Iranian Research Organization for Science and Technology (IROST), Tehran, Iran

Nanotechnology Applications in Forest Products: Past, Present and Future

Douglas J. Gardner
University of Maine
231 AEWC Building
Orono, Maine 04469

Email: douglasg@maine.edu

Extended Abstract

Nanotechnology is the understanding and control of matter at dimensions of roughly 1 to 100 nanometers, where unique phenomena enable novel applications. Encompassing nanoscale science, engineering and technology, nanotechnology involves imaging, measuring, modeling, and manipulating matter at this length scale. Nanotechnology research and development (R&D) in the U.S. is high priority research across all segments of science and engineering since the enactment of the National Nanotechnology Initiative (NNI) in 2001. The forest products industry in the U.S. developed a nanotechnology research roadmap in 2005 and more recently in 2010, recognized the study of cellulose-based nanomaterials as a signature research initiative. Nanotechnology research roadmaps have been developed and applied to forest products globally. Research focus areas for nanotechnology applications in forest products include: polymer composites and nanoreinforced materials; self-assembly and biomimetics; cell wall nanostructure; nanotechnology for sensors, processing and process control; and analytical methods for nanostructure characterization.

At first glance, applications of nanotechnology in forest products might appear to be a relatively new development, but in actual fact, nanoscale materials have been used in the production of sized and coated paper for over a century. Colloidal materials which are systems consisting of a mechanical mixture of particles between 1 nm and 1000 nm dispersed in a continuous medium, usually water, are commonly used in paper chemicals, as well as in paints and coatings to protect wood. The terminologies used to describe nanomaterials become important because the term nanotechnology was first coined in 1974. Even though the term nanotechnology is relatively new, we have been in fact utilizing nanomaterials in production of man made materials for many centuries and a number of good examples can be found in the popular scientific media including glazings for pottery, carbon nanofiber reinforced steel, emulsions for food, etc.

In considering nanotechnology and forest products, we can apply nanomaterials to forest products in the form of coatings, biocides and modified resins or we can derive nanomaterials from wood. Nanomaterials derived from renewable biomaterials like wood, especially cellulose and lignin, will undoubtedly play a large role in future nanotechnology research efforts. High profile nanotechnology applications in forest products include optically transparent cellulose nanofiber paper and optically transparent cellulose nanocomposites for flexible LED displays. Wood protection applications have been a significant focus of nanotechnology including the utilization of nanobiocides and

nanocarrier delivery systems in wood preservatives. Wood coating applications of nanotechnology are now becoming common in the consumer marketplace where coatings with improved scratch and abrasion resistance, hydrophobicity, ultraviolet light blocking and dust free surfaces are touted by commercial manufacturers.

Cellulose nanomaterials are a large focus of research across the world as evidenced by four comprehensive literature reviews appearing in the peer reviewed literature in 2010. Cellulose fibers on the nanoscale are prepared in four different forms: 1) bacterial cellulose nanofibers, 2) cellulose nanofibers by electrospinning, 3) micro- or nano-fibrillated cellulose plant cell fibers, and 4) nanorods or cellulose whiskers. Processing techniques have a significant impact on the adhesion properties of the resulting cellulose nanofibers in composite material applications. The behavior of cellulose surfaces in polymers as well as their interaction with different chemicals is of great importance in their current and future applications in nanocomposites. The mechanical performance of nanocomposites, for instance, is dependent on the degree of dispersion of the fibers in the matrix polymer and the nature and intensity of fiber-polymer adhesion interactions. Challenges in the scale-up of producing commercial quantities of cellulose nanofibrils for materials applications include: scalable homogenization processing methodologies, adequate methods to dry the fibrils and maintain the nanoscale dimensions, and reduction in energy requirements and production costs.

Future needs of nanotechnology in forest products include the ability to have scalable nano-manufacturing by adapting conventional manufacturing processes or developing novel process equipment. For example, a goal might be to adopt papermaking processes where we currently self assemble wood cells on the micron and millimeter length scale at 60 miles per hour (100 kilometers per hour). Novel composite manufacturing processes will need to be developed for automobiles, adhesives, ballistic applications, coatings, biomedical applications as well as drug delivery. Concerns, challenges and opportunities of nanotechnology in forest products will include addressing consumer perception issues of sustainability as well as health risks. There may be market opportunities to improve existing products with nanotechnology such as the development of intelligent packaging.

It appears that we may be on the cusp of significant commercial applications of novel nanotechnology applications in forest products. The current applications of nanomaterials in wood protection and wood coatings as well as the near to market potential for some cellulose nanofibril material applications is an exciting development in the forest products industry. Perhaps the future is now?

Transparent Polymer Composites Reinforced by Nanocrystalline Cellulose

James Snyder, Chemist
Hong Dong, Chemist
Joshua Steele, Chemist
Ken Strawhecker, Chemist
Joshua Orlicki, Chemist
U.S. Army Research Laboratory, Aberdeen Proving Ground, Maryland

Richard S. Reiner, Chemical Engineer
Alan W. Rudie, Supervisory Research Chemist
Forest Products Laboratory, Madison, Wisconsin

The demand for lighter and stronger materials across Army platforms is promoting the development of lightweight composites. Traditional reinforcement materials such as polymers, carbon, and ceramics incur penalties with respect to processing costs to achieve high specific strength, and they typically frustrate transparency. In contrast, cellulose fibers provide a renewable, low-cost alternative with favorable properties that include low densities and high specific strength and modulus (Samir and others 2005, van den Berg and others 2007, Sturcova and others 2005). Recent work by Nogi and others (2009) demonstrating transparency of bacterial cellulose nanofibers in thin sheets as well as in nanocomposites (Nogi and others 2005) indicates potential applicability for nanocellulose in transparent composite defense applications.

At the U.S. Army Research Laboratory (ARL), low-cost, high-performance cellulosic reinforcement of transparent composites is being investigated by means of advanced nanostructured architectures, improved cellulose-matrix interfaces, and characterization of bulk laminates. This parallel approach enables simultaneous development of several critical properties and facilitates more rapid transition of the technology into useful components. The U.S. Forest Service is providing most of the cellulose nanomaterials and surface modifications for the project, including efforts to scale up the laboratory procedures for using wood pulp to produce cellulose nanocrystals (CNC) using a modification of the procedure reported by Gray and others and the larger and less crystalline nanofibrillated cellulose (NFC) using the TEMPO oxidation technique (Saito and others 2006).

Solvent-dispersed blends of polymer and cellulose nanoparticles were cast into films and thin laminates for initial evaluation of optical and mechanical properties at high loadings. Polymethylmethacrylate (PMMA) was used in this study as a test matrix. Films suitable for optical testing were cast from solution in N,N- dimethylformamide at 60 °C under standard atmospheric pressure onto a tempered glass plate. The solution casting methods investigated here are not ideal for thicker laminates and are presented for baseline testing only (Figs. 1 and 2).

Initial optical characterization was performed using a Gardner Haze-Gard Plus analyzer (BYK-Gardner, Columbia, Maryland) to investigate the transmittance, haze, and clarity of each specimen. The target sample thickness was 0.8 mm. The optical properties in our films demonstrated a reduction in transmittance and clarity and an increase in haze with CNC loading. The decline in optical properties with CNC loading may arise from the processing method used here, because solvent casting frequently generates voids and variations in thickness. Although the films investigated appeared well-formed and smooth, it is unclear whether the trends are inherent to the nanoparticle loadings or whether optical properties degrade due to poorly formed particle-matrix

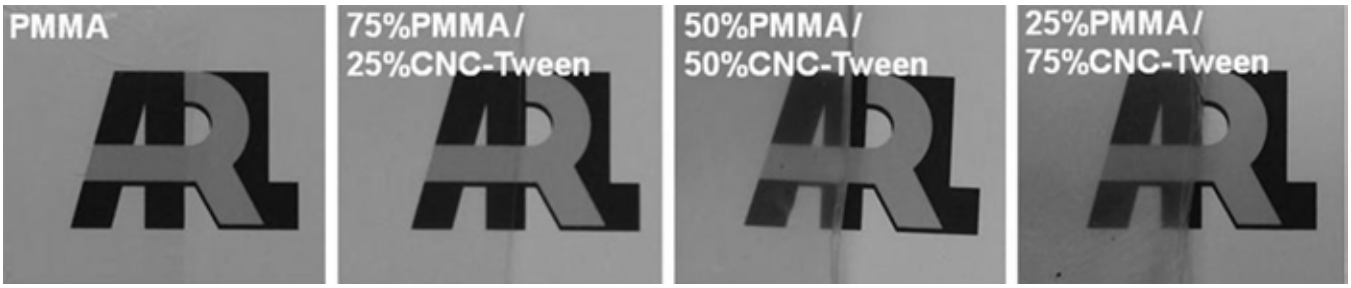

Figure 1. Solution cast PMMA films with increasing concentrations of CNC modified with Tween-40.

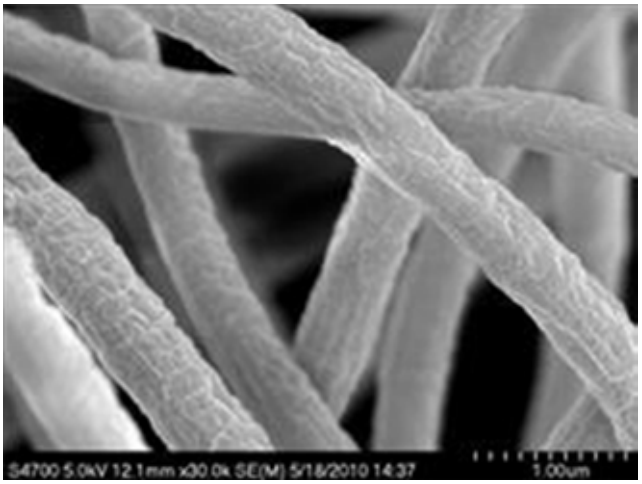

Figure 2. Electrospun PMMA fibers reinforced with 17 wt% CNCs.

interfaces and/or film imperfections. Continuing studies are focused on advanced processing procedures to better quantify optical properties in thicker laminates.

To achieve more control over CNC dispersion and interfacing with the matrix, high-performance fibers and porous networks are being developed that remain transparent in laminates. The initial focus has been on production of cellulose-polymer composite nanofibers of various composition using electrospinning, which uses an external electrostatic field to generate small fibers with diameters on the nanometer scale (Huang and others 2003). These CNC-based nanofibers are expected to possess enhanced mechanical properties in strength, modulus, and resistance to fracture. The highly interpenetrated and porous framework of a nanofiber web may then be used to reinforce polymer composites. Moreover, controlled orientation of CNCs in the polymer matrix is possible using one-dimensional alignment of CNC-based polymer nanofibers. The diameter of the fibers is small and controllable to be in the nanometer range to promote optical transparency.

Electrospun PMMA reinforced with CNCs yielded uniform and smooth nanofibers at all concentrations considered in this study, up through 40 wt% CNC. The average diameters of the fibers ranged from 500 to 200 nm. Fourier transform infrared (FT-IR) spectroscopy was used to confirm the incorporation of CNCs in PMMA. The local moduli of the nanofibers were studied by nanoindentation of fibers electrospun directly onto glass cover slip substrates. Transverse loadings were performed using a TI-950 nanoindenter (Hysitron, Inc., Minneapolis, Minnesota) and employing a 500-nm-radius cone-shaped diamond probe. Indentation depths were typically between 100 and 200 nm. A plot of nanoindentation modulus, *E*, as a function of CNC concentration (Fig. 3) indicates a trend of increasing modulus as CNC loading increases. At 33 wt% CNC the modulus is about 25% higher than that of the neat PMMA nanofiber.

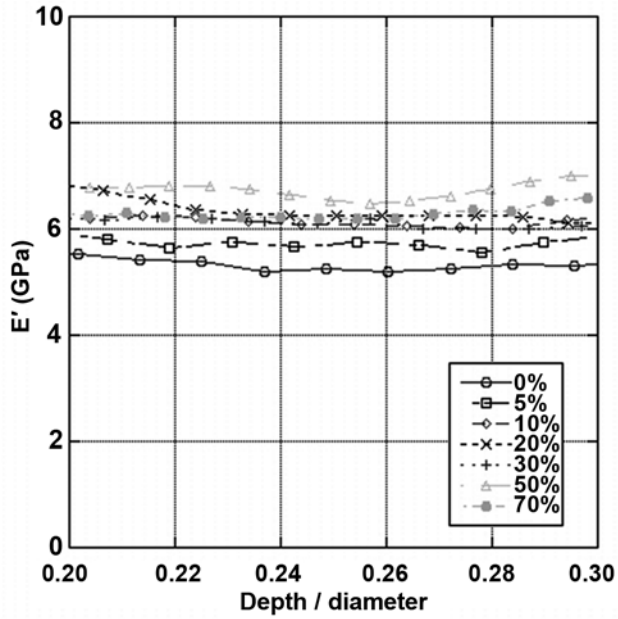

Figure 3. Nanofiber modulus as a function of fiber diameter and CNC concentration.

A slight dip at higher concentrations may be indicative of CNC aggregation.

The fibers were collected on a rapidly rotating mandrel, aligning the electrospun fibers. The orientation of CNC in a CNC/PMMA fiber was investigated by etching PMMA out from fibers with drops of tetrahydrofuran (THF). Homogeneously dispersed and highly aligned CNCs introduced into PMMA fibers were observed along the fiber axis, likely caused by high shear force in the electrospinning process. Several layers of 33 wt% CNC/PMMA nanofibers were stacked into a mold with excess PMMA powder and pressed at 150 °C to yield CNC-reinforced PMMA composites. In these trial laminates, the final CNC concentration was 1 wt%. The nanofibers were found to integrate seamlessly into the pressed matrix to form CNC-reinforced PMMA sheets, and noticeable degradation of transmittance was not detected relative to a 100% PMMA laminate. The optical and mechanical properties of PMMA with CNC nanocomposite fibers are currently being characterized at a greater range of formulations.

More refined control over cellulose architecture may be derived from defining the network prior to matrix integration. We have therefore used gelled networks of NFC as a starting point for these networks. Removing the solvent yielded aerogels that were subsequently backfilled with resin and cured to form the composite. In an alternative method, the solvent was directly displaced with resin, maintaining a finer cellulosic network and better optical properties. Mechanical properties, currently under evaluation, are expected to improve not only from the specific property of NFC, but also from the hydrogen bonding that constructs the network.

In conclusion, we have successfully fabricated nanofibers and thin films of cellulose-polymer transparent composites. Controlled integration of nanostructured cellulose in polymer matrices is essential to maintain the desired optical qualities of the composite while still providing enhanced levels of mechanical reinforcement. Our results indicate that cellulose reinforcement of transparent materials is feasible, which would enable a potential route to low-cost, scalable composite structures using these bioderived resources.

References

Huang, Z.; Zhang, Y.; Kotaki, M.; Ramakrishna, S. 2003. A review on polymer nanofibers by electrospinning and their applications in nanocomposites. Composites Science and Technology. 63: 2223–2253.

Nogi, M.; Handa, K.; Nakagaito, A.; Yano, H. 2005. Optically transparent bionanofiber composites with low sensitivity to refractive index of the polymer matrix. Applied Physics Letters. 87: 243110.

Nogi, M.; Iwamoto, S.; Nakagaito, A.; Yano, H. 2009. Optically transparent nanofiber paper. Advanced Materials. 21: 1595–1598.

Saito, T.; Nishiyama, Y.; Putaux, J.; Vignon, M.; Isogai, A. 2006. Homogeneous suspensions of individualized microfibrils from TEMPO-catalyzed oxidation of native cellulose. Biomacromolecules. 7: 1687–1691.

Samir, A.; Alloin, F.; Dufresne, A. 2005. Review of recent research into cellulosic whiskers, their properties and their application in nanocomposite field. Biomacromolecules. 6: 612–626.

Sturcova, A.; Davies, G.; Eichhorn, S. 2005. Elastic modulus and stress-transfer properties of tunicate cellulose whiskers. Biomacromolecules. 6: 1055–1061.

van den Berg, O.; Capadona, J.; Weder, C. 2007. Preparation of homogeneous dispersions of tunicate cellulose whiskers in organic solvents. Biomacromolecules. 8: 1353–1357.

Enhancing Durability of Wood-Based Composites with Nanotechnology

Carol A. Clausen, Supervisory Research Microbiologist
Forest Products Laboratory, Madison, Wisconsin

Abstract

Wood protection systems are needed for engineered composite products that are susceptible to moisture and biodeterioration. Protection systems using nano-materials are being developed to enhance the durability of wood-based composites through improved resistance to biodeterioration, reduced environmental impact from chemical leaching, and improved resistance to ultraviolet (UV) degradation. Three approaches will be presented: (1) direct application of nano-metals to wood-based products, (2) slow release of biocides embedded in nano-polymer matrices, and (3) controlled delivery of biocides with a nano-carrier. In the first approach, wood was vacuum impregnated with nano-sized particles of metals commonly used in wood preservative formulations (e.g., zinc and copper). Nano-zinc oxide particles were shown to be leach resistant, protected against UV degradation, and acted as a termite toxicant when compared to soluble zinc, a key component of the wood preservative ammoniacal copper zinc arsenate and zinc borate. In the second approach, self-assembling hyperbranched nano-polymers were loaded with an organic biocide. The complex surface of the nano-polymer encapsulated the biocide until a change in the physical environment (i.e., elevated heat or moisture) triggered its release. Nano-polymer encapsulation could provide long-term protection of composites as a surface treatment. In the third approach, nano-tubules made from an inert material served as a carrier for organic biocides. Loaded nano-tubules released the biocide in a slow, controlled fashion and provided superior protection of heat-labile organic biocides during the fabrication process compared to treatment with the biocide alone. Loaded nano-tubules may be used for surface application, pressure impregnation, or as an additive to engineered products.

Introduction

Nano-materials often exhibit novel physical and physiochemical properties that differ significantly from larger particles of the same material (Clausen 2007, Clausen and others 2011). Recent research looks at ways these properties can be exploited in the development of new preservative systems. Opportunities exist for using advances in nanotechnology to enhance the moisture tolerance of composites in traditional markets such as building materials. Embedding biocides in nano-polymer matrices or controlling delivery of biocides with nano-carriers is being evaluated to improve the durability of engineered composite products. The status of research on nano-metals, nano-polymer matrices, and nano-carriers is presented and discussed.

Results and Discussion

Nano-Metals

Either used alone or in combination with existing biocides, nano-metals may play an important role in the next generation of wood protection products. Nano-metals are created by altering particulate size either in the liquid phase (e.g., metal oxide sols, colloidal metals), gas phase (e.g., flame synthesis, plasma-based vapor phase synthesis), or solid phase (e.g., high energy ball milling). Nano-metal preparations of silver, zinc, copper, and other metals have high dispersion stability and low viscosity, allowing for more uniform particulate distribution over a surface (Clausen 2010, Kartal and others 2009).

Dispersion stability coupled with the controlled uniformity of pyrolyzed particles may greatly improve durability of solid and composite wood products in a number of applications: (1) preservative penetration in commercial lumber species, (2) treatability of refractory wood species that are of low commercial value, (3) organic treatments for engineered composites, (4) stability of finishes and coatings for aboveground applications, (5) nonleachable or hydrophobic treatments for both solid and composite materials, (6) photostability of treated wood, and (7) leach resistance of aqueous treatments.

In the presence of moisture, metals oxidize, which results in the release of metal ions. The ionic form of the metal is often the form that is responsible for microbial inhibition (Clausen 2010, Dorau and others 2004). Smaller particles having a higher surface area result in a greater area available for oxidation. Particles with diameter less than 100 nm are required in order to have the necessary surface area to allow a continuous release of metal ions. The size of the metal particle has also been shown to affect microbial inhibition; the smaller the particle, the greater the antimicrobial activity (Nair and others 2009, Reddy and others 2007). Properties of nano-zinc oxide (nano-ZnO) particles were evaluated for their ability to alter physical and biological deterioration of southern pine.

When southern pine sapwood was vacuum impregnated with 30-nm particles of zinc oxide, virtually no leaching occurred in a laboratory leach test, even at the highest retention of 13 kg/m^3 (Clausen and others 2010a). Unleached

Figure 1. Weathering of nano-ZnO treated southern pine after 12 months of outdoor exposure. Unexposed surface (specimens on right) refers to the underside of the individual "exposed surface" specimens shown on the left.

samples were protected from UV damage after 12 months of outdoor exposure; photostability was visibly obvious on both exposed and unexposed surfaces compared with untreated controls (Fig. 1) (Clausen and others 2010b). Graying was markedly diminished, although checking occurred in all specimens. Nano-ZnO treatment at a concentration of 2.5% or greater also provided substantial resistance to water absorption following 12 months of outdoor exposure compared with untreated and unweathered southern pine. In laboratory tests against termites and decay fungi, zinc oxide (30 nm) caused moderate termite mortality in a no-choice bioassay but gave mixed results for inhibition of decay fungi (Kartal and others 2009, Clausen and others 2010b). A subsequent study on the effect of particle size compared 30-nm and 70-nm particles. Specimens were evaluated for leach resistance and termite mortality in laboratory tests (Clausen and others 2011). Results showed that there was no difference in leach resistance (<4%) or termite mortality (Fig. 2). Eastern subterranean termites consumed less than 10% of the leached nano-ZnO-treated wood, with 93% to 100% mortality in southern pine treated with both 30-nm and 70-nm ZnO particles.

Because engineered composites have a lower moisture tolerance than does solid wood, the unique properties of nano-ZnO (i.e., leach resistance, resistance to water absorption, photostability, and termite resistance) are characteristics that could greatly improve the durability of engineered composites.

Nano-Polymer Matrices

Nano-polymer matrices offer a sophisticated method for biocide encapsulation and controlled delivery. Self-assembling nano-polymers, called hyperbranched fluoropolymer–poly(ethylene glycol) (HBFP–PEG) cross-linked networks, were first created by melding two normally incompatible polymers and crosslinking the mixture (Fig. 3) (Bartels and others 2007). The complex subsurface of the resulting hyperbranched nano-polymer has unusual tensile strength and provides nanoscale channels for the uptake and release of "guest" molecules such as biocides. The size of the channels, which have been likened to the holes in a sponge, can be customized to accommodate the guest molecule of choice. The nano-polymer is able to encapsulate and hold a chemical until a change in the physical environment (e.g., humidity, temperature, or pH) triggers its release. This technology has been successfully demonstrated for applications ranging from anti-fouling agents (Gudipati and others 2004) to fragrances.

The cross-linked HBFP–PEG45 nano-polymer was loaded with an experimental multi-component biocide formulation containing carvone as an indicator molecule.

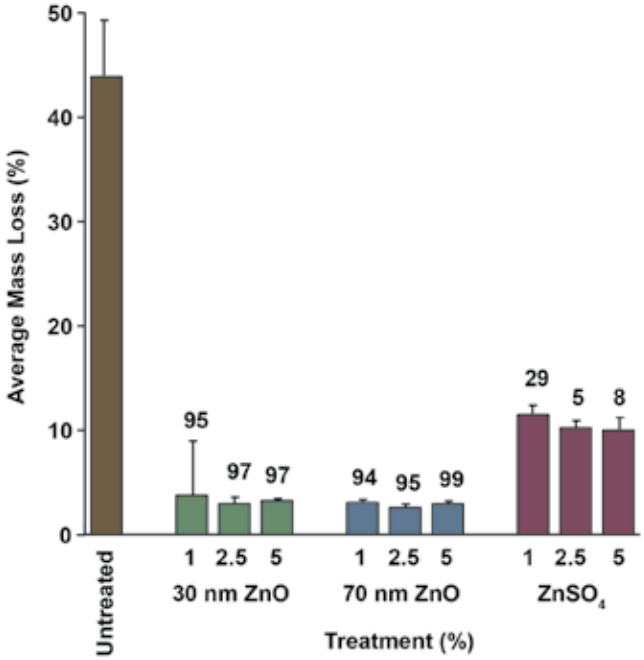

Figure 2. Eastern subterranean termite resistance to southern pine treated with nano-zinc oxide and soluble zinc sulphate indicated by mass loss, i.e., wood consumption. The number above each column represents the average percent termite mortality for that treatment group.

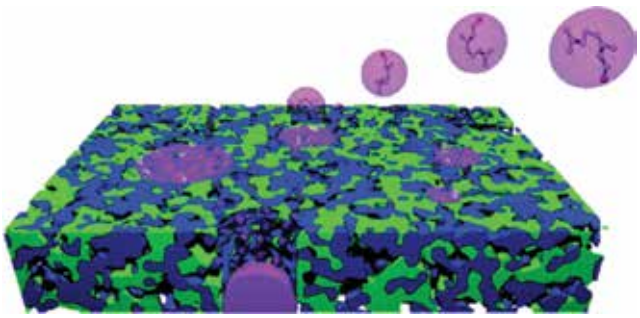

Figure 3. Self-assembling nano-polymer networks act like the holes in a sponge to hold biocides (depicted in purple) until changes in the environment trigger their release (Brown and others 2005, Bartels and others 2007).

The loaded polymer matrix was evaluated for controlled release of the biocide over a range of temperatures from 25 to 75 °C. Gravimetric changes in the loaded nano-polymer following an 8-h exposure to 25, 40, or 75 °C are shown in Table 1. Following isothermal release, the nano-polymer matrices were extracted in methylene chloride and quantitatively analyzed with GC-MS for residual carvone (Table 1).

Results showed that as temperature increased, more of the volatile indicator molecule was released from the matrix with isothermal weight loss reaching 100% after exposure to 75 °C. Quantitative results from the GC-MS analysis suggested that isothermal weight loss alone could not reliably predict release of the biocide above 25 °C. Biocides encapsulated in customized nano-polymer networks could provide prolonged protection as surface treatments for engineered composites.

Table 1—Carvone analysis of loaded HBFP–PEG45 following isothermal release at varying temperatures

Temperature (°C)	Carvone loaded (µg)	Isothermal weight loss (%)	Carvone extracted (µg)
Control	—	0	0
25	297	35.5	101
40	348	95.4	48.5
75	303	100	20.9

Nano-Carriers

Several nano-carrier systems are recognized that may find an application in the field of wood protection, particularly for increased durability of engineered composites (e.g., oriented strandboard (OSB)). For example, a patented nano-carrier system uses 100-nm plastic beads embedded with biocide (Laks and Heiden 2004). Based on the type of polymer comprising the bead, pore size in the bead, biocide viscosity and solubility, biocide-embedded nanoparticles can be designed for slow, controlled release of the biocide. Other cylindrical, tubule-shaped materials (i.e., nano-tubules) made from ceramics, clay, metal, or lipids that have been used as carriers in various medical and industrial applications are now being evaluated for use in engineered composites. Some properties of nano-carriers that would benefit the field of wood protection include

- delivery and placement of biocide,
- slow release of a biocide, and
- release of the biocide upon exposure to certain environmental conditions, such as high humidity.

Protection of heat-labile organic biocides during panel fabrication has greatly limited the applications of newly developed biocides and the number of treatment options for engineered composites.

When developing controlled-release nano-tubules for biocide delivery in composites, a considerable number of variables must be optimized prior to proof of concept. How to precisely control release of a biocide, whether the nano-tubules are compatible with resin used to fabricate the composite, whether the resin itself may be a barrier to release of the biocide, and calculating and regulating actual release rate were examined in the preliminary stage of this project. Methodology was development for analyzing the thermal stability of nano-tubules loaded with a commercial biocide over a range of temperatures from 170 to 190 °C and time. Release rate of the biocide was based on leach resistance, and residual efficacy was evaluated following leaching using two microbial assays that measured the zone of fungal

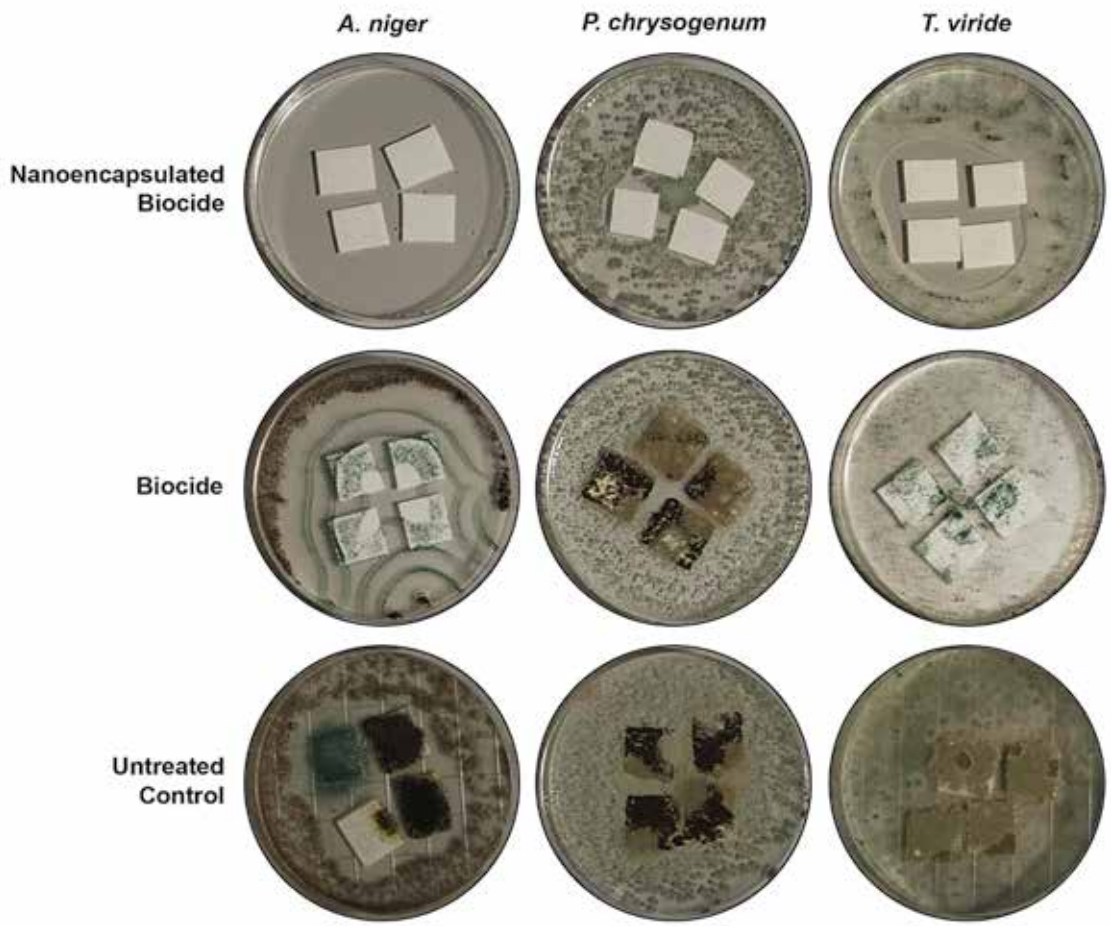

Figure 4. Paper samples treated with biocide-loaded nano-tubules, biocide alone, and untreated controls challenged with three mold fungi.

inhibition in a Petri plate and fungal resistance in a simulated environmental chamber.

Biocide-loaded nano-tubules were incorporated into OSB, medium density fiberboard (MDF), and paper. Samples of nano-treated OSB were tested for modulus of rupture (MOR), modulus of elasticity (MOE), density, moisture swelling, and antifungal resistance in laboratory tests. Preliminary studies on engineered composites demonstrated thermal protection, slow release, and enhanced mold inhibition for the biocide loaded into nano-tubules compared to controls that incorporated either biocide alone or nano-tubules alone. Figure 4 shows the results of paper treated with biocide-loaded nano-tubules and exposed to three mold fungi, *Aspergillus niger*, *Penicillium chrysogenum*, and *Trichoderma viride*. Controls are untreated paper and paper treated with the biocide. Not only are the mold fungi completely inhibited on the surface of samples treated with loaded nano-tubules, but the clearing zone surrounding the samples demonstrates the release of biocide from the nano-tubules. Improved protection of paper treated with biocide-loaded nano-tubules is obvious compared to paper treated with the biocide alone or to untreated paper controls.

Similar results were seen for OSB and MDF that were treated with biocide-loaded nano-tubules compared with untreated controls (Fig. 5). Treated and untreated specimens were placed on Petri dishes of malt extract agar, sprayed with a suspension of *Aspergillus niger* mold spores, and incubated for 4 weeks according to the ASTM D 4445–10 standard laboratory test for controlling sapstain and mold fungi on unseasoned lumber (ASTM 2010). Mold growth occurred on the agar surface and on the surface of untreated test specimens, but mold growth was completely inhibited on specimens treated with biocide-loaded nano-tubules. Release of biocide from the nano-tubules is also evident from the clearing zone surrounding test specimens on agar plates.

Conclusions

Advances in the development of nanotechnology for improved durability of engineered composites are in progress. Unique properties such as photostability, leach resistance, and biocide behavior against biodeteriorating organisms have been identified for select nano-metals. Such properties are desirable for development of new preservative systems. Encapsulating biocides in designer nano-polymer matrices

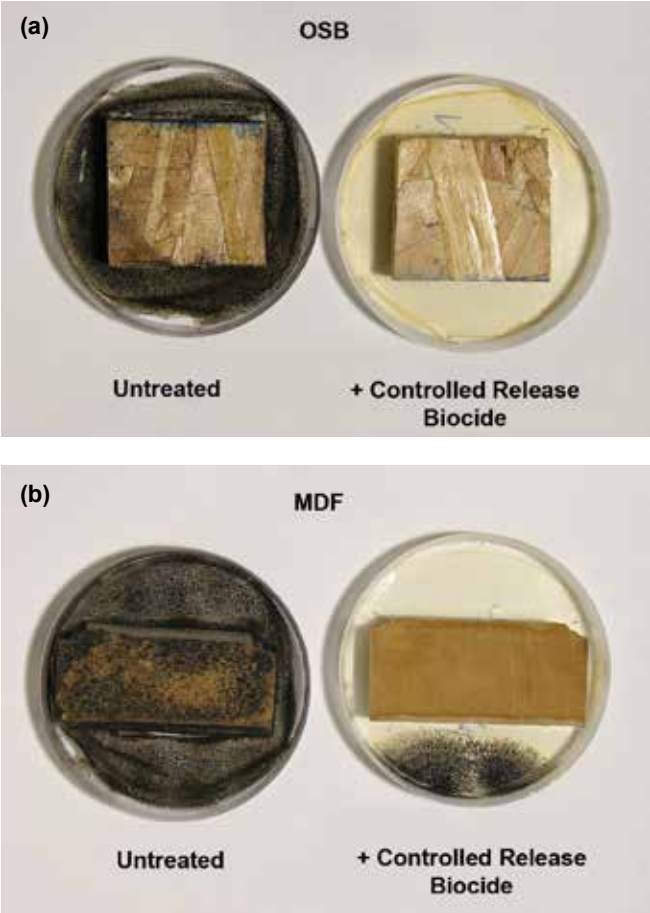

Figure 5. Oriented strandboard (OSB) (top) and medium density fiberboard (MDF) (bottom) either untreated or treated with biocide-loaded nano-tubules were challenged with the mold fungus, *Aspergillus niger.*

are promising delivery systems that release the biocide when triggered by a specific change in the environment. Nano-polymer matrices are ideal for surface treatments of solid and composite wood products. Nano-carriers, such as nano-tubules, can be loaded with organic biocides for targeted delivery that is protected from heat during the fabrication process. Loaded nano-tubules undergo controlled release of biocide to provide prolonged protection of composites from fungal growth.

Literature Cited

ASTM. 2010. Standard test method for fungicides for controlling sapstain and mold on unseasoned lumber (laboratory method). ASTM Standard D 4445–10. Volume 11.01. West Conshohocken, PA: American Society for Testing and Materials: 446–450.

Bartels, J.W.; Cheng, C.; Powell, K.T.; Xu, J.; Wooley, K.L. 2007. Hyperbranched fluoropolymers and their hybridization into complex amphiphilic crosslinked copolymer networks. Macromolecular Chemistry and Physics. 208(15): 1676–1687.

Brown, G.O.; Bergquist, C.; Ferm, P.; Wooley, K.L. 2005. Unusual, promoted release of guests from amphiphilic cross-linked polymer networks. Journal of American Chemical Society. 127(32): 11238–11239.

Clausen, C.A. 2007. Nanotechnology: implications for the wood preservation industry. IRG/WP/07-30415. Stockholm, Sweden: International Research Group on Wood Protection. 13 p.

Clausen, C.A. 2010. Characterizing wood protection properties of nano-metals. Research in Progress RIP-4723-014. Madison, WI: USDA Forest Service, Forest Products Laboratory.

Clausen, C.A.; Green, F., III; Kartal, S.N. 2010a. Weatherability and leach resistance of wood impregnated with nanozinc oxide. Nanoscale Research Letters. 5: 1464–1467.

Clausen, C.A.; Yang, V.W.; Arango, R.A.; Green, F., III. 2010b. Feasibility of nanozinc oxide as a wood preservative. In: Proceedings of the American Wood Protection Association. Birmingham, AL: American Wood Protection Association. 105: 255–260.

Clausen, C.A.; Kartal, S.N.; Arango, R.A.; Green, F., III. 2011 Role that particle size and leach resistance plays in termite mortality on nano-zinc oxide-treated wood. Nanoscale Research Letters. 6:465.

Dorau, B.; Arango, R.; Green, F., III. 2004. An investigation into the potential of ionic silver as a wood preservative. Proceedings, Woodframe Housing Durability and Disaster Issues Conference. Madison, WI: Forest Products Society: 133–145.

Gudipati, C.S.; Greenlief, C.M.; Johnson, J.A.; Prayongpan, P.; Wooley, K.L. 2004. Hyperbranched fluoropolymer (HBFP) and linear poly(ethylene glycol) (PEG) based amphiphilic crosslinked networks as efficient anti-fouling coatings: an insight into the surface compositions, topographies and morphologies. Journal of Polymer Science, Part A: Polymer Chemistry. 42(24): 6193–6208.

Kartal, S.N.; Green, F., III; Clausen, C.A. 2009. Do the unique properties of nano-metals affect leachability or efficacy against fungi and termites? International Biodeterioration & Biodegradation. 63: 490–495.

Laks, P.; Heiden, P.A. 2004 (June 22). Compositions and methods for wood preservation. U.S. Patent 6,753,035.

Nair, S.; Sasidharan, A.; Divya Rani, V.V.; Menon, D.; Manzoor, K.; Raina, S. 2009. Role and size scale of ZnO nanoparticles and microparticles on toxicity toward bacteria and osteoblast cancer cells. Journal of Material Science: Materials in Medicine. 20 (Suppl. 1): 235–241.

Reddy, K.M.; Feris, K.; Bell, J.; Windgett, D.G.; Hanley, C.; Punnoose, A. 2007. Selective toxicity of zinc oxide nanoparticles to prokaryotic and eukaryotic systems. Applied Physics Letters. 9: 2139021–2139023.

Artificial ligaments/tendons based on cellulose nanofibers

Aji P Mathew and Kristiina Oksman
Department of Engineering Materials and Mathematics
Division of Manufacturing and Design of Wood and Bionanocomposites, Luleå
Univeristy of Technology, 97753 Luleå, Sweden
E mail: aji.mathew@ltu.se; kristiina.oksman@ltu.se

Abstract
In the recent years several composite materials were developed and studied with an aim to obtain suitable materials to replace natural ligaments and tendons. While developing artificial tendons or ligaments, properties like biocompatibility, mechanical properties as well as resistance to in vivo moisture and temperature conditions need to be considered. Biomaterials based on cellulose nanofibers isolated from softwood were developed, with an aim to be used as artificial ligament/ tendons. Two types of composites; 1) All cellulose nano composites 2) The studies indicated that nanocelluloses have inherent properties like low toxicity, biocompatibility and biodegradability together with excellent mechanical properties which makes cellulose based nano composites an excellent candidate in biomedical applications. Prototypes in the form of tubes or braids were developed and tested *in vivo* in rats to further explore and optimise its application as ligament/ tendon replacement.

Introduction:
Research in the field of artificial ligaments and tendons indicates that mechanical performance comparable to that of natural ligaments/tendons and biocompatibility are the primary requirements for materials considered for artificial ligament /tendon application. In the recent years several composite materials were developed and studied with an aim to obtain suitable materials to replace natural ligaments and tendons.[1, 2] Artificial tendon made of composites consisting of poly (HEMA) reinforces with polyethylene terephthalate (PET) fibres as well as PET reinforced polyurethane composites for use as ligament prostheses were reported earlier. [1,3] While developing artificial tendons or ligaments biocompatibility, mechanical properties as well as resistance to in vivo moisture and temperature conditions and cyclic loading conditions needs to be considered. Since natural tissues function at 37 ^{o}C it is advantageous to measure the properties at this temperature though elevated temperatures may dehydrate the specimen and affect its properties.[1,-4]
The current report is unique because of the use of biobased raw materials with remarkable mechanical properties for developing the ligament or tendon substitute. The nanocellulose fibres were isolated from wood using chemical and mechanical treatments and were utilized by itself or in combination with collagen, to develop composite materials having mechanical properties similar or better than natural ligaments or tendons. Nanosized cellulose fibers used is expected to result in a homogeneous and uniform product as well as improved fibre-matrix interaction owing to high surface area available for nanocelluloses. The processing and properties of the nano composites, especially in the body conditions of 37° C and high relative humidity conditions (98 %) are reported here. This study is expected to provide valuable insights on the use of nanosized cellulose fibres in the development of artificial ligaments and tendons. The in vitro biocompatibility studies on these nanofiber based composites materials were looked into and were finally fabricated into prototypes and is being evaluated for in vivo biomechanical performance.

Experimental

Materials

Nanofibers were isolated from softwood dissolving pulp (supplied by Domsjö Fabriker AB, Sweden)by mechanical fibrillation method which is reported else where.5 [1]Collagen used in this study was kindly supplied by Resorba Wundversorgung GmbH & Co.KG, Nurnberg, Germany, in the form of collagen suspension of 0.5 wt% in acetic acid medium with a pH of 3.5. This collagen was isolated from horses.

Figure 1 shows the used cellulose nanofibers with diameters in the range of 12-39 nm and collagen nanofibers at pH 7, having diameter in the range of 80-150 nm.

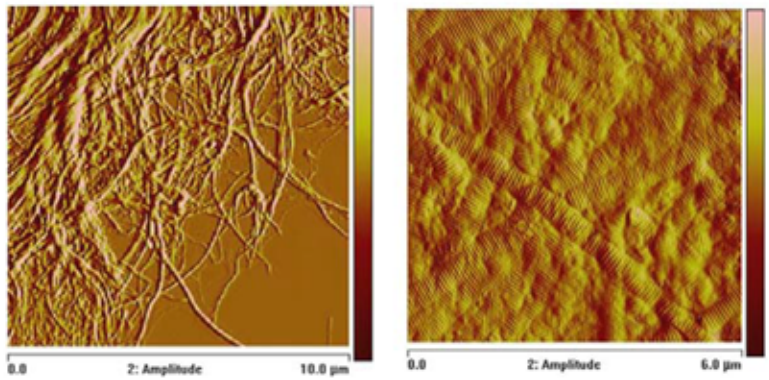

Figure 1 The AFM height images of cellulose nanofibers(left) and collagen nanofibers (right)

Processing Methods

Composite 1: Nanofiber suspensions (0.5 wt%) were used to prepare nanofiber mats using a filter press under vacuum and subsequent drying. The nanofiber mats were partiallay dissolved using ionic liquids followed by precipitation in water and washing with distilled water residual ionic liquid. The samples were finally dried in a hot press

Composite 2: Nanofiber suspensions were thoroughly mixed with collagen suspension and casted on Petri dishes to obtain flat films. These films were neutralised and cleaned by water washing. These films were subsequently crosslinked and washed and dried in vacuum oven for 12 hrs at 35 °C.

Prototype development:

i) Prototypes for ligaments/tendons were developed based on the all-cellulose nano composites. The cellulose nanofiber films were prepared and coated with ionic liquid. These coated films were rolled into tubules and kept at 80 °C for 90 min to carry out partial dissolution. After that it is kept immersed in water for 12 hrs to stop the dissolution and precipitate the dissolved cellulose. This is rinsed in a water bath for 48 hrs to remove all residual ionic liquids.

ii) Prototypes of crosslinked collagen-cellulose nano composites were obtained from the films of the nano composites. The films were cut into strips and braided manually to prototypes with a diameter of 8 cm and width of 1cm.

RESULTS AND DISCUSSION

Composite 1

Mechanical Properties: Mechanical properties of the developed materials were tested in room conditions as well as in simulated body conditions to evaluate its potential as ligament/tendon substitutes. The data from tensile testing (room and simulated body conditions) are given in Table 1.

Table 1. Tensile properties of nanofiber based composites in room conditions in room condition and simulated body conditions and after sterilization.

Sample	TS (MPa)	Strain (%)
Nanofiber mat	105.9 ± 5.5	6.5 ± 1.5
All Cell Comp	112.2 ± 6.5	5.0 ± 1.0
Nanofiber mat (SBC)	64.5 ± 4.9	23.4 ± 2.1
All Cell Comp (SBC)	36.2 ± 3.3	21.3 ± 3.8
Nanofiber mat (SBC), ster	25.1 ± 1.4	20.1 ± 1.6
All Cell Comp (SBC), ster	29.1 ± 1.7	27.7 ± 4.4
Collagen-Cell	96.2 ±12.2	1.4 ± 0.5
X-Collagen –Cell	186.2 ± 34.2	2.4 ± 0.5
Collagen-Cell(SBC)	35.1 ± 2.7	28 0± 3.1
X-Collagen -Cell(SBC)	42.3 ± 4.7	19.0 ± 4.2
Collagen-Cell(SBC) ster	37.2 ± 3.7	17.6 ± 4.7
X-Collagen-Cell(SBC) ster	57.8 ± 12.7	15.1 ± 4.1

The data shows that the nanofiber networks as well as the composites obtained by partial dissolution have very strength in the range of 110 MPa and modulus of 6-8 GPa.In simulated body conditions, the strength and modulus decreased drastically for the nano composites where as the strain at break increased, compared to the corresponding dried ones In order to further confirm the suitability of these materials in biomedical application these materials were tested after sterilization using gamma radiations. It was found that sterilization the material properties were lower in both room and simulated body conditions compared to the corresponding non-sterilized ones. The partially dissolved mats exhibited strength of 30MPa and a strain of 30 % at 37 °C and 95% RH, after sterilization and the properties of these materials are still with in the acceptable range for use in ligament or tendon application.

Biocompatibility: Cytocompatibility of these materials was studied to understand cell adhesion and growth of HOC and HEC cells on all cellulose nano composites. It was found that all cellulose nano composites favoured cell adhesion and growth and the cell density increased after 3 days for both type of cells and was especially favourable for HOC and 80% cells were retained after 3 days. This study indicated that these materials are non-cytotoxic and cytocompatible.

Composite 2

Mechanical Properties: Tensile testing of f collagen and cellulose nanofibers based nanocomposites are given in Table 1. The table shows the data of the tensile testing in room conditions as well as in simulated body conditions of 98% RH and 37 C. In addition the most promising materails based on these studies were sterilized using gamma rays and tested again in simulated body conditions. The increase in mechanical properties is remarkable in these composites and the crosslinked as well as uncrosslinked nano composites showed better mechanical properties than both collagen and the cellulose nanofibers. The crosslinked

materials showed higher strength than their uncrosslinked counter parts where as the strain at break showed a reverse trend. This synergistic effect indicates good chemical compatibility between the two phases, as well as good dispersion. Additionally the in situ pH induced fibrillation of collagen seems to have positive impact on the mechanical characteristics of these materials.The materials were tested at high humidity and 37 °C, in order to obtain some inputs on the performance of these materials in simulated body conditions. In the case of wet samples that simulated body conditions the strength and modulus decreased compared to the dry samples, where as the strain at break increased. The data from the tensile studies in wet conditions showed that all the developed materials are very close to the reported values of natural ligament or tendon, especially at 75% nanofiber content.

Biocompatibilty: Cytocompatibility of these materials was studied to understand cell adhesion and growth on these substrates. It was found that crosslinked collagen –cellulose nanocomposite surfaces favoured cell adhesion and growth and the cell density increased after 15 days.(See figure 2) This study indicated that the crosslinked collagen –cellulose composite is non-cytotoxic and cytocompatible.

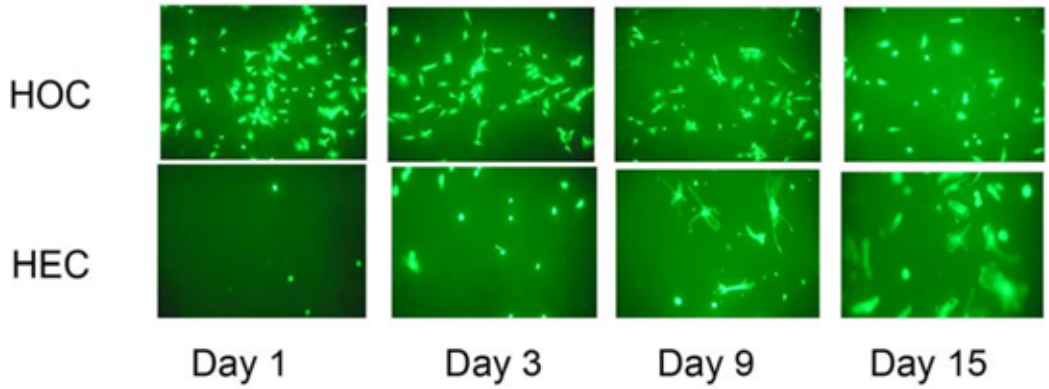

Figure 2. Biocompatibility of sterilized crosslinked collagen- cellulose nanocomposites

Prototypes

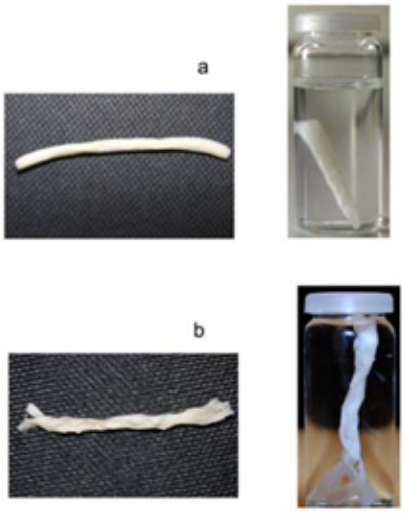

Figure 3 Developed prototypes based on a) All-Cellulose nanocomposites and b) X-collagen-cellulose nanocomposites, in dry room conditions and in PBS medium

The photographs of the prototypes are shown in Figure 3. Both the prototypes were stable in PBS medium and maintained its structural and dimensional stability. It is expected that the developed prototype will have excellent mechanical properties and stability in body conditions and at the same time is non-toxic and biocompatible Further, in vivo biomechanical tests on the prototypes to evaluate its suitability as ligament/tendon substitute are under progress and will be reported subsequently.

CONCLUSION

Cellulose nanofiber based composite materials were developed to be used as the load-bearing component of ligament/tendon substitutes. The nanocellulose composites with nanofibers alone and in combination with collagen were developed for this application. The mechanical properties of the studied composites in simulated body conditions closely matched the mechanical requirement as ligament/ tendon replacement. The initial studies indicated that nanocelluloses having inherent properties like low toxicity, biocompatibility and biodegradability together with excellent mechanical properties are potential candidates to develop cellulose based nano composites for biomedical applications. Prototypes based on these composites are being evaluated for in vitro studies for biocompatibility and in vivo studies for biomechanical performance in order to develop these materials to a commercial application level.

Acknowledgement

European Commission is gratefully acknowledged for the financial support under project NMP4-CT-2006-033277 TEM-PLANT. We acknowledge Dorothée Pierron and Marie-Franciose Harmad' Laboratoire d'Evaluation des Matériaux Implantables (LEMI), France for the biocompatibility studies.

References

1. Iannace S, Sabatini G, Ambrosio L and Nicolais L, Mechanical behaviour of composite artificial ligaments and tendons, Biomaterials, 16, 675-680 (1995)

2. Meyers MA, Chen P-Y, Lin Y-MA., Seki Y.Biological Materials: Structure and mechanical properties. Prog. Mater. Sci: 53 : 1-206 (2008).

3. Santis R.De., Sarracino F, Mollica F, Netti PA, Ambrosio L and Nicolais L, Continuous fibre reinforced polymers as connective tissue replacement, Comp. Sci. Tech, 64, 861-871 (2004).

4.Migliaresi C and Nicolais L, Composite materials for biomedical applications, Int. J. Artif. Organs, 3, 114-118 (1980).

5. Mathew AP, Stelte W. Oksman K., Mechnaical ioslation of nanofibesr and thier utilization in novel nanocomposites for medical applications, 10th International Conference of Wood & Biofiber Plastic Composites, 11-12 May 2009, Madison, Wisconsin, USA. 2009.

Nanocellulose/Conducting Polymer Nanocomposite Films Based on Bacterial Cellulose

Byoung-Ho Lee[1], Hyun-Ji Lee[1], Taekjun Chung[1], Hyun-Joong Kim[1,2]

[1]*Lab. of Adhesion & Bio-Composites, Program in Environmental Materials Science,*
[2]*Research Team for Biomass-based Bio-Materials, Research Institute for Agriculture and Life Sciences,*
Seoul National University, Seoul 151-921, Republic of Korea
Corresponding author: hjokim@snu.ac.kr (www.adhesion.org)

Abstract

Bacterial cellulose/conducting polymer nanocomposites were prepared by the in-situ chemical oxidative polymerization of aniline or pyrrole and bacterial cellulose. Polyaniline conducting polymer nanocomposites with bacterial cellulose fibers were prepared and characterized. In both nanocomposites, the bacterial cellulose was fully encapsulated with polyaniline or polypyrrole by direct in-situ polymerization of the respective monomers using the oxidant and dopant. These bacterial cellulose/conducting polymer nanocomposite materials exhibited the inherent properties of both components. The deposition of a conducting polymer on the bacterial cellulose surface was characterized by scanning electron microscopy, conductivity and cyclic voltammetry measurements.

1. Experimental

1.1. Material

Bacterial cellulose was cultivated using the cultivation method reported below. Aniline monomer and pyrrole monomer were purchased from Sigma Aldrich. Ammonium persulfate (APS) and Ferric chloride as the oxidant were purchased from Duksan Pure Chemical Co., LTD. p-Toluenesolfonic acid as the dopant was purchased from Sigma Aldrich.

1.2. Polymerization of conducting polymer on the bacterial cellulose surface

Bacterial cellulose with a HCl aqueous solution was used as a source for the bacterial cellulose/PANi nanocomposites. Aniline was added to distilled water containing bacterial cellulose. An aqueous HCl solution (35 wt%) was added dropwise to the above-prepared solution until the pH of the solution was 3, and stirred for 1 h under vigorous stirring. APS as an oxidant and p-TSA as a dopant dissolved in distilled water was added to the aniline/bacterial cellulose solution. The monomer : oxidant : dopant molar ratio was kept at 4:1:2. The polymerization of aniline was carried out at room temperature for 2 h. After polymerization, the BC/PANi nanocomposites were obtained.

The method for manufacturing the BC/PPy nanocomposite was similar to that of the BC/PANi nanocomposites. Firstly, pyrrole was added to distilled water containing bacterial cellulose. $FeCl_3$ or APS as the oxidant and p-TSA as the dopant dissolved in distilled water were added to the above prepared beaker. The monomer : oxidant : dopant molar ratio was kept at 4:1:4. The polymerization of pyrrole was carried out below 5 °C for 30 min. After polymerization, the BC/PPy nanocomposites were obtained. Table 1 is lists the composition of the nanocomposites.

1.3. Measurements

FE-SEM was used to characterize the polymerization surface of bacterial cellulose/conducting polymers.

All specimens used for the conductivity measurements were obtained by the polymerized nanocomposites. A four-probe conductivity apparatus was used for the conductivity tests.

Cyclic voltammograms were recorded on aqueous solutions and performed in a standard three-electrode cell setup utilizing an Autolab with the nanocomposite as the working electrode. A platinum plate and Ag/AgCl were used as a counter and reference electrodes, respectively.

2. Results and Discussion

As shown in Figure 1(a) and (b), the surfaces of the nanocomposite were covered completely with polyaniline on the surface of bacterial cellulose. The PANi on the sample doped with p-TSA had a similar nano-granular morphology to the non doped PANi sample. In addition, the grain size was estimated to be ~100 nm.

Figure 1(b) shows the surface morphology of bacterial cellulose/PPy nanocomposite. The PPy coating was composed of small uniform spheres, ~ 100 to 200 nm in diameter, which were fused together to fully encapsulate the bacterial cellulose fiber. In all cases, nanocomposites with four different PPy using the different oxidants and dopants had a globular morphology with some different sizes. PPy particles nucleated and grew on the bacterial cellulose surface. Regular spherical shape particles were observed. Johnston et al. (Johnston et al., 2005) reported that interfacial adhesion between PPy and cellulose fiber was due to the formation of hydrogen bonds between the pyrrole ring and cellulose surface. All the PPy particles on the bacterial cellulose surface had a spherical shape and controlled size, ~100 to 200 nm in diameter. In addition, in the case of PPy1 and PPy2, the individual bacterial cellulose was actually fully covered with PPy. However, the formation of PPy3 and PPy4 was different. The PPy had a cauliflower like morphology. These morphological properties show that oxidant or dopant has a significant effect on the particle shape and size of conducting polymers on the surface of the bacterial cellulose fiber.

Room temperature electrical conductivity measurements were carried out on bacterial cellulose/conducting polymer nanocomposite films using a four probe method. Table 6 lists the conductivity of the nanocomposite. The calculated electrical conductivities ranged from 0.8 to 1.3 S/cm for the BC/PANi nanocomposites and 0.2 to 2.3 S/cm for the BC/PPy nanocomposites, whereas the bacterial cellulose sheet was insulating. This considerable increase in electrical conductivity from insulating to semiconducting is significant. It was reported that the electrical conductivity of PANi depends on the degree of doping, oxidation state, particle morphology, crystallinity, interior intrachain interactions, molecular weight, etc (Abdiryim et al., 2007; Stafstr et al., 1987; Zhang et al., 2002). The conductivity of the BC/PANi1 nanocomposite was higher than that of BC/PANi2, which was not doped with p-TSA. Therefore, the doping level affects the electrical conductivity.

Table 2 lists the conductivity of nanocomposites of PPy on bacterial cellulose doped with p-TSA. The BC/PPy1 nanocomposites provided the highest conductivity, which used $FeCl_3$ as the oxidant and p-TSA as the dopant during polymerization. Little difference between (BC/PPy1, BC/PPy2) and (BC/PPy3, BC/PPy4) was observed. This suggests that the oxidant affects the conductivity. In particular, chloride ions have a good influence on the electrical conductivity. Therefore, the BC/PPy1 and BC/PPy2 nanocomposite show higher conductivity than BC/PPy3 and BC/PPy4. As mentioned above, nanocomposites using p-TSA as the dopant have a high doping level, so that the nanocomposites using p-TSA show higher electrical conductivity than the nanocomposites without p-TSA. Richardson reported that the

difference in the oxidant and dopant had a large effect on the electrical conductivity of wood cellulose-based polypyrrole composites (Richardson et al., 2006).

Table 1 Composition of nanocomposites.

Sample name	Bacterial cellulose	Monomer		Oxidant		Dopant
		Aniline	Pyrrole	APS	$FeCl_3$	p-TSA
BC/PANi1	○	○		○		○
BC/PANi2	○	○		○		
BC/PPy1	○		○		○	○
BC/PPy2	○		○		○	
BC/PPy3	○		○	○		○
BC/PPy4	○		○	○		

Table 2 The electrical conductivity values of nanocomposites.

Samples	Electrical conductivity (S/cm)
PANi1	1.3
PANi2	0.8
PPy1	2.3
PPy2	2.0
PPy3	0.5
PPy4	0.2

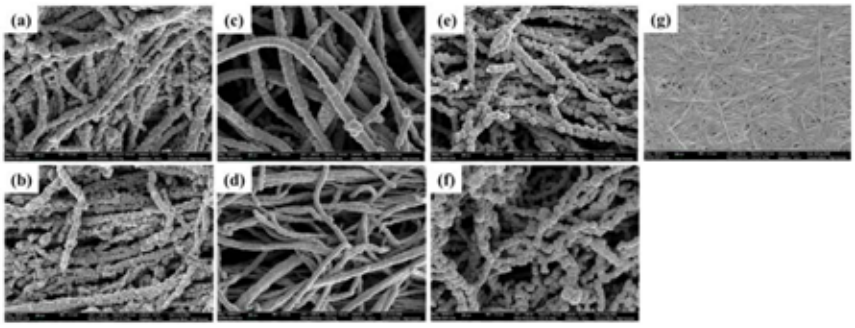

Figure 1. FE-SEM images of (a) BC/PANi1, (b) BC/PANi2, (c) Bc/PPy1, (d) BC/PPy2, (e) BC/PPy3, (f) BC/PPy4 nanocomposite sheets and (g) pure BC.

References

Abdiryim T, Jamal R, Nurulla I. 2007. Doping effect of organic sulphonic acids on the solid-state synthesized polyaniline. J Appl Polym Sci 105(2):576-584.

Johnston JH, Moraes J, Borrmann T. 2005. Conducting Polymers on Paper Fibres. Synth Met 153(1-3):65-68.

Richardson M, Johnston J, Borrmann T. 2006. Electronic properties of intrinsically conducting polymer-cellulose based composites. Current Applied Physics 6(3):462-465.

Stafstr, ouml, m S, Br, eacute, das JL, Epstein AJ, Woo HS, Tanner DB, Huang WS, MacDiarmid AG. 1987. Polaron lattice in highly conducting polyaniline: Theoretical and optical studies. Phys Rev Lett 59(13):1464.

Zhang Z, Wei Z, Wan M. 2002. Nanostructures of Polyaniline Doped with Inorganic Acids. Macromolecules 35(15):5937-5942.

EUCALYPTUS MICRO AND NANOFIBRES FOR REINFORCEMENT OF POLYMERIC NANOCOMPOSITES

G. H. D. Tonoli [a], L. A. Caixeta [b], J. M. Marconcini [b], A. C. Corrêa [b], M. A. Pereira-da-Silva [c], L. M. Mendes [a], Luiz H. Capparelli Mattoso [b]

[a] *Department of Forest Science. Universidade Federal de Lavras, C. P. 3037, 37200-000, Lavras, MG, Brazil. *Corresponding author - Phone/Fax: + 55 35 3829-1411, email: gustavotonoli@yahoo.com.br, lourival@dcf.ufla.br*

[b] *Laboratório Nacional de Nanotecnologia para o Agronegócio (LNNA), Embrapa Instrumentação Agropecuária, Caixa Postal 741, São Carlos, SP. CEP 13560-970, Brazil. leandrocaixeta@ymail.com, marconcini@cnpdia.embrapa.br , mattoso@cnpdia.embrapa.br , carol_correa@hotmail.com*

[c] *Instituto de Física de São Carlos, Universidade de São Paulo, C.P. 369, 13560-970, São Carlos, SP, Brazil. maps@ifsc.usp.br*

EXTENDEND ABSTRACT

Nowadays, there is a growing interest in the use of more environment-friendly materials and polymers of natural occurrence, such as cellulose, for developing materials. Cellulose is a versatile polymer that can be extracted in a nanofibre form, leading to a material with mechanical strength just limited by the forces among adjacent atoms. The micro/nanofibres have be used for different commercial applications: pharmaco (Villanova et al., 2011), dietary food (Okiyama et al., 1993), packaging (Siro and Plackett, 2010), special papers (Sehaqui et al., 2011) and especially as reinforcement in polymer matrices (Gardner et al. 2008). The geometric properties of the nanocellulose structures (shape, length and diameter) depend mainly on the origin of the cellulose and the extraction process (Ahola et al., 2008).

Several sources of cellulose have been used to obtain cellulose nanostructures with different morphologies and crystalinities; however, the potential use of wood short fibres for production of nanofibres has been insufficiently explored. In tropical regions, eucalyptus is a fast growing hardwood species with good fibre qualities and relatively cheap market price. Among kraft pulps, bleached eucalyptus kraft pulp (BEKP) is the most abundant and has been becoming increasingly more available than others. A proper choice of starting cellulose materials can reduce energy consumption in the micro/nanofibres production, a key issue for industrial up-scaling. Although eucalyptus pulp has been widely employed in the paper industry throughout the world, there is limited information in the scientific literature concerning its use as raw-material for production of micro/nanofibres designed for different aplications. Eucalyptus pulp presents shorter fibres than pinus pulp for example, which can suggest that the same occurs if it is broken the hierarquical structure of the fibre cell wall. The important is that the smaller the fibre length (which generally relates to lower aspect ratio), the easier the fibre dispersion.

Cellulose micro/nanofibres can be obtained from mechanical and chemical approaches. Between the mechanical procedures it can be cited: refining and sonification, which lead to micro and nanofibres. Refining is carried out in the presence of water, usually by passing the suspension of pulp fibres through a refiner composed by a relatively narrow gap between the rotor and the stator. The main effect of refining

in cellulosic fibre structure as a result of mechanical action is the fibrillation of the fibres. Sonification is carried out in a fibre suspension in order to separate the fibrils bundles in the fibre cell wall through cavitation. Between the chemical procedures it can be reported: enzymatic hydrolises with cellulases giving origin to micro and nanofibres; and acid hydrolises with sulphuric or hydrochloric acid leading to nanocristaline particles (whiskers). The amorphous regions around the cellulose microfibrils are destroyed by acid hydrolysis under a controlled period of time and temperature, keeping the crystallites intact. The acid hydrolysis is selective in amourphous cellulose, resulting in colloid suspensions of well-defined cellulose nanocrystals. In the present study, fibres and micro/nanofibres extracted from bleached eucalyptus Kraft pulp were investigated in terms of morphology (optical mycrosccopy - OM, atomic force microscopy - AFM and scanning transmission electron microscopy – STEM), chemical composition (elemental analysis), crystallinity (XRD), zeta-potential, and thermal stability (TG).

As expected it was observed the yield decrease from a yield of 65% to 61% with the increase of hydrolises time (from 30 min to 60 min), as a consequence of the disintegration of amorphous cellulose and degradation of the crystalline reginons during hydrolysis (Bondeson et al., 2006). The X-ray difractograms (XRD) of the fibres and micro/nanofibres showed a well defined peak around $2\theta = 22{,}5^{o}$ that is characteristic of cellulose I. Sonified micro/nanofibres presented lower crystalinity index due probably to the cavitation occurred, which acts separating the glucose chains in the cellulose nanocrystals, no glucose solubilisation is expected. The decrease of crystalinity was also observed in refined fibres due to the shearing of the crystalites during the mechanical treatment suffered by the fibres. Nanofibres obtained by hydrolysis presented higher crystalinity index than the others due to remotion of amorfous cellulose, hemicelluloses and residual lignin, then resulting in the majority the crystalites formed by well organized glucose chain. The increase in crystallinity with the time of hydrolysis was also undoubtedly due to the removal of hemicelluloses and lignin, which exist in the amorphous regions

Acid hydrolises decreased the onset degradation temperature of the nanofibres as also observed elsewhere by Teixeira et al. (2010) for cotton nanofibres. Thermal analyse of the fibres and micro/nanofibres showed two stages of thermal degradation. The first stage occurred at temperatures of 150 to 350 ^{o}C, with weigth loss of around 70% and 40% for fibres and micro/nanofibres respectively. The second stage is the thermal degradation between 350 and 525 ^{o}C. Decomposition of the starting fibre and micro/nanofibres occurred in several stages, indicating the presence of different components that decompose at different temperatures. Hydrolised nanofibres (30 min and 60 min) presented low decomposition temperatures and began to degrade from around 180 ^{o}C and 210 ^{o}C, probably owing to the decomposition of remanescent degraded hemicelluloses and lignin. Thermal degradation occurred first in the chains with sulphate groups for cellulose nanofibres obtained by acid hydrolises, because they promote the dehydration reactions that release water and catalize the cellulose degradation reactions (Corrêa et al., 2010). Furthermore, the substitution of OH groups by sulphate groups decreases the activation energy for cellulose chain degradation. This will limit the use of some of the present nanofibres to polymers that do not require high processing temperatures (e.g. above 180 ^{o}C) for extrusion.

In conclusion, it was showed that eucalyptus cellulose micro/nanofibres can be isolated using mechanical fibrillation (refining and sonification) and chemical (acid hydrolysis) processes. Nanofibres obtained here presented distint morphological characteristics that can be used for engineering of polymeric composites, with the possibility of impact differently in their mechaninal performances. Sonificated

nanofibres presented similar diameters and higher length than crystaline nanofibres (whiskers). The present work contributes to the wide spreading of different methods for micro/nanofibres production for polymer reinforcement.

ACKNOWLEDGEMENTS
Financial support for this research was provided by FAPESP, FAPEMIG and CNPq.

REFERENCES

Ahola S, Osterberg M, Laine J. Cellulose nanofibrils - adsorption with poly(amideamine) epichlorohydrin studied by QCM-D and application as a paper strength additive. Cellulose (2008) 15:303-314.
Bondeson D, Mathew A, Oksman K. Optimization of the isolation of nanocrystals from microcrystalline cellulose by acid hydrolysis. Cellulose (2006) 13:171-180.
Corrêa AC, Teixeira EM, Pessan LA, Mattoso LHC. Cellulose nanofibers from curaua fibers. Cellulose (2010) 17:1183-1192
Gardner DJ, Oporto GS, Mills R, Samir MASA (2008) Adhesion and surface issues in cellulose and nanocellulose. J Adhesion Sci Technol 22:545-567.
Okiyama A., Motoki M., Yamanka S.: Bacterial cellulose IV. Application to processed foods. Food Hydrocolloids, 6, 503-511 (1993).
Sehaqui H, Allais M, Zhou Qi, Berglund LA. Wood cellulose biocomposites with fibrous structures at micro- and nanoscale. Composites Science and Technology 71(3) 382-387, 2011.
Siro I, Plackett D (2010). Microfibrillated cellulose and new nanocomposite materials: a review. Cellulose, 17, 459-494.
Teixeira EM, Corrêa AC, Manzoli A, Leite FL, Oliveira CR, Mattoso LHC. Cellulose nanofibers from white and naturally colored cotton fibers. Cellulose (2010) 17:595-606.
Villanova JCO, Ayres E, Carvalho SM, Patrício PS, Pereira FV, Oréfice RL. Pharmaceutical acrylic beads obtained by suspension polymerization containing cellulose nanowhiskers. European Journal of Pharmaceutical Sciences 42(4) 406-415, 2011.

Impact Properties and Characteristic Impact Resistance Model of Cellulose Nanofibril-Filled Polypropylene Composites

Han-Seung Yang[1,2*], Douglas J. Gardner[1†] and Jacques W. Nader[1]

[1]*AEWC-Advanced Structures and Composites Center*

[2]*Forest Bioproducts Research Institute (FBRI)*

University of Maine

Orono, ME 04469-5793, USA

*: First author.

e-mail: hanseung.yang@maine.edu

Tel: +1-207-581-2182 Fax: +1-207-581-2074

†: Corresponding author.

e-mail: douglasg@maine.edu

Tel: +1-207-581-2846 Fax: +1-207-581-2074

ABSTRACT

Notched and unnotched Izod impact strength of cellulose nanofiber (CNF) and microfibrillated cellulose (MFC)-filled impact modified polypropylene (PP) composites were evaluated and compared with microcrystalline cellulose (MCC)-filled composites. Izod impact strength and fracture initiation resistance values were investigated and a characteristic impact resistance model was developed to evaluate the impact fracture mechanism of cellulose nanofibril-filled PP composites. As filler content increased, both notched and unnotched impact strength decreased because of the agglomeration of the filler, which caused the cracks to easily propagate in the composite. CNF and MCC-filled composites showed higher impact resistance than MFC-filled composites as filler loading increased but CNF and MFC-filled composites showed higher characteristic impact resistance than MCC-filled ones. It was found that impact resistance is not the only evaluation criteria, but in addition, the characteristic impact resistance is another evaluation tool to describe the material's unique impact characteristics. The unnotched impact energies were considerably larger than the notched impact energies because the unnotched impact energies are a measure of crack propagation, and also of crack initiation. Impact modified PP used in this study is more fracture resistant, but more crack sensitive than conventional PP.

Key words: Notched and unnotched Izod impact; cellulose nanofiber; microfibrillated cellulose; microcrystalline cellulose; characteristic impact resistance model; crack propagation; crack initiation

INTRODUCTION

Recently, organic/inorganic nanoscale material-filled composites have attracted a great deal of interest from researchers because these composites often exhibit superior properties that are synergistically derived from the filler and matrix polymer (Svoboda et al 2002). Especially, cellulose nanofibril-filled thermoplastic composites have been studied extensively because they are an alternative to inorganic filler reinforced thermoplastic nanocomposites in terms of low cost and mitigation of health and environmental concerns. Because cellulose materials are totally biodegradable, while inorganic nano fillers such as nanoclay, silica, mica and carbon nanofibers are not, cellulose nanocomposites are viewed to be an environmentally friendly composite material and interest in cellulose

nanocomposites has increased in recent years (Mi et al 1997). Cellulose is a renewable natural polymeric material which has special properties such as biocompatibility, long-term durability and extreme heat resistance over a wide temperature range (Zugenmaier 2006). In addition, relative high-strength, high stiffness and low density are positive properties, therefore, natural fillers can be a replacement for synthetic fillers to reinforce plastics used in the automotive industry, packaging, and furniture production (Alemdar and Sain 2008).

From the point of view of polymer matrices, thermosetting polymers are both expensive and brittle. There is an increasing need for developing favorable polymer composite materials that can serve industrial needs and provide an economical substitute while maintaining properties similar to those composites. Polypropylene (PP) is suitable as a matrix polymer because of its low price and favorable properties such as good stiffness, lightweight, good weathering ability, design flexibility and good mechanical properties (Mi et al 1997). To be suitable for mass production, polymeric materials must be economical and easily available using well-established and reliable technologies. These conditions are clearly accomplished by PP-based reinforced composites. In fact, PP matrix composites can be produced with many different types of fillers using widely applied processing techniques such as injection molding and compression molding. Recent developments in natural filler reinforced composites have shown that it is possible to obtain high performance materials utilizing environmentally friendly reinforcements. PP is among the most utilized polymer matrices as a consequence of its recyclability and low processing costs (Manchado et al 2000). To improve the competitiveness of PP for engineering plastic applications, it is an important objective in PP compounding to simultaneously increase its dimensional stability, heat distortion temperature, stiffness, strength, and impact resistance without sacrificing easy processing (Svoboda et al 2002).

Certain composite applications need high strength and brittleness, while others need good stiffness and ductility. Fracture toughness and impact resistance are among the most important mechanical properties of a material when impact loading is applied. Determination of fracture characteristics, therefore, is extremely important (Hristov et al 2004). Especially for application in motor vehicle exteriors such as bumpers and impact-resistant panels, fracture initiation and propagation mechanisms are a key factor of a material's property requirements. There are few reported investigations dealing with analyses of the individual stages of the fracture process under impact loading applications (Hristov et al 2004, Yang et al 2004, Oksman and Clemons 1998 and Stark and Rowlands

2003) .

In this study, impact properties of cellulose nanofiber (CNF) and microfibrillated cellulose (MFC)-filled impact modified polypropylene (PP) composites were evaluated and compared with microcrystalline cellulose (MCC)-filled composites by means of notched and unnotched Izod impact tests including discussion of individual impact energy behavior during fracture and development of a characteristic impact resistance model. A fracture initiation resistance concept is developed to characterize the different fracture mechanisms between notched and unnotched Izod impact tests and a characteristic impact resistance model was also developed to describe material's unique impact characteristics. The purpose of this study is to investigate the effect of cellulose nanofibril fillers as well as microcrystalline cellulose on the impact properties of thermoplastic polymer composites and to analyze fracture processes during applied impact loading.

EXPERIMENTAL PROCEDURE

Materials

Matrix Polymer

The polypropylene (PP) used as the thermoplastic matrix polymer was supplied by Polystrand Co., in the form of impact modified copolymer pellets with a density of 900 kg/m^3 and a melt flow index of 35 g/10 min (230°C/2,160 g). The product's commercial name was FHR Polypropylene AP5135-HS and it was stored in sealed packages.

Reinforcing Fillers

The cellulose materials used as natural reinforcing fillers in the composites were microcrystalline cellulose (MCC) for the comparison purposes, cellulose nanofiber (CNF) and microfibrillated cellulose (MFC). The product name of the MCC was Sigmacell® Cellulose Type 50 supplied by Sigma-Aldrich Co.; the CNF was Arbocel Nano MF 40-10 supplied by J. Rettenmaier & Söhne GMBH Co., Germany; and the MFC was Lyocell L010-4 supplied by EFTec™ Co. CNF was in the form of a suspension with a solids content of 10 wt.%. MFC was in the form of wet fiber web with a solids content of 15 wt.%. CNF is in the form of rod-like short fiber 50 - 300 nm in diameter and 6 - 8 in aspect ratio, MFC is in the form of long fiber 50 - 500 nm in diameter and 8,000 - 80,000 in aspect ratio, and MCC is in the form of particle 50 µm in average diameter and 1 - 2 in aspect ratio. The MCC was stored in sealed containers after being oven dried for 24 h at 103°C. The CNF

and MFC were stored in a refrigerator at 5 - 10°C in sealed packages before being used.

Sample Preparation

The MCC was dried to a moisture content of less than 1 wt.% using a forced air oven at 103°C for at least 24 h and then stored in sealed containers in an environmental chamber prior to compounding. The CNF and MFC were stored in sealed containers in a refrigerator at 5 - 10°C prior to compounding. A Brabender Prep-mixer® was employed to compound the MCC, CNF and MFC with the PP, with the latter being used as a matrix polymer. During the CNF and MFC mixing with PP, the cellulose nanofibril suspension and wet fiber webs were slowly and carefully fed into the bowl mixer in low amounts for each attempt, otherwise the water would evaporate explosively and violently. The process temperature and torque changes were measured in real time. The sample preparation procedure consisted of three general processes, viz. melt blending, grinding and injection molding. Compounding was performed at 190°C for 40 min with a screw speed of 60 rpm. The blended mixture was granulated using a lab scale grinder, the ground particles were stored in sealed packs to avoid unexpected moisture infiltration after first being oven dried for at least 24 h at 103°C. Seven levels of filler loading (1, 2, 3, 4, 6, 8 and 10 wt.%) for MCC, CNF and MFC were used in the sample preparation. Cellulose fillers were blended with PP for 40 min, ground and then stored in sealed containers in an environmental chamber prior to injection molding. The samples used for the Izod impact tests were injection molded at 246°C, using an injection pressure of 17.25 MPa. The width, length and depth of the impact test samples were in accordance with ASTM D 256-06. After injection molding, the test samples were conditioned before testing at 23±2°C and 50±5% RH for at least 40 h according to ASTM D 618-99.

Test Methods

Izod Impact Tests

Notched and unnotched Izod impact strength tests were conducted using a Ceast pendulum impact tester (Model Resil 50B) according to ASTM D 256-06 at 23±2°C and 50±5% RH in the environmentally conditioned mechanical testing room. Each value obtained represented the average of six samples and in the case where COV (coefficient of variance) exceeded 5%, the number of samples was increased to twenty.

Scanning Electron Microscopy (SEM)

Studies on the morphology of the Izod impact fracture surfaces of the composites were carried out using an AMR 1000 (AMRay Co.) scanning electron microscope (SEM). Images were taken at 10 kV with 200× SEM micrograph magnifications. All samples were sputtered with gold before the microscopic observations were made.

RESULTS AND DISCUSSION

Notched and unnotched Izod Impact Strength

The notched and unnotched Izod impact samples were tested and **Fig. 1** shows the Izod impact strengths of the composites at different filler loadings. Both notched and unnotched Izod impact strength of the composites decreased as the filler content increased. The agglomerated filler particles generated filler-filler contacts where there was no interfacial adhesion in the matrix polymer, which caused any cracks to easily propagate in the composite since no crack initiation energy was required (Yang et al 2004). These micro-cracks caused decreased impact strength of the composites (Yang et al 2006a), however, a previous study reported that the addition of a compatibilizing agent could improve filler dispersion and the impact resistance of the composites (Svoboda et al 2002 and Yuan et al 2008). Based on previous research results (Zhang et al 2003 and Zhang et al 2004), it can be assumed that impact strength of the composites should be enhanced by nano reinforcement but in real applications, no researchers have successfully enhanced the impact strength of the composites by incorporating nanoparticles. Previous research results (Zhang et al 2003 and Zhang et al 2004) indicate that the impact strength increased as filler loading increased up to low filler content such as 2 - 6 wt.% but decreased as filler loading was increased further. The decrease in impact strength of the composites was usually caused by poor dispersion of filler particles. If the filler particles are dispersed thoroughly in the matrix polymer, cracks will occur only at the filler-matrix interface. In the case when small particles are incorporated in the matrix, crack length increases considerably during the process of fracture. Increases in crack length leading to increases in energy absorption before fracture (Bledzki et al 2009) should enhance impact strength.

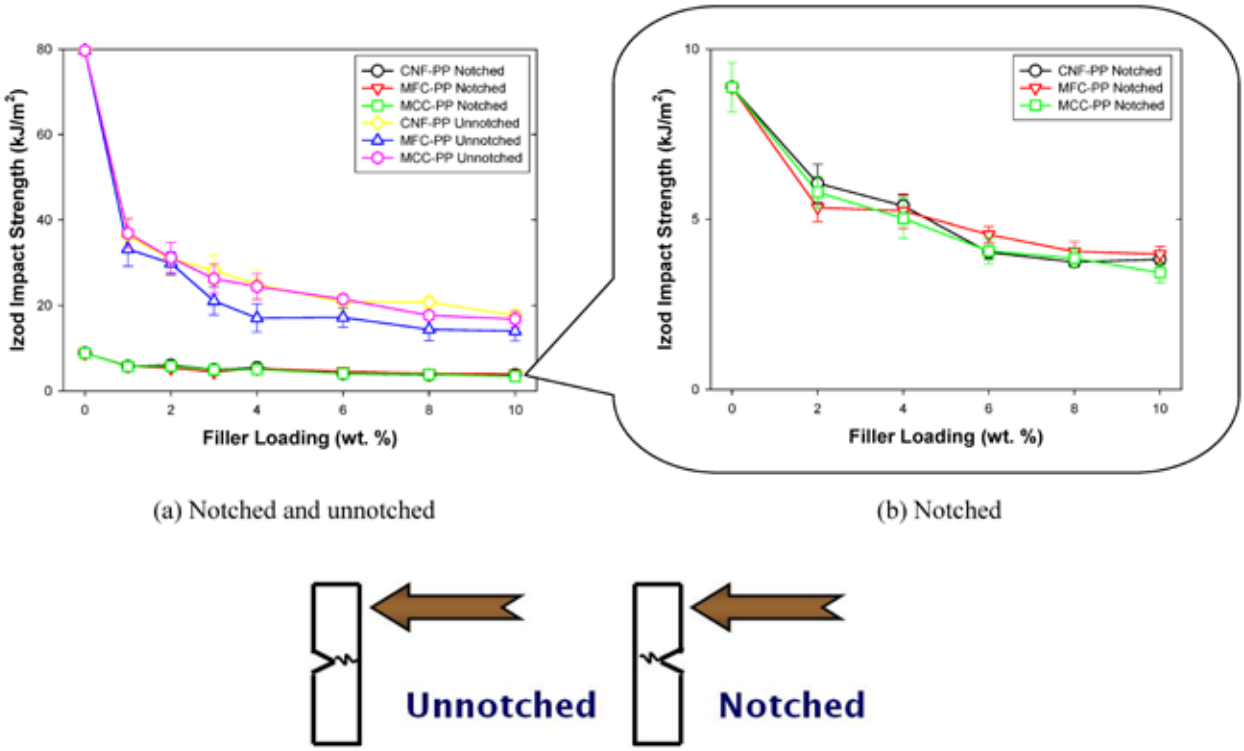

(a) Notched and unnotched (b) Notched

Fig. 1. Notched and unnotched Izod impact strengths of the composites at different filler loadings.

This is the ideal concept but in real applications, filler particles tended to agglomerate with each other and there were many filler-filler contacts in the composites which are more crack sensitive than the filler-matrix interface as shown in **Fig. 2**. This is the major reason for a decrease in impact strength as filler loading increases in the composites. Especially cellulose nanofibril fillers strongly tend to agglomerate with each other during drying or the melt mixing process by hydrogen bonding because the raw cellulose nanofibrils are produced in a form of aqueous suspension. Therefore, preventing agglomeration and achieving good dispersion of cellulose nanofibril reinforcements in polymer composites is one of the key points of future research.

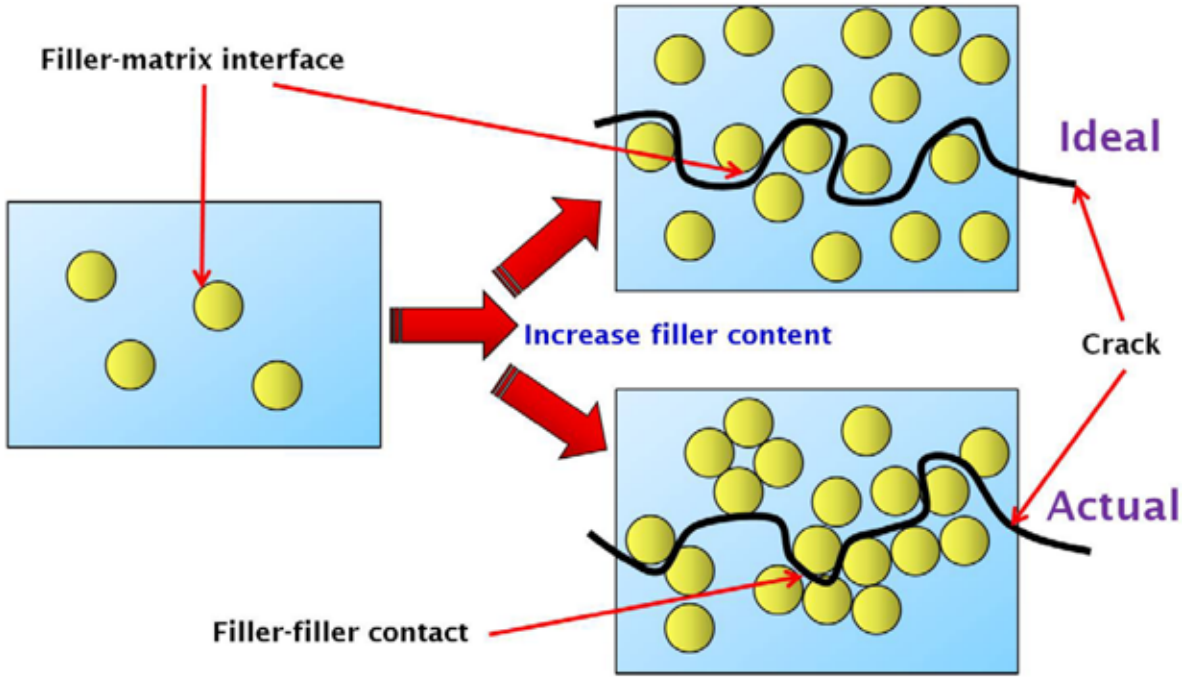

Fig. 2. Crack at the interface during the impact fracture in the composites.

The unnotched impact strength of CNF-filled PP composites displayed higher values than the other fillers as loading increased, which was attributed to the larger agglomerations of fillers in the MFC and MCC-PP composites while the CNF-filled PP composites exhibited less agglomerations as shown in **Fig. 3**. Agglomerated particles or fibers caused poor stress transfer to the matrix polymer and this led to lower impact strength of the composites as shown in **Fig. 1**. The notched samples exhibited lower impact strength than the unnotched samples. The notched tip is the stress concentrating point when impact occurs, and the easy propagation of the crack results in the low impact strength in the notched sample (Yang et al 2004). In the case of the unnotched samples, the filler–matrix interface is the stress concentrating point and crack propagation begins at micro-cracks in the composite. Previous researchers reported that maleic anhydride grafted polypropylene (MAPP) compatibilizer had little or no effect on the notched impact strength but appeared to increase the unnotched impact strength of the composites (Oksman and Clemons 1998 and Stark and Rowlands 2003), which was attributed to the improved interfacial adhesion causing a higher impact resistance in the case of the unnotched impact test. The unnotched sample made with 100 wt.% of polypropylene exhibited significantly higher impact strength than the sample made with 1wt.% filler loading.

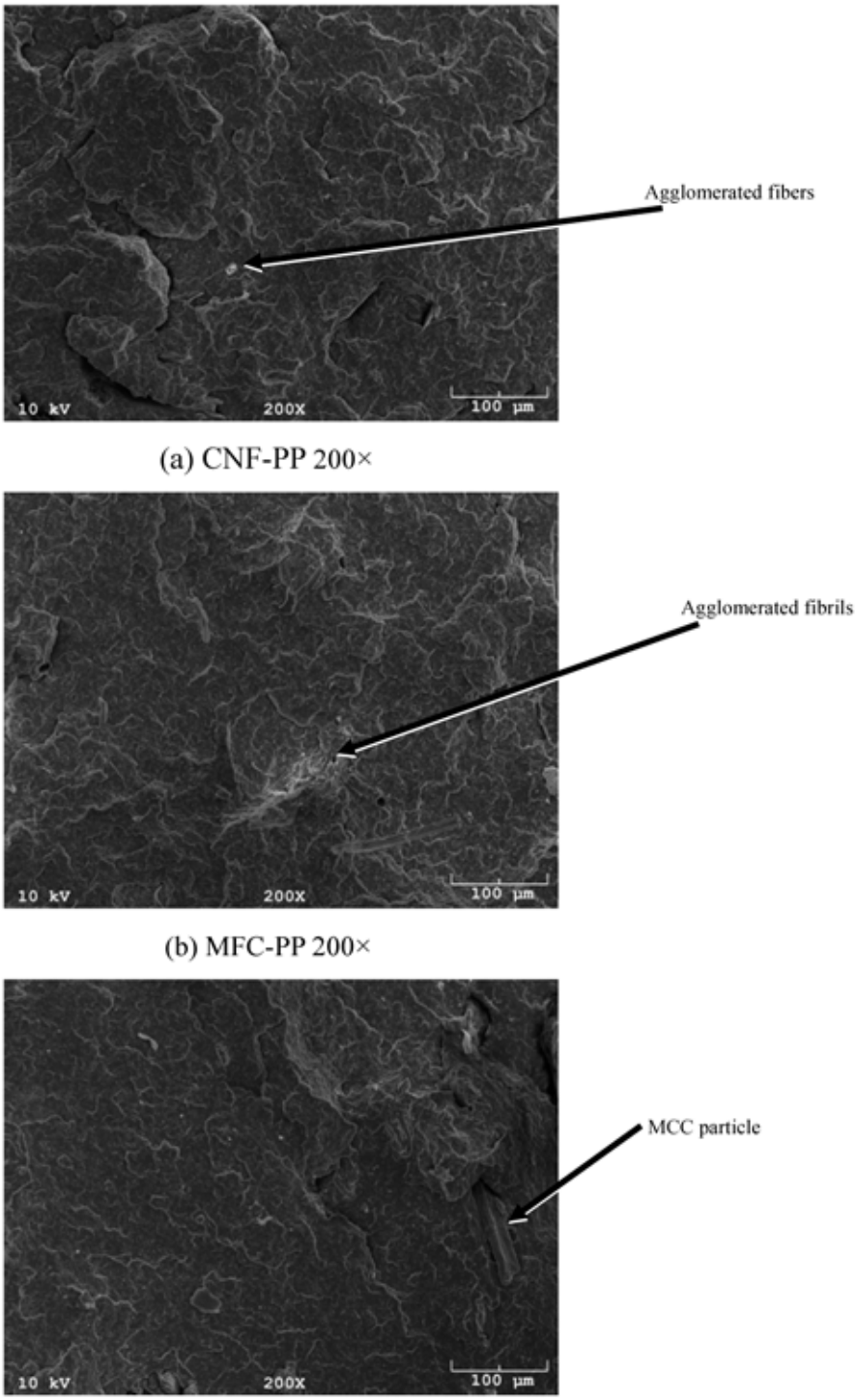

Fig. 3. SEM micrographs of the composites unnotched impact samples away from the notch (3 wt.% of filler loading).

The unnotched Izod impact energies were considerably larger than the notched Izod impact energies because of the different fracture processes involved in the notched and unnotched samples. The impact properties were affected by the crack initiation and the crack propagation mechanism between the filler and the matrix polymer (Yang et al 2006b).

There are several photographs in **Fig. 4** which describe notched and unnotched impact fracture behavior. **Fig. 4** (a) is a notched sample and the crack easily propagated from the notched tip. **Fig. 4** (b) is an unnotched sample, impact loading applied at the opposite side of notched tip and the crack was initiated and then propagated from the impact point. In this case, stress whitening occurred at the impact point. **Fig. 4** (c) is a fracture end of the notched sample and almost no stress whitening occurred, but **Fig. 4** (d) is a fracture end of the unnotched sample and stress whitening occurred at the opposite side of the notched tip.

(a) Notched sample

(b) Unnotched sample

(c) Fracture end of notched sample

(d) Fracture end of unnotched sample

Fig. 4. Fracture surfaces of notched and unnotched impact samples (3 wt.% of filler loading).

The unnotched sample impact behavior was controlled to a considerable extent by fracture initiation processes which, in turn, were controlled by stress concentrations occurring at defects in the composite system. Notched impact behavior was controlled to a greater extent by factors affecting the propagation of fractures initiated by the stress concentration at the notched tip. In other words, the unnotched Izod impact energies are not only a measure of crack propagation, but also of crack initiation (Yang et al 2004 and Yang et al 2007a). This is because the notched impact energy comprises only the crack propagation, whereas the unnotched impact energy consists of the crack initiation and crack propagation in the composite system (Yang et al 2007b).

Fracture initiation resistance can be calculated by subtracting notched impact strength from unnotched impact strength and is shown in **Fig 5**.

$FI_R = I_U - I_N$

where FI_R is fracture initiation resistance, I_U is unnotched and I_N is notched impact strength, respectively. The fracture initiation resistance of CNF-filled PP composites showed higher values than the other samples, which was attributed to the large agglomerations of the other fillers and displays a similar trend to graph in **Fig. 1** (a).

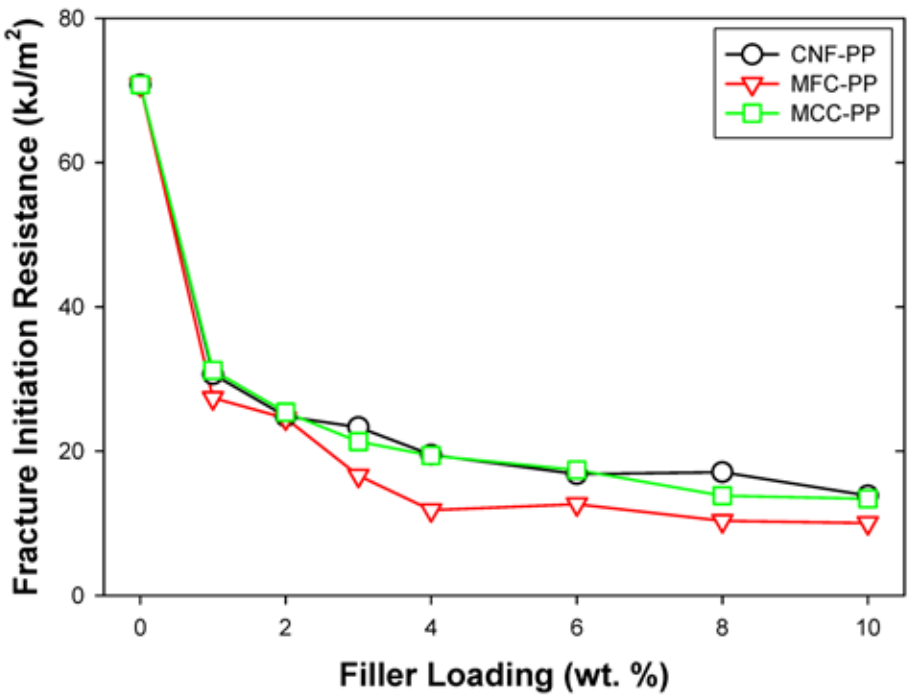

Fig. 5. Fracture initiation resistances of the composites at different filler loadings.

Fig. 6 shows the comparison between conventional PP (homo PP) and impact modified PP used in this study. The matrix polymer's resistance to crack propagation has an influence upon notched impact strength, while unnotched impact strength was affected by the energy consumed due to plastic flexural deformation prior to crack initiation (Yang et al 2006b). From **Fig. 6** (b), the unnotched impact strength of the impact modified PP used in this study was nearly twice the conventional PP, but the notched impact strength was lower than conventional PP. This means that the impact modified PP was more fracture resistant than the conventional PP while more crack sensitive than conventional PP. In other words, when impact loading is applied, impact modified PP is hard to initiate but easy to propagate cracks compared with the conventional PP. In the case of the notched sample made with 100 wt.% PP with the notched tip, the crack was initiated at the impact occurrence, but the unnotched specimen had no such defect and therefore showed significantly higher impact strength. The addition of the filler led to the creation of an interface between the filler and the matrix polymer, which then constituted the stress concentrating and crack initiating point, and this caused significantly reduced impact strength in the unnotched sample (Yang et al 2004 and Yang et al 2007a).

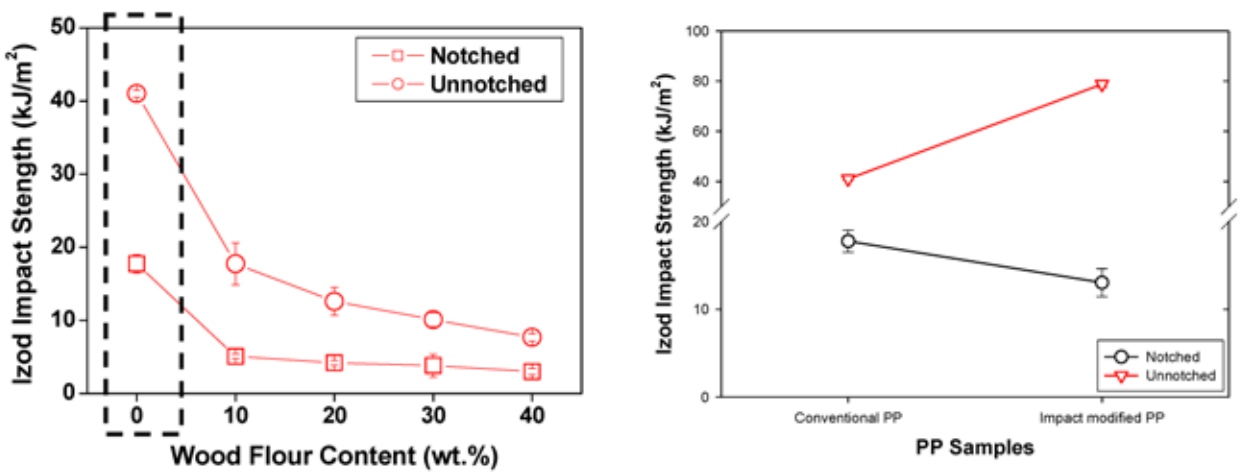

(a) Wood flour-conventional PP

(b) Comparison between conventional and impact modified PP

Fig. 6. Notched and unnotched Izod impact strength comparison between conventional PP and impact modified PP ((a): courtesy of Yang et al 2006b).

Characteristic Impact Resistance Model

During the evaluation of impact fracture surfaces, it was observed that stress whitening occurred at the impact point when the crack initiated and then propagated from the end of fracture initiation zone to the slip-stick point. Beyond the slip-stick point, there was no impact resistance in this brittle fracture zone. The area between the fracture initiation zone and slip-stick point can be described as a fracture propagation zone as shown in **Fig. 7**.

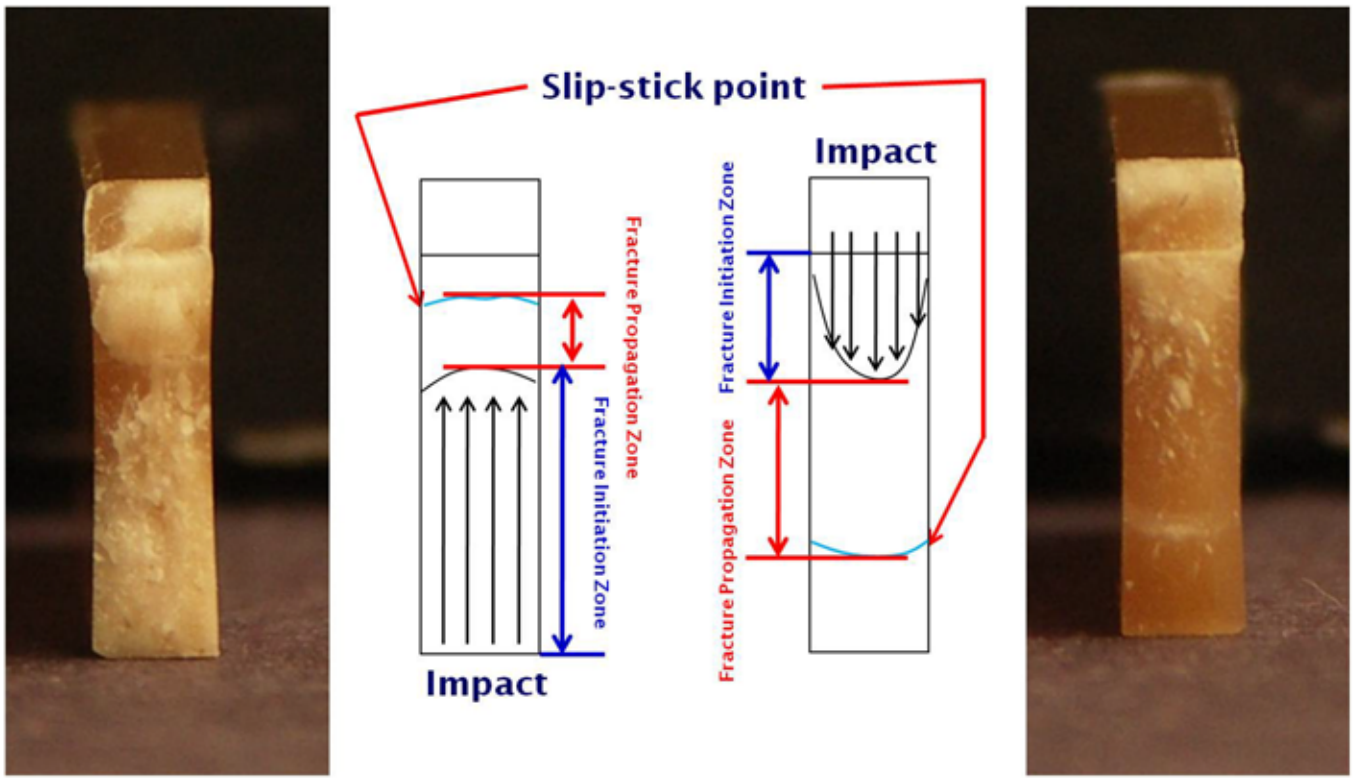

(a) Unnotched sample (b) Notched sample

Fig. 7. Fracture initiation and propagation zone of notched and unnotched Izod impact samples (3 wt.% of filler loading).

It also has been found that the length of the fracture initiation zone is directly proportional to fracture initiation resistance of the composite samples as filler loading increases. Therefore, the relationship between fracture initiation zone length and fracture initiation resistance can be established using a regression function as shown in **Fig. 8**. Among the possible regression functions, a single exponential 3 parameter function provided the best fit with the empirical data. By drawing a regression line at the fracture initiation zone length of 0 that intersects with the y axis (fracture initiation resistance) of the graph, although this extreme situation will never happen in real applications, which imaginably means no energy was consumed to initiate impact fracture, but all impact energy was consumed to propagate fracture. This is the boundary condition and the y intercept value can be described as a characteristic fracture propagation resistance as summarized in eq. (1).

$$y = C_1 + a_1 e^{b_1 x} \quad (1)$$

If $x = 0$, $y = C_1 + a_1$ (characteristic fracture propagation resistance)

Where x = fracture initiation zone length (m), y = fracture initiation resistance (kJ/m^2) and C_1, a_1, b_1 = constants calculated by regression. The regression functions including C_1, a_1 and b_1 values are as follows;

$y = 6.55 + 0.03e^{(1050.75x)}$ $R^2 = 0.9986$ (CNF-PP)

$y = 1.28 + 0.08e^{(919.32x)}$ $R^2 = 0.9967$ (MFC-PP)

$y = -16.87 + 1.55e^{(549.96x)}$ $R^2 = 0.9963$ (MCC-PP)

In the case of $x = 0$, $y = 6.58$ (CNF-PP), 1.36 (MFC-PP) and -15.32 (MCC-PP). The minus value of characteristic fracture propagation resistance in the MCC-PP composite sample means that there is no resistance during fracture propagation in the boundary condition. This is a unique characteristic when the material is at the boundary condition and CNF- and MFC-filled PP composites are more resistant than MCC-PP in terms of characteristic fracture propagation resistance. For example, if all impact energy is consumed to propagate fracture, the largest energy will be required in the CNF-PP composite samples while the MCC-PP samples will require no energy which means just brittle fracture will occur.

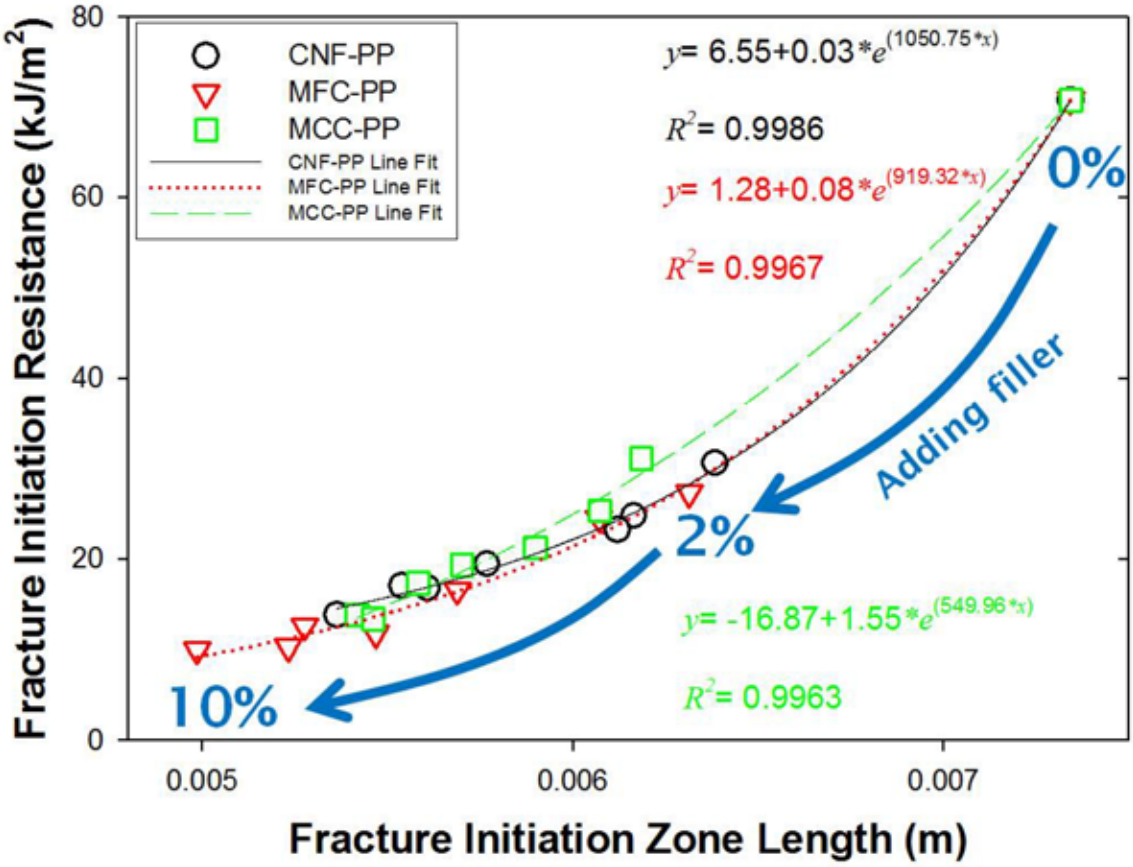

Fig. 8. Relationship between fracture initiation zone length and fracture initiation resistance.

On the other hand, the length of the fracture propagation zone was inversely proportional to fracture initiation resistance of the composite samples as filler loading increased. Therefore, the relationship between fracture propagation zone length and fracture initiation resistance can be established as shown in **Fig. 9**. By drawing a regression line at the fracture propagation zone length of 0 that intersects with the y axis (fracture initiation resistance) of the graph which imaginably means all energy was consumed to initiate impact fracture but no energy was consumed to propagate fracture. This is another boundary condition and the y intercept value can be described as a characteristic fracture initiation resistance in eq. (2).

$$y = C_2 + a_2 e^{-b_2 x} \qquad (2)$$

If $x = 0$, $y = C_2 + a_2$ (characteristic fracture initiation resistance)

Where x = fracture propagation zone length (m), y = fracture initiation resistance (kJ/m^2) and C_2, a_2, b_2 = constants calculated by regression. The regression functions including C_2, a_2 and b_2 values are as follows;

$y = 9.24 + 165.10e^{(-1176.28x)}$ $R^2 = 0.9963$ (CNF-PP)
$y = 3.11 + 154.55e^{(-986.29x)}$ $R^2 = 0.9975$ (MFC-PP)
$y = -0.09 + 146.27e^{(-863.68x)}$ $R^2 = 0.9948$ (MCC-PP)

In the case of $x = 0$, $y = 176.34$ (CNF-PP), 157.66 (MFC-PP) and 146.18 (MCC-PP). This is a unique characteristic when the material is in the boundary condition, for example, if all energy is consumed to initiate fracture, the largest energy will be required in the CNF-PP composite samples while the MCC-PP samples will require the smallest amount of energy. This result is different from **Fig. 5** where fracture initiation resistance of CNF, MCC- filled PP composites is higher than MFC-PP composites. This means that the apparent values such as impact strength and fracture initiation resistance are not the only tool to evaluate a material's unique characteristics when the material is in extreme/boundary conditions.

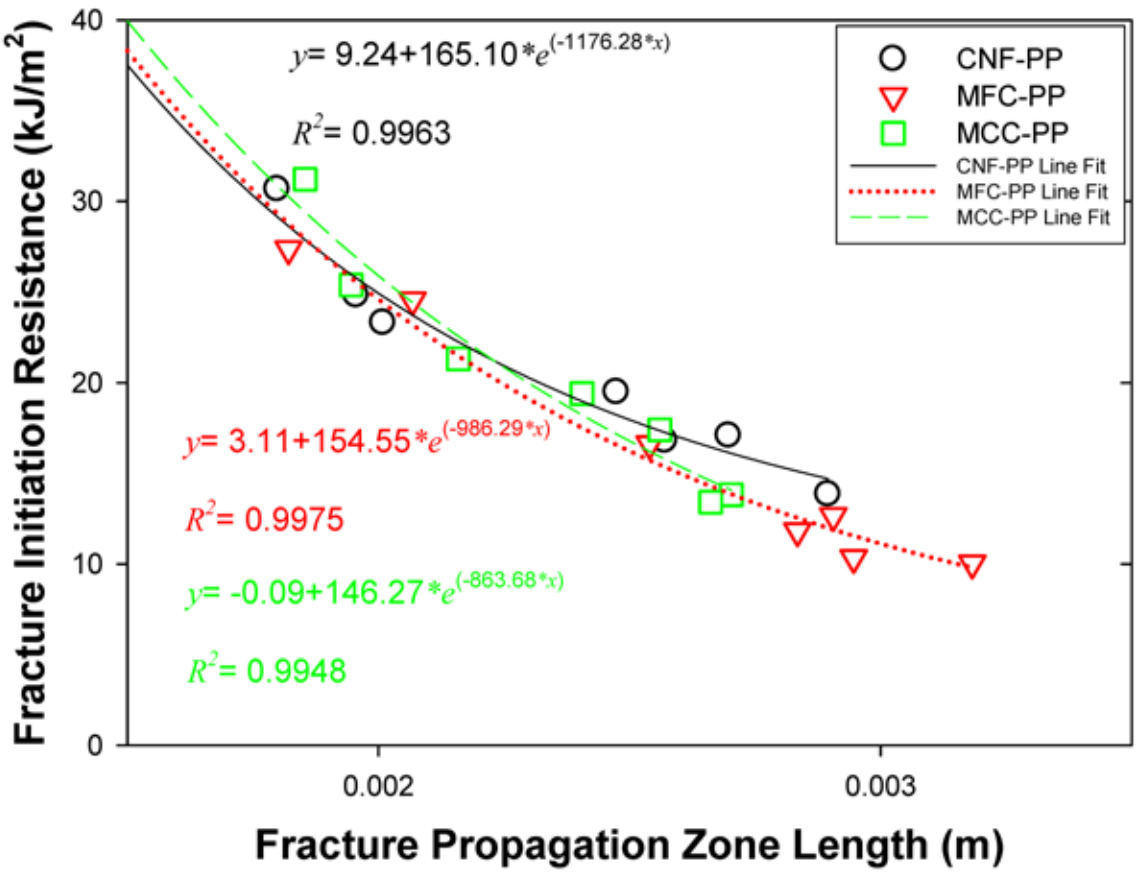

Fig. 9. Relationship between fracture propagation zone length and fracture initiation resistance.

There are two possible scenarios comparing two different materials in terms of impact resistance as shown in **Fig. 10**. In case 1, both fracture initiation resistance and characteristic fracture propagation resistance of material A are better than material B, therefore material A is recommended. Meanwhile in case 2, fracture initiation resistance of material A is higher than material B, but in terms of characteristic fracture propagation resistance, material B is better than material A. This means that once fracture is initiated, material B is more resistant than material A. Material A in case 2 applies to MCC-PP and material B applies to CNF-PP and MFC-PP in this study. Considering all the possible end user environments, it is important for structural designers or material manufacturers to understand the practical implications of impact behavior depending on the specific applications, and also, will be helpful to determine proper materials to be utilized. The characteristic impact resistance model will be a new and valuable analysis tool to investigate unique characteristics of nanocomposite materials.

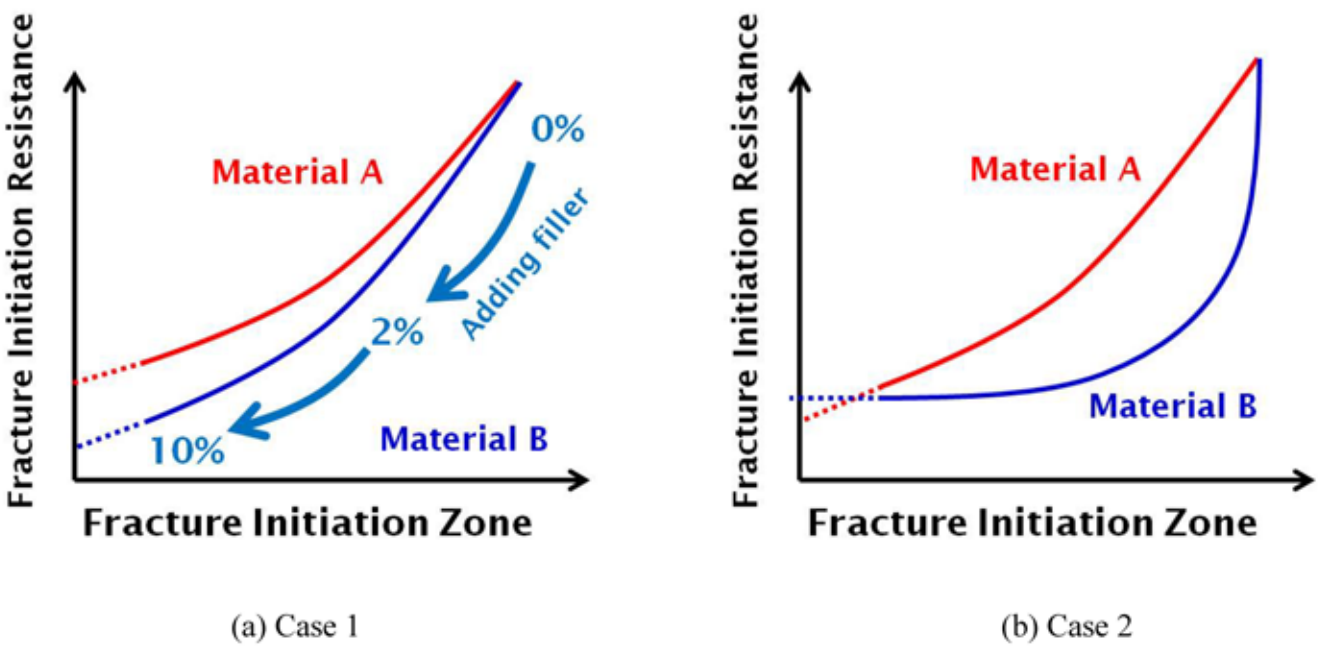

Fig. 10. Case study of two different materials using characteristic impact resistance model.

CONCLUSIONS

CNF was found to offer better impact strength and resistance than MCC as the filler loading increased, which was attributed to the larger size of the MCC. The impact properties were affected by the crack initiation and crack propagation mechanism between the filler and the matrix polymer. The unnotched Izod impact energy was considerably larger than the notched Izod impact energy, and this was due to the different fracture processes involved in the notched and unnotched Izod impact samples. It was found that the impact modified PP used in this study was more fracture resistant while more crack sensitive than conventional PP. CNF and MCC-filled composites showed higher impact resistance than MFC-filled composites as filler loading increased but CNF and MFC-filled composites showed higher characteristic impact resistance than MCC-filled ones. It was found that both impact resistance and characteristic impact resistance are tools to describe a material's unique impact characteristics.

ACKNOWLEDGEMENT

Funding for this research was provided by the National Science Foundation under Grant No. EPS-05-54545 and the US Army W912HZ-07-2-0013.

LITERATURE CITED

Alemdar, A. and M. Sain. 2008. Biocomposites from Wheat Straw Nanofibers: Morphology, Thermal and Mechanical Properties. Composites Science and Technology 68(2): 557-565.

Bledzki, A. K., A. Jaszkiewicz and D. Scherzer. 2009. Mechanical Properties of PLA Composites with Man-made Cellulose and Abaca Fibres. Composites: Part A 40(4):404-412.

Hristov, V. N., R. Lach and W. Grellmann. 2004. Impact fracture behavior of modified polypropylene/wood fiber composites. Polymer Testing 23(5): 581-589.

Manchado, M. A. L., J. Biagiotti, L. Torre and J. M. Kenny. 2000. Effects of Reinforcing Fibers on the Crystallization of Polypropylene. Polymer Engineering and Science 40(10): 2194-2204.

Mi, Y., X. Chen and Q. Guo. 1997. Bamboo Fiber-reinforced Polypropylene Composites: Crystallization and Interfacial Morphology. Journal of Applied Polymer Science 64(7): 1267-1273.

Oksman. K. and C. Clemons. 1998. Mechanical Properties and Morphology of Impact Modified Polypropylene-Wood Flour Composites. Journal of Applied Polymer Science 67(9): 1503-1513.

Stark, N. M. and R. E. Rowlands. 2003. Effects of Wood Fiber Characteristics on Mechanical Properties of Wood/Polypropylene Composites. Wood and Fiber Science 35(2): 167-174.

Svoboda, P., C. Zeng, H. Wang, L. J. Lee and D. L. Tomasko. 2002. Morphology and Mechanical Properties of Polypropylene/Organoclay Nanocomposites. Journal of Applied Polymer Science 85(7): 1562-1570.

Yang, H. S., H. J. Kim J. Son, H. J. Park, B. J. Lee and T. S. Hwang. 2004. Rice-husk Flour Filled Polypropylene Composites; Mechanical and Morphological Study. Composite

Structures 63(3-4): 305-312.

Yang, H. S., H. J. Kim, H. J. Park, B. J. Lee and T. S. Hwang. 2006a. Water Absorption Behavior and Mechanical Properties of Lignocellulosic Filler-Polyolefin Bio-Composites. Composite Structures 72(4): 429-437.

Yang, H. S., M. P. Wolcott, H. S. Kim, S. Kim and H. J. Kim. 2006b. Properties of Lignocellulosic Material Filled Polypropylene Bio-Composites Made with Different Manufacturing Processes. Polymer Testing 25(5): 668-676.

Yang, H. S., H. J. Kim, H. J. Park, B. J. Lee and T. S. Hwang. 2007a. Effect of Compatibilizing Agents on Rice-Husk Flour Reinforced Polypropylene Composites. Composite Structures 77(1): 45-55.

Yang, H. S., M. P. Wolcott, H. S. Kim, S. Kim and H. J. Kim. 2007b. Effect of Different Compatibilizing Agents on the Mechanical Properties of Lignocellulosic Material Filled Polyethylene Bio-composites. Composite Structures 79(3): 369-375.

Yuan, Q., D. Wu, J. Gotama and S. Bateman. 2008. Wood Fiber Reinforced Polyethylene and Polypropylene Composites with High Modulus and Impact Strength. Journal of Thermoplastic Composite Materials 21(3): 195-208.

Zhang, J., S. Wang, L. Lu, D. Li and X. Yang. 2003. Preparation and Performance of High-Impact Polystyrene (HIPS)/Nano-TiO_2 Nanocomposites. Journal of Applied Polymer Science 87(3):381-385.

Zhang, Q. X., Z. Z. Yu, X. L. Xie and Y. W. Mai. 2004. Crystallization and Impact Energy of Polypropylene/CaCO3 Nanocomposites with Nonionic Modifier. Polymer 45(17): 5985–5994.

Zugenmaier, P. 2006. Materials of Cellulose Derivatives and Fiber-reinforced Cellulose–polypropylene Composites: Characterization and Application. Pure and Applied Chemistry 78(10): 1843-1855.

Synthesis of Hybrid Porous Cellulose/Metal Nanocomposites

Tao Wang, Research Assistant Professor
Center for Nano Science and Technology and Department of Electrical Engineering
University of Notre Dame, Notre Dame, Indiana

Zhiyong Cai, Supervisory Research Materials Engineer
Forest Products Laboratory, Madison, Wisconsin

Abhijit Biswas, Research Associate Professor
Center for Nano Science and Technology and Department of Electrical Engineering
University of Notre Dame, Notre Dame, Indiana

Lei Liu, Research Assistant Professor
Advanced Diagnostics and Therapeutics and Department of Electrical Engineering
University of Notre Dame, Notre Dame, Indiana

Abstract

Highly porous metals with millimeter-sized cellular structures have found a broad range of applications from energy absorption to machine construction due to their interesting combinations of physical/mechanical properties, structural morphology, and low densities. However, the mechanical properties of these metals scale adversely with the relative density, and therefore the porous materials retain only a fraction of the bulk values. Recent studies on nanoporous metallic materials have revealed a dramatic improvement in mechanical properties, such as yield strength, as the dimensions of the pores approach submicron to nanometer range. These encouraging results point to a promising approach to bridge the gap between high strength and high porosity. The reason for this enhancement is attributed to the significant size effect of the nanoscale ligament in addition to the relative density. Nevertheless, the implementation of such a material is severely hampered due to critical challenges in search of viable manufacturing routes and materials. By using celluloses nanofibers, we aim to design and synthesize hybrid porous cellulose/metal nanocomposite materials with proper metallization processes. In this presentation, we will report our initial results in the construction of three-dimensional (3D) microfibrillated cellulose nanocomposites and their potential applications in terahertz devices. Our future work will focus on investigation of conformal synthesis of 3D porous nanocomposites.

Acknowledgments

The authors thank the Center for Nano Science and Technology at the University of Notre Dame for financial support and Dr. Alexandru S. Biris for providing scanning electron microscopy (SEM) and atomic force microscopy (AFM) characterization.

Introduction

The pursuit for materials that have versatile functionalities but are yet strong and lightweight has long been a dream of material scientists and engineers. Bulk materials, which have been used since the advent of human activities, almost reach their ends in this context unless a dramatically transformative category of materials is discovered. Instead, a logical alternative is to intelligently engineer porous or cellular materials into a new class whose properties can be well tailored to meet various high-performance needs at very low relative densities. During the past several decades, such a class of material has received much attention due to the combination of functionalities and mechanical properties that it displays, and it has been used in a variety of applications ranging from structural components to functional devices that show interesting combinations of physical/mechanical properties, structural morphology, and lightweightness (Banhart 2001). However, extensive experimental work has concluded that the retained mechanical properties scale adversely by following Gibson and Ashby's theory, which suggests that mechanical properties (e.g., Young's modulus or tensile strength) of the porous metals retain only a fraction of the bulk values (Gibson and Ashby 1999).

In the past few years, nanostructured three-dimensional (3D) metallic foams with much smaller pore dimensions have become a hot research topic. Recent developments include materials made of noble metals such as gold (Au), silver (Ag), and platinum (Pt) (Biener and others 2005, Biener and others 2006, Hodge and others 2007). Inspired by the localized electrochemical corrosion phenomenon occurring with an alloy, the controlled process can be favorably exploited to produce nanoporous metals. This process is called dealloying, which is adopted, for example, to generate Au nanofoams from an initial binary Au–Ag alloy. Surprisingly, mechanical property tests reveal values of the yield stresses

that are significantly higher than that of bulk Au. Furthermore, as the ligament size becomes smaller (i.e., 10 nm), the yield stress approaches the theoretical limit (Biener and others 2005, Biener and others 2006). These findings seem contradictory to the previously described, widely accepted Gibson and Ashby predication, making it necessary to re-evaluate the factors (besides relative density) that determine the strength value at nanometer length scale (Hodge and others 2007). Overall, this research area is in its early infancy. There remain several bottlenecks in understanding such a class of material, and the implementation of such a material is also severely hampered due to critical challenges in the course of further development. One key challenge lies in the synthesis processes, among which dealloying (preferentially etching one element from a binary alloy) is dominant. Another challenge is the availability of viable materials, which are generally limited to noble metals such as Au, Ag, and Pt. None of these is economically preferred for structural applications and other functional situations. Thus, exploration of both new materials and effective synthesis routes are critical to bringing these materials to real-world applications.

Interest in cellulose-based porous nanomaterials has recently received a great boost, not only because the cellulose microfibrils or nanofibers themselves possess excellent tensile properties and modulus, but also because their substantial tunabilities offer enormous potential for creating new hybrid functional nanomaterials. For example, nanofiber networks were used either as constituents or templates to synthesize new functional materials for magnetic aerogels and stiff magnetic nanopaper (Olsson and others 2010), cell regeneration (Barreiro and others 2010), nanoparticle synthesis (Ifuku and others 2009), electrically conducting flexible aerogels (Paakko and others 2008), gas sensor (Huang and others 2005), and catalysis (Shigapov and others 2001). We envision that a combination of atomic-level material deposition with properly designed 3D cellulose nanofiber networks will lead to a new fabrication route toward novel nanocomposites at a true nanoscale and will also enhance the diversity of component metals and alloys. As an initial step, we report our preliminary studies on synthesis of nanocomposites consisting of cellulose nanofibers and magnetic nanoparticles as well as their potential applications in terahertz devices. Our future work will focus on investigation of conformal synthesis of 3D porous nanocomposites.

Experimental

The cellulosic nanofibers were generated through a microfluidizer processor, which is essentially a specialized homogenizer and forces liquid streams through microchannels at extremely high shear rates, resulting in a size reduction of particles in the liquid stream. In this study, eucalyptus (*Eucalyptus grandis, E. amplifolia*) fibers were enzymatically treated to convert some cellulose into fermentable sugars for ethanol production. The remaining coarse fibers were then passed through the microfluidizer until they were reduced to primarily nanofibers. The particles used are silica-encapsulated magnetic oxide Fe_3O_4 nanoparticles with controlled dimensions, which were synthesized following the microemlusion procedure described in Ifuku and others (2009). The nanocomposite samples were prepared by a simple drop-cast method by mixing the nanofibers and particles and subsequently sonicating and coating to a microscope slide. This is followed by baking at 50 °C on a hot plate overnight. As a comparison, the fibers alone were also coated the same way in the absence of magnetite nanoparticles.

Scanning electron microscopy (SEM) was carried out by a JEOL JSM-7000F (JEOL Ltd., Tokyo, Japan) equipped with a field emission gun. Prior to SEM observations, the specimens were coated with thin layers (less than 1 nm) of carbon. Atomic force microscopy (AFM) was performed with Digital Instruments (Veeco) Dimension-3100 (Digital Instruments Veeco Metrology Group, Plainview, New York) under tapping mode. Both the height images and the amplitude images were collected simultaneously. Surface morphology studies were performed by using a SPI Dimension 3100 atomic force microscope that uses standard and advanced scanning probe microscopy (SPM) imaging modes to measure surface characteristics. The terahertz transmission spectroscopy of the cellulose and its composite films was performed on a system consisting of a frequency extension module covering 0.57–0.63 THz and a Schottky diode-based THz detector.

Results and Discussions

Figure 1 shows both SEM images of a sample without magnetite nanoparticles and a nanocomposite sample. It can be clearly seen that a porous cellulosic nanofiber network is present in the nanofiber-alone coating (Fig. 1(a)). When magnetite nanoparticles are added, two distinct regions are observed: one is an aggregated area of nanoparticles (Fig. 1(b)) and another is a networked area of nanofibers (inset of Fig. 1(b)) similar to that in Fig. 1(a). This indicates a phenomenon commonly encountered in particle nanocomposites. The morphological features of the two samples from AFM measurements are shown in Figure 2. It is readily evidenced that the interwoven networks are formed with long cellulose fibers with diameters between 16 and 25 nm (Fig. 2(a)). The phase separation of the particle-enriched region and nanofiber region is also seen in the AFM image (Fig. 2(b)) of the nanocomposite. From the amplitude image, the diameter of the core-shell nanoparticle shown by a pair of red arrows is determined to be 21 nm, but the actual size is slightly smaller due to apex of the AFM tip.

Both the SEM and AFM analyses seem to suggest that the simple preparation procedure yielded a nonuniform but less porous nanofiber matrix. However, the heterogeneous dispersion of the nanoparticles is detrimental to the integrity of the resultant composites and therefore limits the mechanical loading, adhesion, and local magnetic performances. To overcome such a problem, several chemical modification

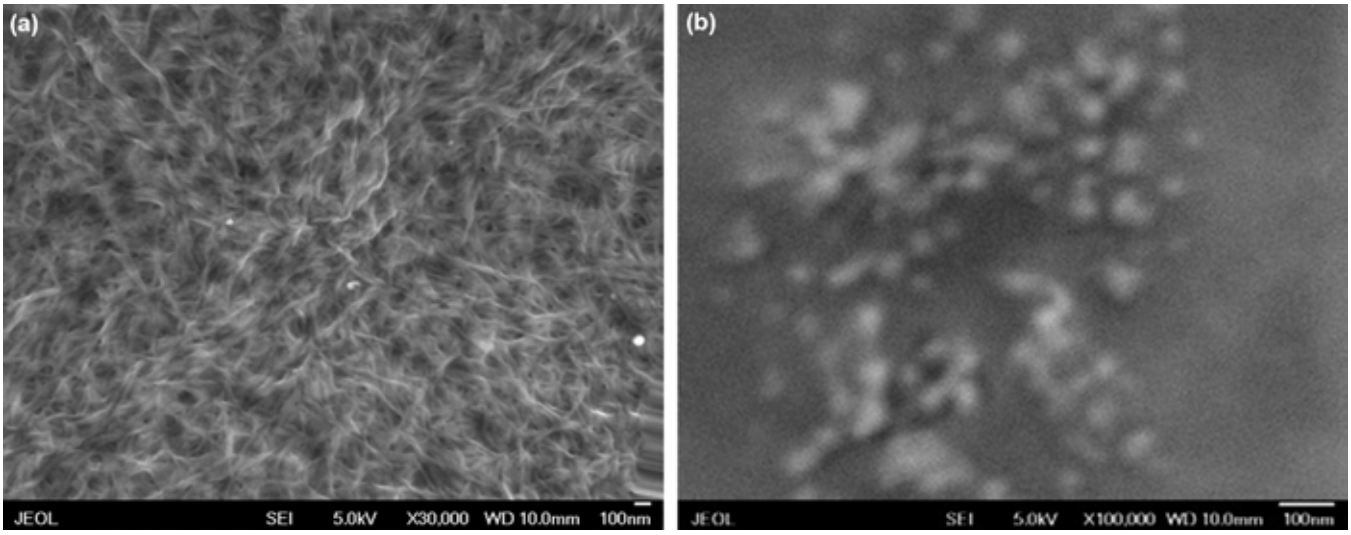

Figure 1. SEM images showing (a) porous cellulosic nanofiber network morphology of the sample without magnetite nanoparticles and (b) magnetite nanoparticles in the nanocomposite sample.

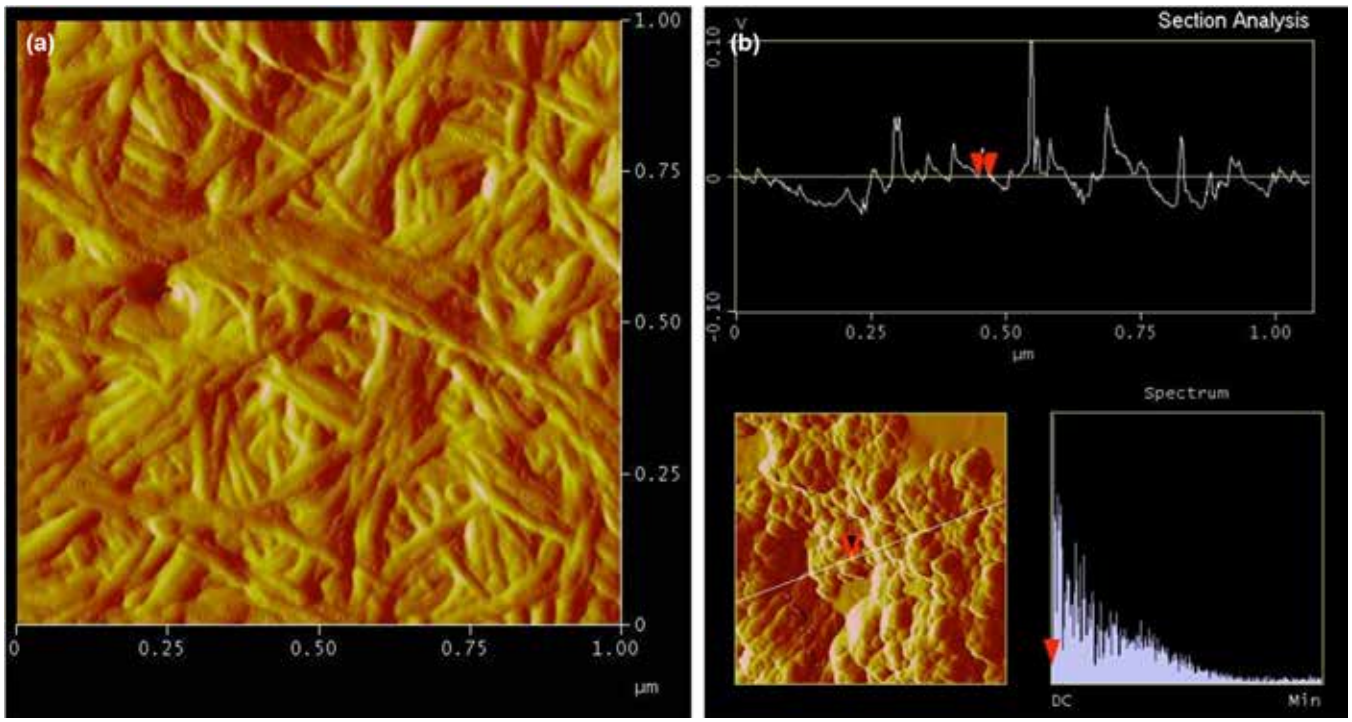

Figure 2. AFM images showing morphology of (a) interwoven network of 16–25-nm-diameter cellulosic nanofibers in the sample without nanoparticles and (b) magnetite nanoparticles in the nanocomposite sample.

mechanisms using coupling agents, such as organosilanes (Paakko and others 2008) and aminopropyl-triethoxylsilane (APTES) (Huang and others 2005), have been explored to modify the interfacial behaviors of the dispersoids and matrices. Because both surfaces of the cellulosic fiber and the silica shell present hydroxyl groups in our system, we will address this issue by investigating and establishing an optimal silanization protocol to achieve not only strong covalent interfacial bonding but also improved particle dispersion.

The THz transmission spectroscopy system (0.57–0.63 THz) was applied to characterize cellulose samples shown in Figure 3. The nanocomposite samples under examination are prepared by dropping and drying liquids on 3-mil Mylar thin films, and the measured data are normalized to the voltage response of the blank Mylar thin film measured using this system for THz transmission. Shown in Figure 3(b) is the THz spectrum of one cellulose sample in the frequency range of 0.57–0.63 THz. Stronger absorption is observed

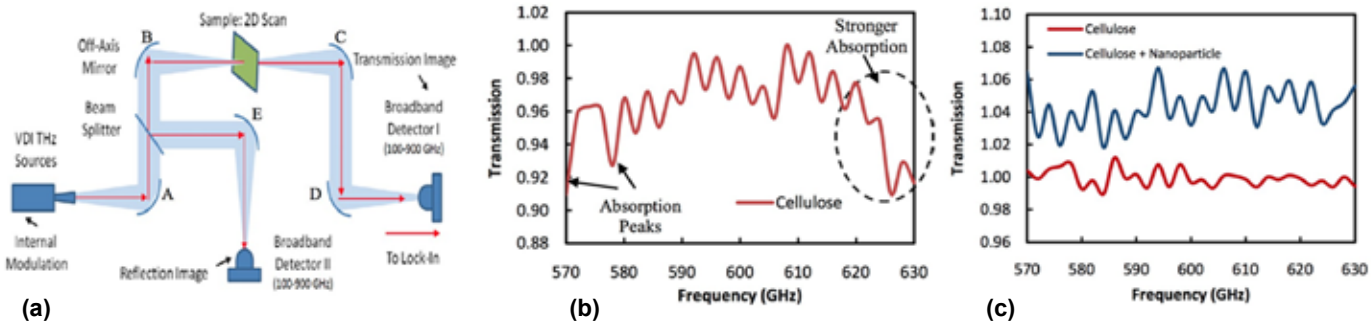

Figure 3. THz transmission spectroscopy of the resultant nanocomposites at 0.57–0.63 THz: (a) configuration of the solid state frequency domain THz system based on quasi-optical, ultra-broadband, Schottky diode detector—system diagram; (b) THz transmission spectrum of cellulose sample, narrow absorption features have been observed; and, (c) THz transmission comparison of cellulose sample and cellulose with magnetic nanoparticles. Enhanced THz transmission is observed for cellulose with nanoparticles sample.

at 0.62–0.63 THz, 0.57 THz, and 0.58 THz. The absorption peaks show narrow frequency bandwidths less than 0.01 THz. These spectral features are difficult to be discovered using conventional time-domain THz techniques and could be used for characterization and identification of cellulose samples. The THz spectrum of cellulose samples with nanoparticles was also measured and compared to cellulose samples under the same preparation conditions, as shown in Figure 3(c). The sample with nanoparticles shows higher transmission than the sample without. In addition, the transmission of the magnetic nanoparticles sample is larger than the one over the entire frequency range of 0.57–0.63 THz, indicating a field enhancement. This property may find applications in THz-based chemical and biological sensing.

Summary

A nanocomposite was prepared by co-deposition of cellulosic nanofibers and core-shell magnetic Fe_3O_4-silica nanoparticles. While a fine interwoven network of the nanofibers is formed, there exist regions where the particles are aggregated. Our future work will focus on developing an optimized silanization protocol to create covalent interfacial bonding and homogenous particle dispersion and evaluating the resultant nanocomposites in magnetic, mechanical, and thermal performances. The THz transmission spectroscopy examination of the nanocomposite films from 0.57 to 0.63 THz suggests strong absorption peaks and enhancement of intensity due to incorporation of magnetic nanoparticles. This may indicate potential usefulness of this cellulose nanocomposite in chemical and biological sensing. Our future work will focus on investigation of conformal synthesis of 3D porous nanocomposites.

References

Banhart, J. 2001. Manufacture, characterisation and application of cellular metals and metal foams. Progress in Materials Science. 46(6): 559–U3.

Barreiro, A.M.; Recouvreux, D.O.S.; Hotza, D.; Porto, L.M.; Rambo, C.R. 2010. Sand dollar skeleton as templates for bacterial cellulose coating and apatite precipitation. Journal of Materials Science. 45(19): 5252–5256.

Biener, J.; Hodge, A.M.; Hamza, A.V.; Hsiung, L.M.; Satcher, J.H. 2005. Nanoporous Au: a high yield strength material. Journal of Applied Physics. 97(2): January 15.

Biener, J.; Hodge, A.M.; Hayes, J.R.; Volkert, C.A.; Zepeda-Ruiz, L.A.; Hamza, A.V.; Abraham, F.F. 2006. Size effects on the mechanical behavior of nanoporous Au. Nano Letters. 6(10): 2379–2382.

Gibson, L.J.; Ashby, M.F. 1999. Cellular solids: structure and properties. 2nd ed. Cambridge, UK: Cambridge University Press.

Hodge, A.M.; Biener, J.; Hayes, J.R.; Bythrow, P.M.; Volkert, C.A.; Hamza, A.V. 2007. Scaling equation for yield strength of nanoporous open-cell foams. Acta Materialia. 55(4): 1343–1349.

Huang, J.; Matsunaga, N.; Shimanoe, K.; Yamazoe, N.; Kunitake, T. 2005. Nanotubular SnO_2 templated by cellulose fibers: synthesis and gas sensing. Chemistry of Materials. 17(13): 3513–3518.

Ifuku, S.; Tsuji, M.; Morimoto, M.; Saimoto, H.; Yano, H. 2009. Synthesis of silver nanoparticles templated by TEMPO-mediated oxidized bacterial cellulose nanofibers. Biomacromolecules. 10(9): 2714–2717.

Olsson, R.T.; Samir, M.A.S.A.; Salazar-Alvarez, G.; Strom, V.; Belova, L.; Berglund, L.A.; Ikkala, O.; Nogues, J.; Gedde, U.W. 2010. Making flexible magnetic aerogels and stiff magnetic nanopaper using cellulose nanofibrils as templates. Nature Nanotechnology. 5(8): 584–588.

Paakko, M.; Vapaavuori, J.; Silvennoinen, R.; Kosonen, H.; Ankerfors, M.; Lindstrom, T.; Berglund, L.A.; Ikkala, O. 2008. Long and entangled native cellulose I nanofibers

allow flexible aerogels and hierarchically porous templates for functionalities. Soft Matter. 4(12): 2492–2499.

Shigapov, A.N.; Graham, G.W.; McCabe, R.W.; Plummer, H.K. 2001. The preparation of high-surface area, thermally-stable, metal-oxide catalysts and supports by a cellulose templating approach. Applied Catalysis A: General. 210 (1–2): 287–300.

An investigation into the mechanical behaviour of surface-modified fibrillated cellulose reinforced composites

M.Sc. Bulota M.*, M.Sc. Hänninen T., Dr. Jääskeläinen A.-S., Dr. Kontturi E., Prof. Hughes M.

Aalto University, School of Chemical Technology, Department of Forest Products Technology
*mindaugas.bulota@aalto.fi

Abstract

Because of its abundance, as well as its high stiffness, cellulose has been recognised as having huge potential in the production of environmentally friendly composite materials. Although research on cellulose reinforced composites has advanced rapidly over the last decade or so (Azizi et al. 2005, Eichhorn et al 2010), there is a need for further investigation into the mechanical behaviour of these materials. Despite the fact that the molecule of interest - cellulose - is the same, there is a significant amount of variation in its reinforcing capabilities resulting from the raw material, the preparation methods, chemical treatments, etc. A well-known property of cellulose is its ability to form stable water suspensions and this has been utilized in the production of composites. However the reinforcement of hydrophobic polymers has been limited due to the hydrophilic nature of cellulose.

In the present study TEMPO-oxidized cellulose fibrils (TOCF), prepared from bleached birch pulp, were used to reinforce poly(lactic) acid (PLA). Acetylation, using acetic anhydride in dimethylformamide (DMF), was carried out in order to facilitate dispersion of the TOFC in a non-polar solvent (chloroform) in which the PLA was dissolved. The degree of acetylation was evaluated by FT-IR spectroscopy. Composites were prepared by solvent casting from a solution of PLA in chloroform containing up to 10 wt% load of acetylated TOFC. The resulting composites had a thickness of approximately 80 μm and were tested in tension according to ISO 527:1996. Further investigation was undertaken with Raman spectroscopy as well as with scanning electron microscopy.

The acetylated TOCF showed significantly improved dispersion in non-polar media, which led to the successful preparation of composite films. The mechanical properties of reinforced PLA exhibited different properties compared to unreinforced PLA. Fracture energy (toughness) was significantly increased at lower weight fractions of TOCF. However, the same effect was not observed at higher weight fractions of reinforcement.

Preparation of composite films

TEMPO-oxidized cellulose fibrils (TOCF) were prepared from bleached birch Kraft pulp according to the method of Saito et al. (Saito et al 2006). After oxidation, the fibrils were stirred in a commercial blender with the addition of deionised water until a transparent gel was formed. The TOCF was solvent exchanged, by two sequential centrifugations at 8000 rpm for 15 min at 20 °C, to and then acetylated. Acetylation took place in a round bottom flask at 105 ± 5 °C for 15 and 120 minutes. Subsequently, acetone was added to wash away the reaction by-products and left overnight, following which the suspension

was solvent exchanged to acetone and from acetone to chloroform. PLA (2002 D Nature Works) was dissolved in chloroform at room temperature and mixed with the acetylated TOCF. The mixture was homogenized and degassed before casting onto a release agent (chemlease 75) treated glass plate. It was kept overnight in a room and finally cured in an oven at 55°C ± 5 for 30 min.

Mechanical testing

Specimens for tensile testing were prepared in accordance with ISO 527:1996. Specimen type 1BA was punched out of the films using a custom made cutting die. There were at least 5 specimens in each group. The thickness of films was up to 100 µm. Specimens were conditioned at +23 °C ± 1 °C and 50 % ± 2 % relative humidity (RH) for at least 72 h before testing. Testing of the composites was performed at a crosshead speed of 20 mm/min.

Results

Dried samples of acetylated and non-acetylated cellulose were investigated using FT-IR spectroscometer FTS 600 (Bio-Rad). The spectra were recorded between 400 cm^{-1} and 4000 cm^{-1}. The results are presented in Figure 1.

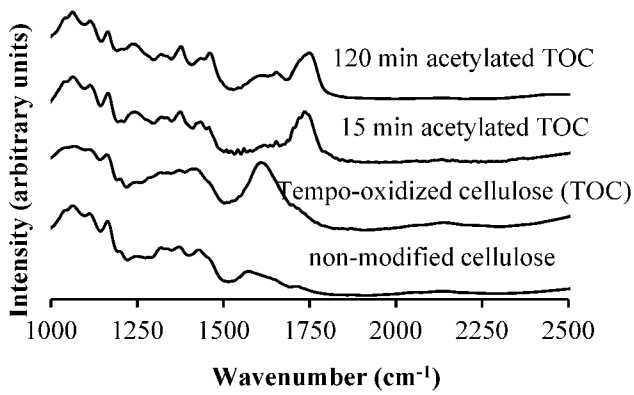

Figure 1.FT-IR spectra of non-modified, tempo-oxidized and acetylated oxidized cellulose.

The tempo-oxidation introduces carboxylic groups on cellulose surface (Saito et al 2007). Therefore the peak in FT-IR spectrum occurs at around 1600 cm^{-1}. It is not visible in the spectrum of the non-modified cellulose. Carboxylic groups are esterified during the acetylation reaction as evanesce of 1600 cm^{-1} peak and appearance of 1750 cm^{-1}peak, corresponding to carbonyl group, indicates. Interestingly the reaction duration did not have a significant effect on the level of acetylation, implying that the accessible hydroxyl groups reacted within the first 15 minutes.

It is known that the dispersion of cellulose in non-polar solvents depends on the degree of substitution (DS) (Tingaut et al. 2010). The dispersion of TOCF was investigated using optical microscopy and Raman spectroscopy, Figure 2.

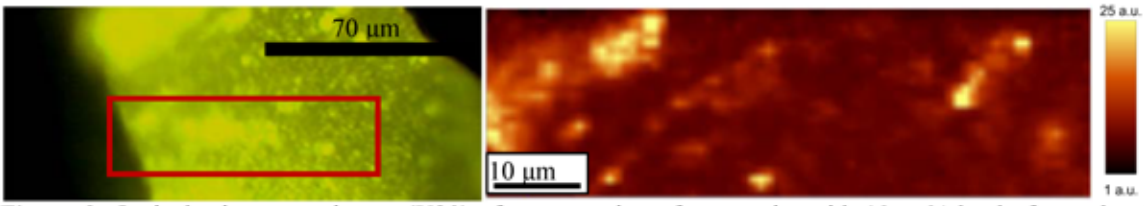

Figure 2. Optical microscope image (X20) of cross-section of composite with 10 wt% load of acetylated TOCF and a Raman map of the area within the rectangular. Scale bar indicates arbitrary intensity units (lighter colour corresponds to higher amount of cellulose).

White areas in the optical image intuitively could be related to cellulose clumps due to aggregation although it could also be other contaminants. The Raman spectra were recorded from the area within the rectangular (Figure 2), at a spacial resolution of 1 µm. The Raman map was constructed by taking the intensity ratio of two distinct peaks: 1095 cm^{-1} corresponding to cellulose and 1130 cm^{-1} corresponding to PLA. The Raman mapping data agrees with the hypothesis that the clumps, visible in the optical microscope image, are cellulose aggregates. However the difference in intensities implies that the PLA matrix impregnated them to a certain extent.

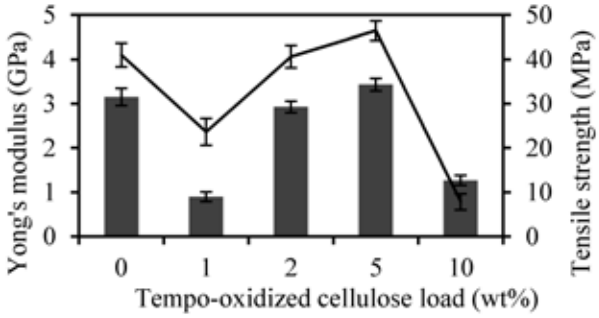

Figure 3. Mechanical properties of composite films reinforced with 15 min acetylated TOCF. Columns represent Young's modulus; curve represents tensile strength. The error bars denotes standard deviation.

The addition of TOCF altered mechanical behaviour of the PLA. The Young's modulus was significantly lower than the unreinforced PLA at 1 wt% load of TOCF. However, with only 2 wt% load the stiffness was comparable with that of pure PLA and at 5 wt% load, a slight (8%) increase in stiffness was observed. At a weight fraction of 10% TOCF the Young's modulus decreased mainly due to the extensive aggregation as shown in Figure 2. The tensile strength followed the similar trend, although exhibiting a somewhat more moderate drop at 1 wt% load in comparison to Young's modulus. The decrease in both Young's modulus and tensile strength was accompanied by large increase in strain to failure and consequently the work of fracture. This is probably due to crazing as extensive "stress whitening" in the test samples was observed.

Conclusions

Tempo-oxidized cellulose reinforced PLA films were successfully prepared. The dispersion of polar cellulose in non-polar chloroform was significantly improved through esterification of the hydrophilic hydroxyl groups. The resultant composites exhibited significantly different mechanical behaviour compared to pure PLA, especially at low weight fractions of reinforcement agent. High values of strain to failure – approx 250%

were observed at low weight fractions of TOFC, although at the expense of strength and stiffness.

Literature cited:

Azizi S. M, A. Said, F. Alloin, and A. Dufresne. 2005. Review of Recent Research into Cellulosic Whiskers, their Properties and their Application in Nanocomposite Field. Biomacromolecules 6:612-26.

Eichhorn, S. J., A. Dufresne, M. Aranguren, N. E. Marcovich, J. R. Capadona, S. J Rowan, C. Weder, W. Thielemans, M. Roman, S. Renneckar, W. Gindl, S. Veigel, J. Keckes, H. Yano, K. Abe, M. Nogi, A. N. Nakagaito, A. Mangalam, J. Simonsen, A. S. Benight. 2010. Review: Current International Research into Cellulose Nanofibres and Nanocomposites. *Journal of Materials Science* 45:1-33.

Saito, T., S. Kimura, Y. Nishiyama and A. Isogai. 2007. Cellulose nanofibers prepared by TEMPOmediated oxidation of native cellulose. *Biomacromolecules* 8:2485.

Saito, T., Y. Nishiyama, J. L. Putaux, M. Vignon and A. Isogai. 2006. Homogeneous suspensions of individualized microfibrils from TEMPO-catalyzed oxidation of native cellulose. Biomacromolecules 7:1687.

Tingaut P., T. Zimmermann and F. Lopez-Suevos. 2010. Synthesis and Characterization of Bionanocomposites with Tunable Properties from Poly(Lactic Acid) and Acetylated Microfibrillated Cellulose. *Biomacromolecules* 11:454-64.

Production and Characterization of Nano-Structured Carbons from Pine Chips

Qiangu Yan, Postdoctoral Research Associate
Department of Agricultural and Biological Engineering, Mississippi State University, Mississippi State, Mississippi

Hossein Toghiani, Associate Professor
Dave C. Swalm School of Chemical Engineering, Mississippi State University, Mississippi State, Mississippi

Fei Yu, Assistant Professor
Department of Agricultural and Biological Engineering, Mississippi State University, Mississippi State, Mississippi

Zhiyong Cai, Supervisory Research Materials Engineer
Forest Products Laboratory, Madison, Wisconsin

Jilei Zhang, Professor
Forest Products Laboratory, Mississippi State University, Mississippi State, Mississippi

Abstract

This study investigated the influences of temperature, heating rate, purge gas type, and flow rate on the production of nano-structured carbons from southern pine wood chips by pyrolysis. Pyrolysis temperatures were between 450 and 1,000 °C with heating rates of 1.0, 10, and 50 °C/min. The purge gases were nitrogen and hydrogen with flow from 100 to 1,000 mL/min. The surface morphology of pine chars was characterized using scanning electron microscopy (SEM) and transmission electron microscopy (TEM). SEM analyses indicated that the surface of pine chips had already started to decompose at 450 °C if nitrogen was used with a flow rate of 500 mL/min, but no nanoparticles were formed. The formation of sphere nanoparticles with a diameter from 50 to 100 nm was observed at 650 °C. More nanoparticles were produced as pyrolysis temperature increased to 1,000 °C, and the particle diameter in the surface was around 20 nm. Pine chars produced with nitrogen gas showed more nanoparticles on the char surface than those with hydrogen. The surface of the pine chars had fewer particles with increased purge gas flow. The particle quantity was increased at higher heating rates. Nano carbon spheres, nano carbon chips, carbon nanofibers, carbon nanotubes, some porous carbon particles, and micro-pores and channels were observed from the chars produced at 1,000 °C.

Introduction

Driven by the shortage of crude oil and environmental concern, research efforts have been made to develop new processes for converting renewable biomass to energy. The biofuels can be achieved from biomass through thermal degradation and biological processes (Kumar and others 2009). Three phases are produced during the thermal transformation of biomass under inert atmosphere: gases, liquids (tars, condensable vapors), and solids (char) (Wampler 2006). The operating conditions such as pyrolysis temperature and heating rate are key factors affecting three phase product fractions (Baumlin and others 2006).

Pyrolysis processes may be conventional or fast pyrolysis, depending on the operating conditions. Conventional slow pyrolysis has been applied for thousands of years, such as for charcoal production (Demirbas 2009). In slow pyrolysis, biomass is heated to 500 °C with vapor residence times ranging from 5 to 30 min. For fast pyrolysis, biomass is rapidly heated in the absence of oxygen. Biomass decomposes to generate vapors, aerosols, and solid char. Fast pyrolysis processes produce 60−75 wt% of liquid bio-oil, 15−25 wt% of solid char, and 10−20 wt% of non-condensable gases (Mohan and others 2006). Carbon content of wood varies from about 47% to 53% due to varying lignin and extractives content (Ragland and Aerts 1991), and 30% to 50% of the carbon in the wood is converted to solid char during the pyrolysis process.

In bio-oil research, most attention has been concentrated on liquid product upgrading and syngas formation and utilization, but the char, an attractive byproduct, has received less attention. Thus far, there is no other value-added use available for this solid residue besides direct combustion for heat production. The synthesis of value-added, carbonaceous nanomaterials from the bio-chars as well as carbon rich and renewable biomass such as wood or agriculture plants can be an attractive option to use carbon resources in a sustainable and "CO_2-neutral" way compared to using fossil resources (Hu and others 2010). Limited studies were found on systematically analyzing the effects of thermal treatment conditions such as temperature, heating rate, purge gas type, and gas flow rate on the surface morphology change of bio-chars produced from biomass and the formation of nanomaterials from these bio-chars. The objective of this study was to investigate the effects of these thermal treatment variables on the formation process of nanomaterials and the surface morphology change of bio-chars pyrolyzed from southern pine clear wood biomass.

The different morphologies and structures of bio-chars can be produced with various operating conditions. Ohata and others (*www.geocities.jp/yasizato/Yoshizawa17.pdf*) heated the sapwood of Hinoki from 400 to 900 °C with a heating rate of 20 °C/min and held it for 120 min at 900 °C. Three nitrogen gas rates of 100, 200, and 1,000 cm^3/min, and three oxygen concentrations of 0.7, 0.3, and 0.06 vol% were investigated. Tube-like carbon fibers were observed on cell walls of the charcoals when the sample was heated at 900 °C in 0.06 vol% of oxygen concentration. It was suggested that cobalt serve as the catalyst and carbon monoxide as the carbon source. Saito and Arima (2002) observed cone-shaped carbon materials inside the cell lumen of pre-heat-treated (300–400 °C) sapwood of Japanese cedar heat-treated at 2,500 °C with argon gas for 1 h. The heating rate, pressure, and cooling rate were 10 °C/min, 10–20 Pa, and 30 °C/min, respectively. There were no carbon particles observed for samples heated less than 2,500 °C.

Carbonized microfibrils and onion-shaped graphitic nanoparticles were observed from 20-year-old Japanese cedar carbonized up to 700 °C for 30 min with a heating rate of 4 °C/min and in an argon gas atmosphere (Hata and others 2000). Onion-like nanoparticles and nano-size pore structures were observed on the surface of Japanese cedar carbonized at 700 °C for 1 h with a heating rate of 10 °C/min (Ishimaru and others 2001). Kurosaki and others (2003) flash-heated the sapwood of Japanese cedar at 800 °C for 1 h and produced well-aligned curved, fragmented, and not-closed graphitic plane carbon structures. But this was not for the slow heating process (in a helium atmosphere at 4 °C /min, gas flow rate 50 mL/min, and pressure 300 kPa) where the cell structure was still maintained. Most particles observed were about 25 nm in diameter, but larger size particles up to 100 nm were also observed, which were elliptical rather than spherical.

It was found that under a high heating rate the biomass char particles underwent plastic deformation (i.e., melted) and developed a structure differing from that of the virgin biomass (Cetin and others 2004). Pressure was also found to influence the physical and chemical structures of char particles. Guerrero and others (2005) characterized the chars from pyrolysis of eucalyptus at different temperatures and heating rates, and the influence of their morphology changes on overall reactivity was investigated. Large internal cavities and a more open structure were observed over the high heating rate char particles. The globular particles with the size of approximately 20 nm were observed in the cell wall sections of sycamore maple heated to 1,100 °C under nitrogen (Herzog and others 2006). After subsequent activation by CO_2 at 900 °C for a dwell time of 0 min, molecular-sized pores with diameters ranging from 3 to 20 nm and particles containing crystallized minerals were observed. There was a fundamental difference in the nanoforms before and after activation. Stacked carbon structures were found in cellulose-rich regions before activation. After activation, additional onion-like, multi-walled clusters were observed.

Hu and others (2008) prepared chars from rice husk at different pyrolysis conditions. Scanning electron microscopy (SEM) images showed that the surface of pores in char particles became increasingly rough in the middle of pyrolysis. Biagini and others (2009) produced the bio-chars from cacao shells and olive cake using a high heating rate and characterized the char morphology after the first step of devolatilization. Different chars were produced in a drop tube reactor by rapid pyrolysis with various nominal temperatures and residence times. It was found that char particle size enlarged at 500–600 °C due to swelling phenomena and bubble formation, and at a higher temperature (800 °C) the final size slightly decreased with respect to the parent material for crack formation and melting of material.

Fu and others (2009) characterized pyrolysis chars from maize stalks with the effects of pyrolysis temperature and heating rate on the char properties investigated. The pyrolysis was performed at atmospheric pressure and temperatures from 600 to 1,000 °C under low and high heating rates. As the temperature increased, maize stalk chars had a slightly less amorphous structure and fewer aliphatic side chains and became more aromatic and ordered. At a high heating rate, progressive increases in porosity development with increasing pyrolysis temperature occurred. The surface area of the chars reached a maximum of 81.6 m^2/g at 900 °C and decreased slightly at a higher temperature. Above 900 °C, structural ordering, pore widening, and/or the coalescence of neighboring pores led to the decrease in the surface area values, resulting in thermal deactivation of the chars. The influence of the heating rate on the surface area was not significant.

Material and Methods

Materials and Heating Device

The southern pine wood chips (>1 mm in length) were dried on an onsite dryer with a maximum moisture content of 10%. Pyrolysis of the pine chips was carried out in a fixed-bed tubular quartz reactor with an outer diameter of 25.4 mm and a length of 120 cm (Fig. 1). A K-type thermocouple was placed inside the tube and embedded in the wood chip sample to monitor the temperature. For each experimental run, 15 g of pine chips (Fig. 2) were packed in the middle of a 25.4-mm O.D. quartz tubular reactor.

Experimental Design

Temperature effect on the morphology of the pine chars was studied at five temperatures (450, 500, 550, 650, and 1,000 °C) with a nitrogen flow under atmosphere pressure.

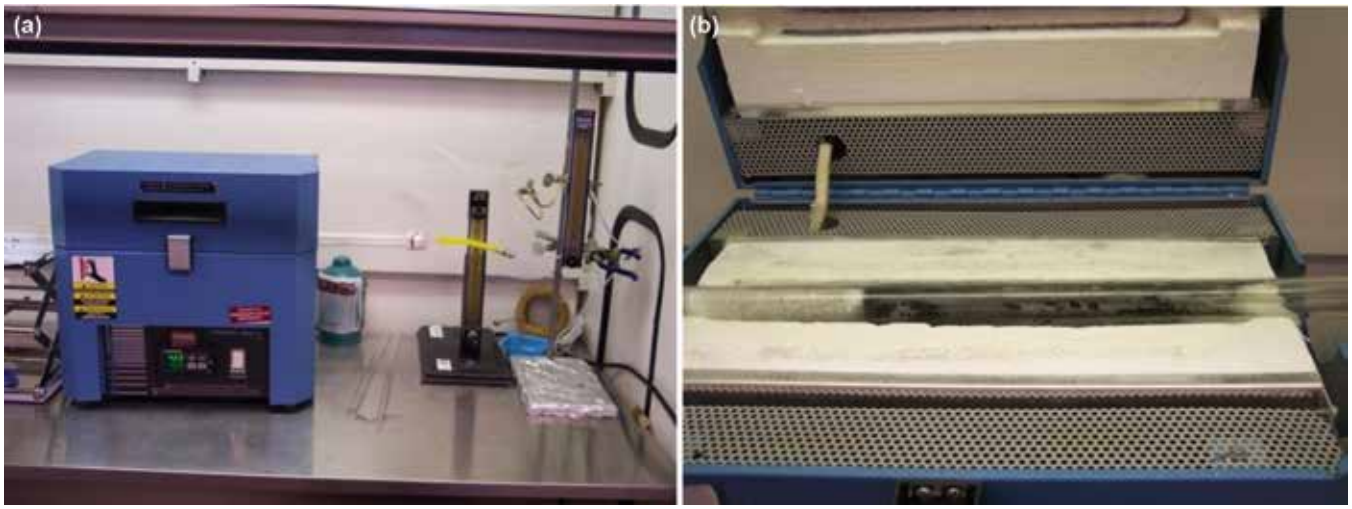

Figure 1. Thermal reaction system (a) and 25.4-mm O.D. quartz reactor (b).

Figure 2. Raw southern yellow pine chips (> 1 mm).

For each of five temperature runs, the gas flow rate, heating rate, and pyrolysis time were 500 mL/min, 10 °C/min, and 30 min, respectively.

Heating rate effect on the morphology of the pine chars was studied using three heating rates (1, 10, and 50 °C/min) under nitrogen atmosphere. For each of three runs, the gas flow rate, final temperature, and pyrolysis time were controlled at 500 mL/min, 1,000 °C, and 30 min, respectively.

Three nitrogen gas flow rates (100, 500, and 1,000 mL/min) were used to investigated the gas flow rate effect on the morphology of the pine chars. For each of three flow runs, the final temperature, heating rate, and pyrolysis time were controlled at 1,000 °C, 30 °C/min, and 30 min, respectively.

Two types of gases (hydrogen and nitrogen) were used to study the effect of gas type on the morphology of the pine chars. For each of the two types of gas runs, the final temperature, heating rate, gas flow rate, and pyrolysis time were controlled at 1,000 °C, 50 °C/min, 500 mL/min, and 30 min, respectively.

Characterization

The morphologies of the raw wood chips and the pine char samples were examined by SEM on a JEOL JSM-6500F instrument (JEOL Ltd., Tokyo, Japan) operating at 5.0 kV. The SEM samples were pre-coated with gold before being introduced into the vacuum chamber. The resulting char samples were soaked in ethanol and sonicated for 20 min. The carbon particles washed from the char surface were collected and examined with a JEOL JEM-100CX II transmission electron microscope (TEM) (JEOL Ltd., Tokyo, Japan) operating at 80 kV.

Results and Discussion

Temperature Effect

The SEM images of the raw pine wood chips and the chars obtained under pyrolysis temperatures of 450, 500, 650, and 1,000 °C are shown in Figures 3 to 7, respectively. Figure 3 shows that the surface of the chip is smooth and clean. There is no dust or devolatilization coking residue on the wood surface. Figure 4 shows that the wood had already started to decompose at 450 °C. Smooth regions on the surface suggested that the wood had begun to melt; however, the decomposition was not significant. No particles were found on the surfaces of the char sample heated up to 450 °C.

The surface of the chars heated up to 500 °C was in the form of continuous melt and decomposition (Fig. 5). The most obvious feature observed on the char at 650 °C was the formation of sphere particles over its surface (Fig. 6) with diameters of 50 to 100 nm. The loss of surface material and the growth of crystalline structure suggested that the

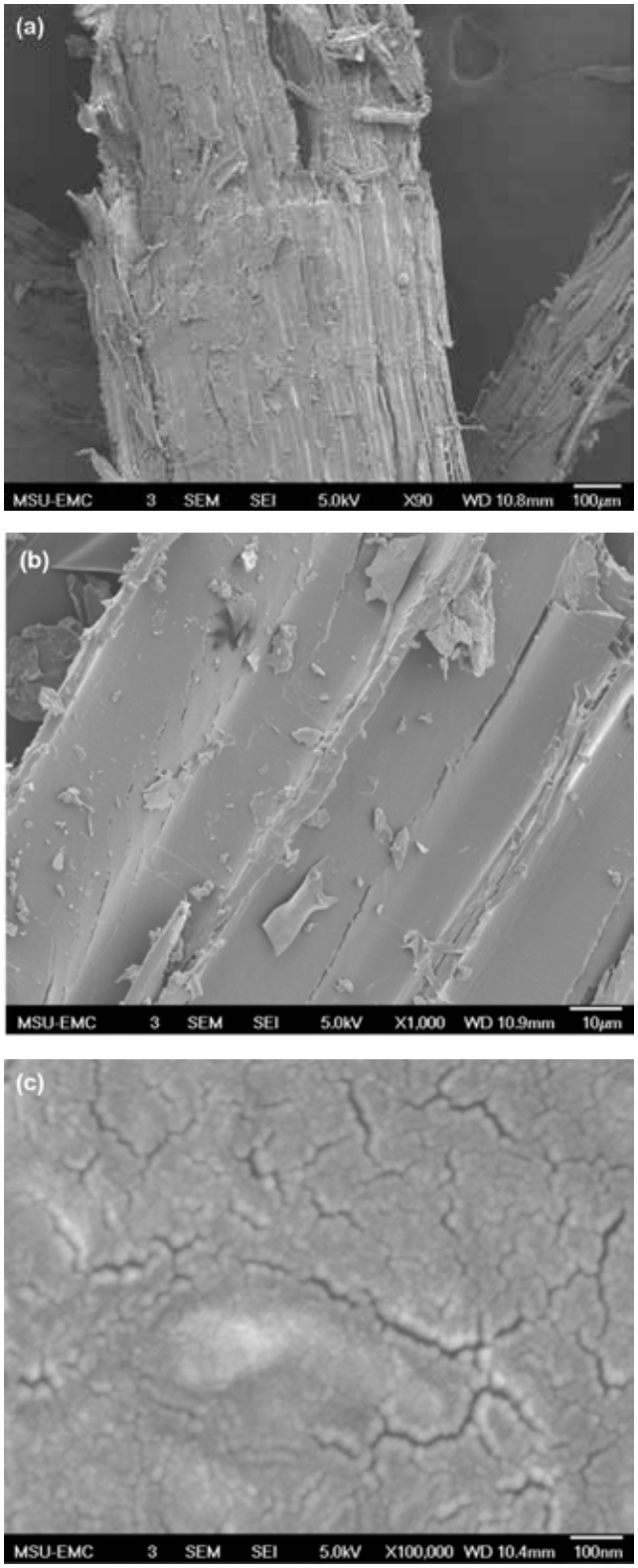

Figure 3. SEM images of surface morphologies of raw pine chips at three magnifications of: (a) ×90; (b) ×1,000; and, (c) ×100,000.

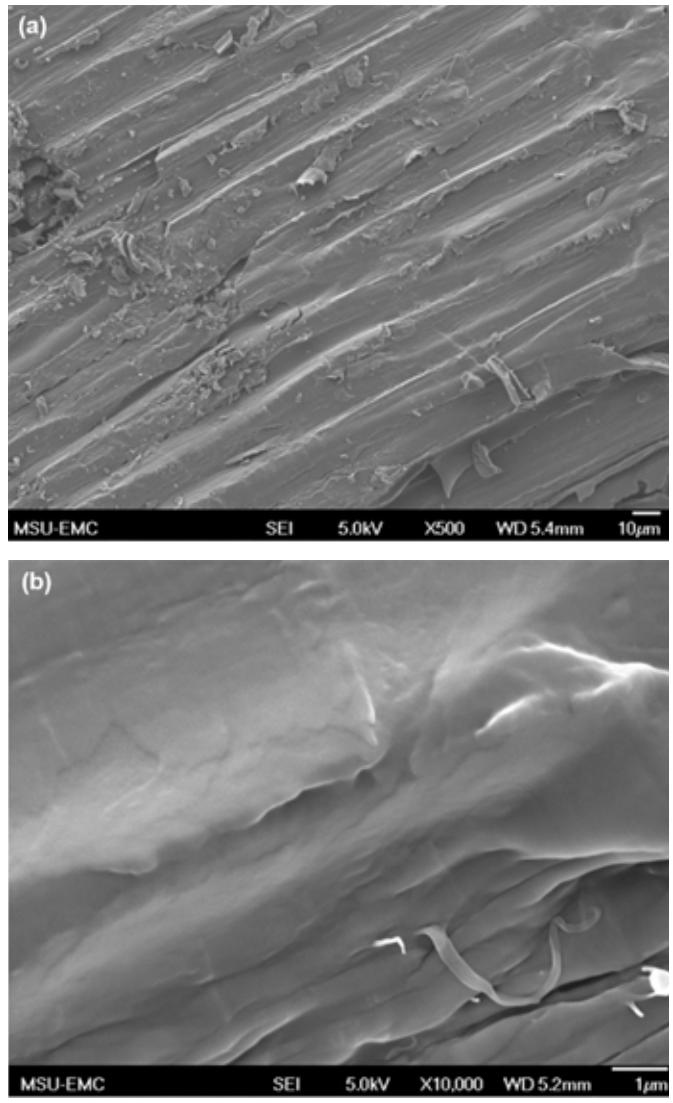

Figure 4. SEM images of surface morphologies of pine chars treated at 450 °C for 30 min, with a nitrogen gas flow rate of 500 mL/min and a heating rate of 10 °C/min at two magnifications of: (a) ×500 and (b) ×10,000.

part of decomposition products precipitated to form the crystalline deposits. When volatile matter is generated, the physical structure of a char changes significantly during the devolatilization. Pyrolysis temperature had a notable impact on the pore structure of biomass char (Hu and others 2008).

As pyrolysis temperature increased to 1,000 °C, the surface of pine chars was covered with more nano sphere particles (Fig. 7). The diameter of the particles appearing on the top of the pine char surface ranged from 50 to 100 nm, whereas the particles underneath the surface were around 20 nm in diameter. The formation of surface nanoparticles indicated that the more volatile products vaporized and redeposited to form the crystalline structures. More micro-pores and micro-channels were observed on the char surface as the pyrolysis temperature increased.

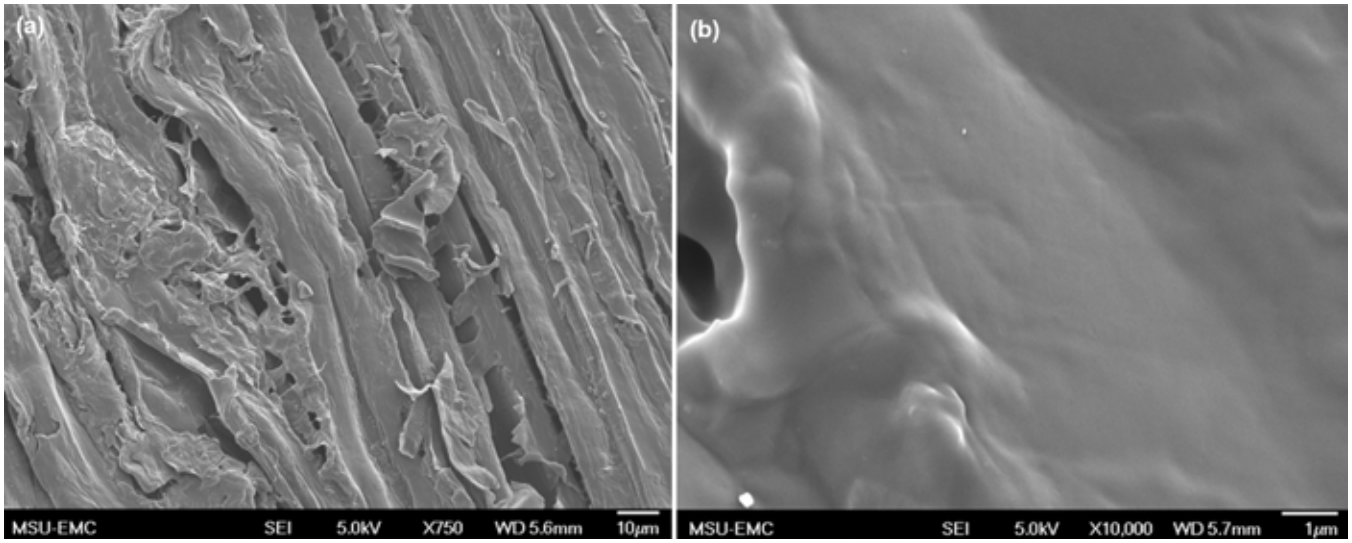

Figure 5. SEM images of surface morphologies of pine chars treated at 500 °C for 30 min, with a nitrogen gas flow rate of 500 mL/min and a heating rate of 10 °C/min at two magnifications of: (a) ×750 and (b) ×10,000.

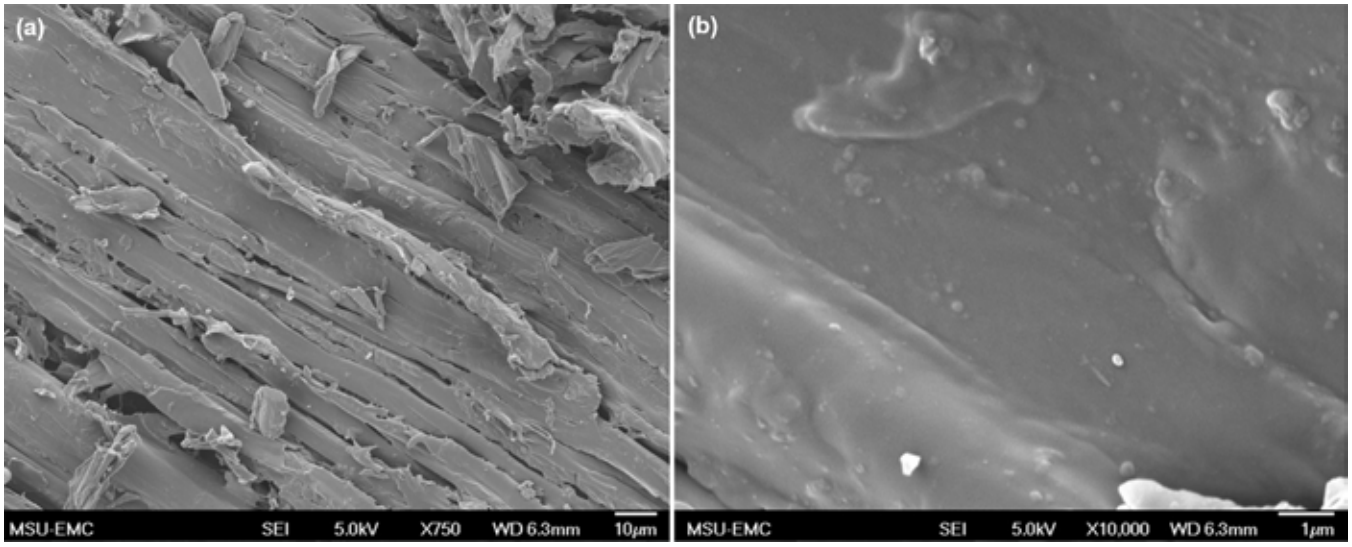

Figure 6. SEM images of surface morphologies of pine chars treated at 650 °C for 30 min, with a nitrogen gas flow rate of 500 mL/min and a heating rate of 10 °C/min at two magnifications of: (a) ×750 and (b) ×10,000.

Heating Rate Effect

SEM images of pine chars from heating rates of 1, 10, and 50 °C /min are shown in Figure 8. For all char samples, sphere-shaped nanoparticles were observed. These particles might be due to pyrolytic carbon deposits resulting from organic volatiles. During carbonization, hydrocarbons release from the samples as volatile matter. Collisions of these compounds with pore walls might bring about cracking and carbon deposition.

The surface with the heating rate of 1 °C/min was smooth, and 50–100 nm particles were distributed over the surface. Under the heating rate of 10 °C/min, the pine char surface is covered with different sizes of smooth, open pores and more particles with 100–200 nm diameters. More and larger particles appeared over the surface of the chars with the rate of 50 °C/min. These particles obtained under high heating rates may be the result of secondary product formation from the precipitation of volatile gases. The higher heating rate leads to a rapid formation of volatile matter, causing a rapid increase of pressure in the wood particle and an explosive release of volatiles (Sharma and others 2001, 2004).

Purge Gas Flow Rate Effect

Figure 9 shows SEM images of pine chars produced with three nitrogen flow rates. The surface of pine chars under 100 mL/min flow rate was covered with nanoparticles with sizes ranging from 10 to 50 nm in diameter, and fewer micro-pores and micro-channels were formed on the

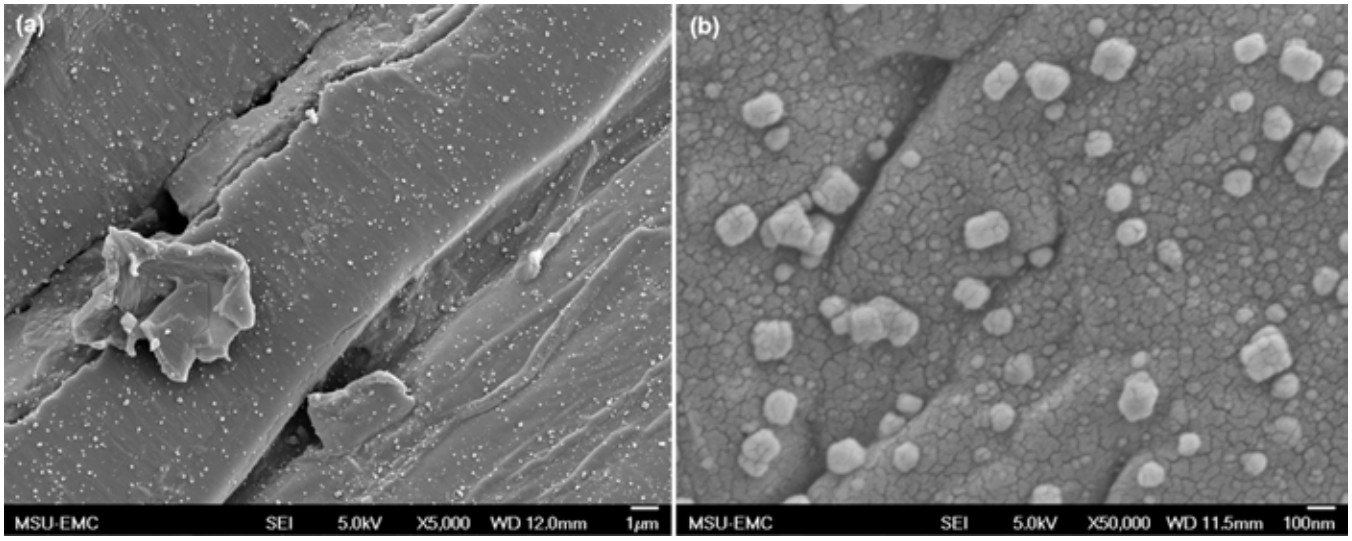

Figure 7. SEM images of surface morphologies of pine chars treated at 1,000 °C for 30 min, with a nitrogen gas flow rate of 500 mL/min and a heating rate of 10 °C/min at two magnifications of: (a) ×5,000 and (b) ×50,000.

surface. The surface of pine chars had fewer nanoparticles and more micro-pores and micro-channels with the increase of the purge gas flow rate from 100 to 1,000 mL/min. In this case, the fast volatile release during pyrolysis leads to loss of porosity of the char, because part of the volatiles would decompose and deposit as the secondary reaction char in the micro-channels or the surface of the char matrix at a low flow rate, whereas the porosity of the char should increase when the purge gas flow rate increases. Therefore, more micro-pores and micro-channels are observed over pine chars produced at the higher purge gas flow rate.

Purge Gas Type Effect

Figure 10 shows SEM images of pine chars purged with nitrogen and hydrogen gases. Many nanoparticles were observed over the surface of the char purged with nitrogen. The char purged with hydrogen had few or no nanoparticles over its surface. Many micro-pores and micro-channels were evenly distributed over the surfaces of chars purged both by nitrogen and hydrogen. The surface of hydrogen-purge chars is relatively smoother compared to nitrogen-purge chars.

Particle Characterization

Figures 11 to 14 show TEM images of nanoparticles washed off from pine chars produced under different thermal treatment conditions. Typically, nano carbon spheres, nano carbon chips, and some porous carbon particles (Fig. 11) were observed for the pine chars produced at 1,000 °C with heating rate of 1 °C/min under a nitrogen flow rate of 500 mL/min, and these particles had the diameters between 20 and 100 nm. Large amounts of nano carbon spheres mixed with porous carbon particles (Fig. 12) were found for the pine chars produced at 1,000 °C, with a 1 °C/min heating rate and a hydrogen flow rate of 500 mL/min, and these carbon spheres were between 20 and 50 nm in diameter.

For the chars produced at 1,000 °C with a 100 °C/min heating rate under a nitrogen flow rate of 500 mL/min, porous carbon particles and carbon nanofibers (or carbon nanotubes (CNTs)) were observed, as shown in Figure 13. It was interesting to find some CNTs formed in the mixture with carbon particles (Fig. 14) when the chars were produced under the condition of 1,000 °C, with 100 °C/min heating rate under a 500 mL/min hydrogen flow. Although no metal catalysts and hydrocarbons or CO were introduced, trace levels of metals (southern pine contains very small amounts of inorganic elements such as Ca, K, Mg, Na, Si, Fe, and Mn) (Koch 1972) in the chars catalytically decomposed the volatile products such as methane, organic compounds, and CO to form carbon nanotubes during the pine pyrolysis process.

Conclusions

The influences of final pyrolysis temperature, heating rate, purge gas type, and flow rate on the surface morphology of pine chars were investigated using SEM and TEM. SEM images of raw pine chips show that the surface is smooth and clean, and there is no dust.

The surface morphologies of pine chars were significantly affected by pyrolysis temperature for the pine chips heated under a nitrogen flow rate of 500 mL/min and a heating rate of 10 °C/min for 30 min. SEM analyses indicated that at 450 °C, pine chips had already started to decompose. The pine char obtained at 500 °C was in the form of a continuous melt and decomposition. No nanoparticles were observed on the char surfaces as temperature increased to 500 °C.

The most obvious feature observed was the formation of sphere particles over the surface of the pine chars heated up to 650 °C, where particle diameters ranged from 50 to 100 nm. As temperature increased to 1,000 °C, the char

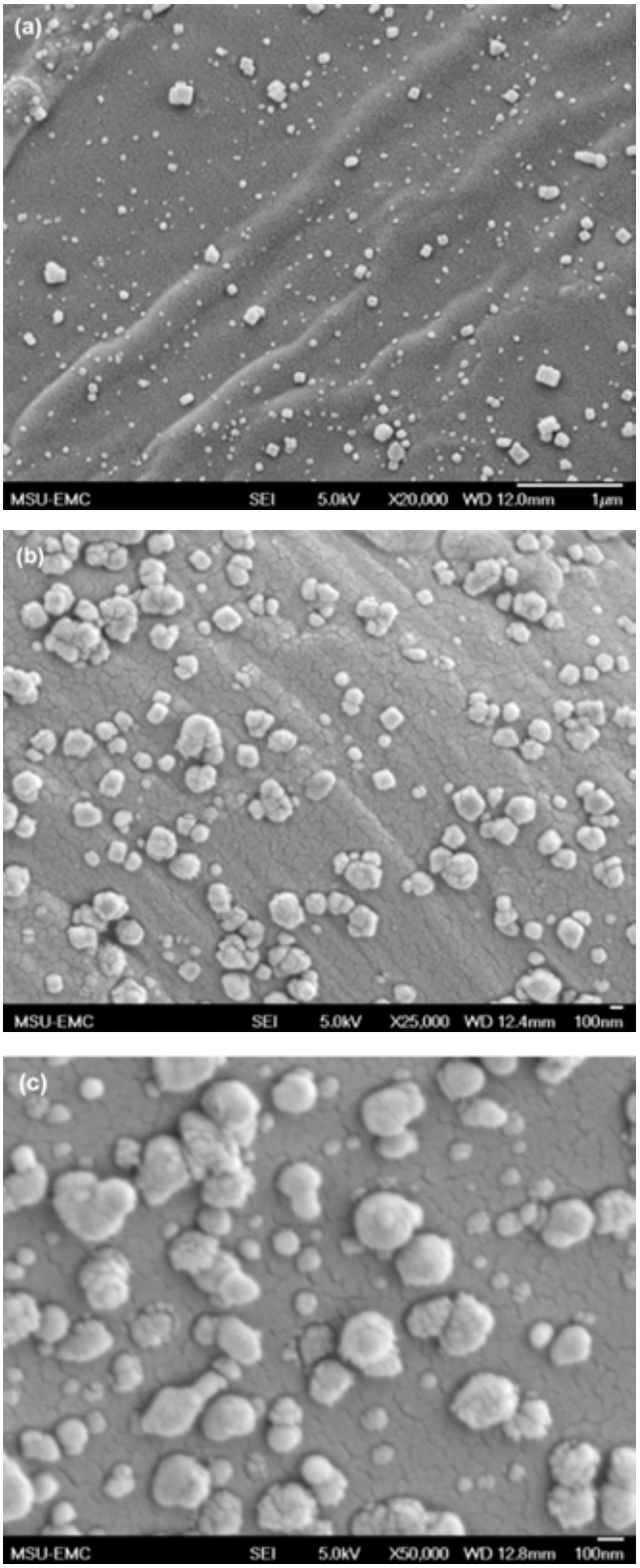

Figure 8. SEM images of surface morphologies of pine chars produced at three heating rates: (a) 1 °C/min; (b) 10 °C/min; and, (c) 50 °C/min to the final temperature of 1,000 °C for 30 min, with a nitrogen gas flow rate of 500 mL/min.

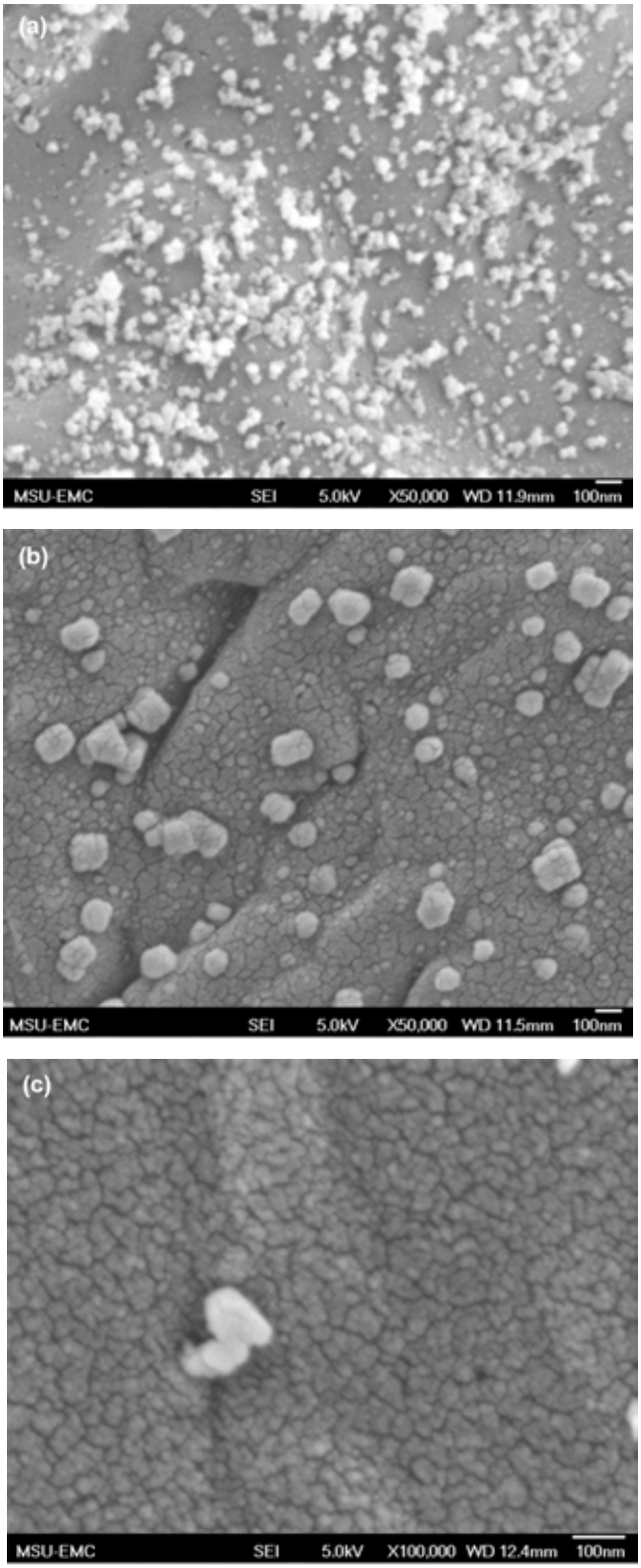

Figure 9. SEM images of surface morphologies of pine chars heated to a final temperature of 1,000 °C, with a heating rate of 30 °C/min for 30 min under three nitrogen flow rates: (a) 100 mL/min; (b) 500 mL/min; and, (c) 1,000 mL/min.

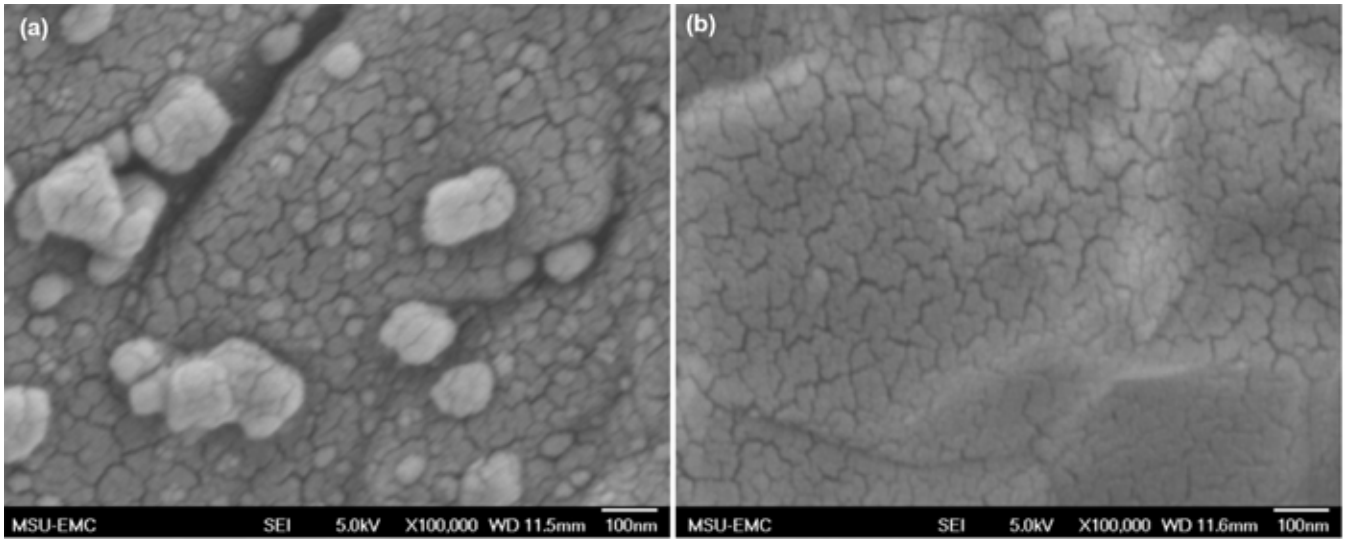

Figure 10. SEM images of surface morphologies of pine chars heated to a final temperature of 1,000 °C, with a heating rate of 50 °C/min for 30 min using purge gases of (a) nitrogen and (b) hydrogen gases of a constant flow rate of 500 mL/min.

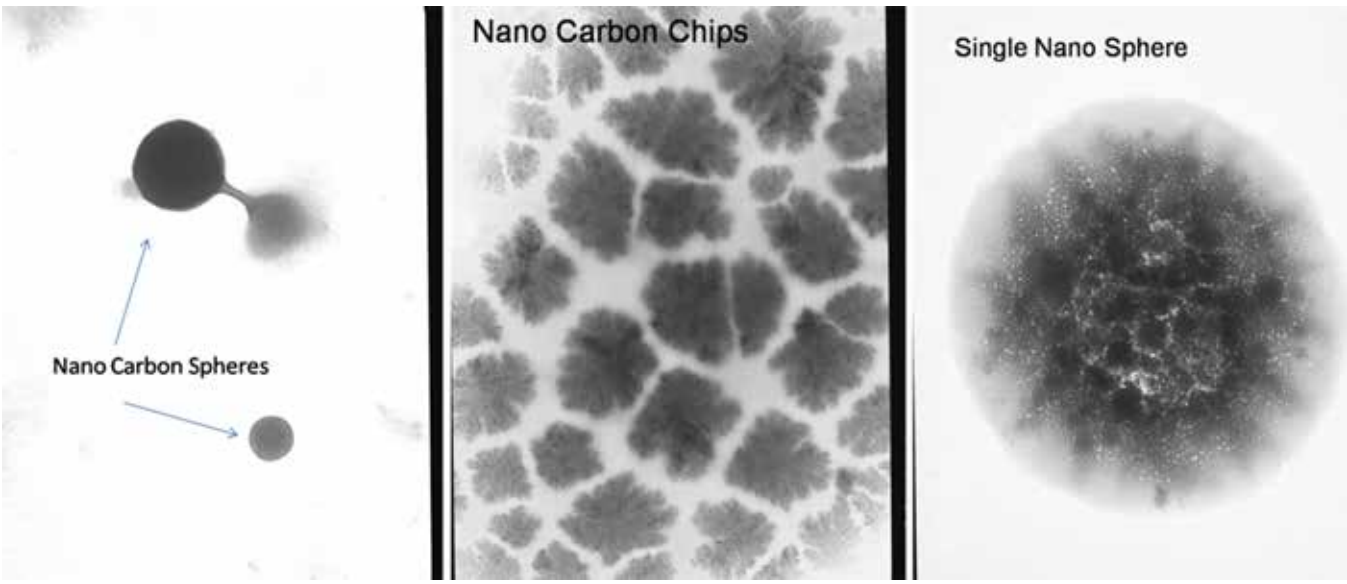

Figure 11. TEM images of carbon particles (20–100 nm in diameter) washed off from pine chars heated to the final temperature of 1,000 °C for 30 min, with a heating rate of 1 °C/min under a nitrogen flow rate of 500 mL/min.

surface was covered with more nano sphere particles. The particles distributed on top of the char surface range from 50 to 100 nm in diameter, whereas the particles underneath the char surface were about 20 nm in diameter. More micro-pores and micro-channels were seen on the pine char surfaces as the temperature increased to 1,000 °C.

The heating rate has a significant influence on the surface morphology of pine chars pyrolyzed at 1,000 °C for 30 min with a nitrogen gas flow rate of 500 mL/min. The size and quantity of nanoparticles on the pine char surface increased as the heating rate increased from 1 to 50 °C/min. Different sizes of smooth, open pores can be produced on the pine char surface with a heating rate of 50 °C/min.

The lower the nitrogen gas flow rate, the more nanoparticles and fewer micro-pores and micro-channels are formed on the pine char surface. Also, the higher the nitrogen gas flow rate, the fewer nanoparticles and the more micro-pores and micro-channels there were. The surface of pine chars purged with nitrogen yielded significantly more nanoparticles than those purged with hydrogen. Both chars purged with nitrogen and hydrogen had many evenly distributed micro-pores and micro-channels, but the surface of

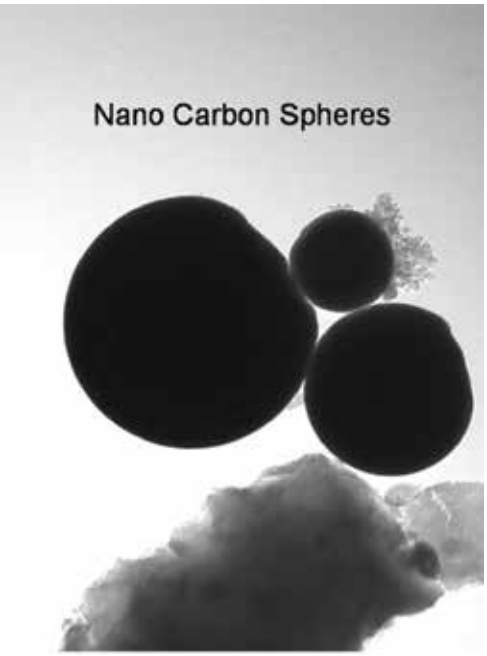

Figure 12. TEM image of carbon particles washed off from pine chars produced at the final temperature of 1,000 °C for 30 min, with a heating rate of 1 °C/min and a hydrogen flow rate of 500 mL/min.

hydrogen-purged chars was relatively smooth compared with the nitrogen-purged chars.

Literature Cited

Baumlin, S.; Broust, F.; Bazer-Bachi, F.; Bourdeaux, T.; Herbinet, O.; Ndiaye, F.T.; Ferrer, M.; Lédé, J. 2006. Production of hydrogen by lignin fast pyrolysis. International Journal of Hydrogen Energy. 31(15): 2179–2192.

Biagini, E.; Simone, M.; Tognotti, L. 2009. Characterization of high heating rate chars of biomass fuels. Proceedings of the Combustion Institute. Waltham, MA: Elsevier, Inc. 32(2): 2043–2050.

Cetin, E.; Moghtaderi, B.; Gupta, R.; Wall, T.F. 2004. Influence of pyrolysis conditions on the structure and gasification reactivity of biomass chars. Fuel. 83(16): 2139–2150.

Demirbas, A. 2009. Biorefineries: for biomass upgrading facilities. 2nd ed. Berlin, Germany: Springer. (14 October 2009).

Fu, P.; Hu, S.; Xiang, J.; Sun, L.; Li, P.; Zhang, J.; Zheng, C. 2009. Pyrolysis of maize stalk on the characterization of chars formed under different devolatilization conditions. Energy & Fuels. 23(9): 4605–4611.

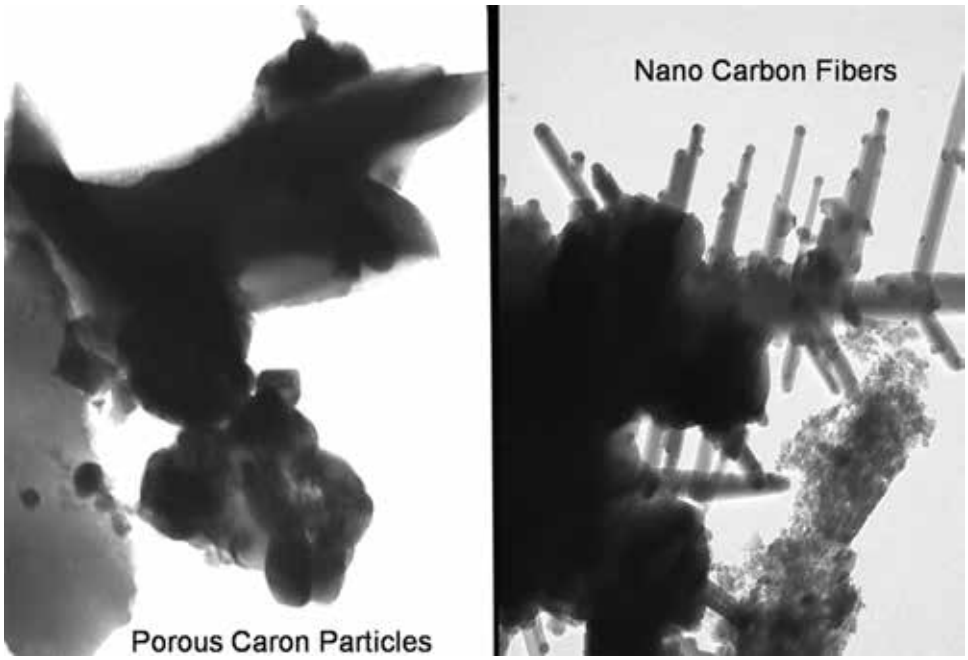

Figure 13. TEM images of carbon particles washed off from pine chars produced at the final temperature of 1,000 °C for 30 min, with a heating rate of 100 °C/min and a nitrogen flow rate of 500 mL/min.

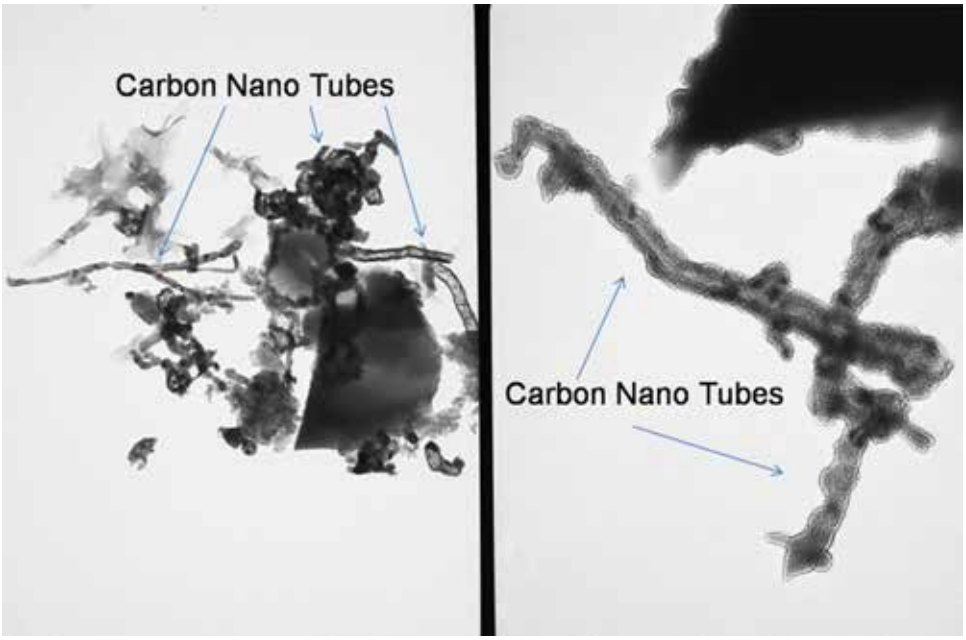

Figure 14. TEM images of carbon particles washed off from pine chars produced at the final temperature of 1,000 °C for 30 min, with a heating rate of 100 °C/min and a hydrogen flow rate of 500 mL/min.

Guerrero, M.; Ruiz, M.P.; Alzueta, M.U.; Bilbao, R.; Millera, A. 2005. Pyrolysis of eucalyptus at different heating rates: studies of char characterization and oxidative reactivity. Journal of Analytical and Applied Pyrolysis. 74(1–2): 307–314.

Hata, T.; Imamura, Y.; Kobayashi, E.; Yamane, K.; Kikuchi, K. 2000. Onion-like graphitic particles observed in wood charcoal. Journal of Wood Science. 46: 89–92.

Herzog, A.; Reznik, B.; Chen, T.; Graule, T.; Vogt, U. 2006. Structural changes in activated wood-based carbons: correlation between specific surface area and localization of molecular-sized pores. Holzforschung. 60: 85–92.

Hu, B.; Wang, K.; Wu, L.; Yu, S.H.; Antonietti, M.; Titirici, M.M. 2010. Engineering carbon materials from the hydrothermal carbonization process of biomass. Advanced Materials. 22: 813–828.

Hu, S.; Xiang, J.; Sun, L.; Xu, M.; Qiu, J.; Fu, P. 2008. Characterization of char from rapid pyrolysis of rice husk. Fuel Processing Technology. 89(11): 1096–1105.

Ishimaru, K.; Vystavel, T.; Bronsveld, P.; Hata, T.; Imamura, Y.; Hosson, J.D. 2001. Diamond and pore structure observed in wood charcoal. Journal of Wood Science. 47: 414–416.

Koch, P. 1972. Utilization of the southern pines. Agric. Handb. SFES-AH-420. Asheville, NC: U.S. Department of Agriculture, Forest Service, Southern Forest Experiment Station.

Kumar, P. [and others]. 2009. Industrial & Engineering Chemistry Research. 48(8): 3713–3729.

Kurosaki, F.; Ishimaru, K.; Hata, T.; Bronsveld, P.; Kobayashi, E.; Imamura, Y. 2003. Microstructure of wood charcoal prepared by flash heating. Carbon. 41: 3057–3062.

Mohan, D.; Pittman, C.U.; Steele, P.H. 2006. Pyrolysis of wood/biomass for bio-oil: a critical review. Energy & Fuels. 20(3): 848–889.

Ohata, M.; Yoshizawa, N.; Youshizawa, S. Tube-like carbon fabricated by carbonization of wood. www.geocities.jp/yasizato/Yoshizawa17.pdf. (Accessed 5 January 2010).

Ragland, K.W.; Aerts, D.J. 1991. Bioresource Technology. 37(1991): 161–168.

Saito, Y.; Arima, T. 2002. Growth of cone-shaped carbon material inside the cell lumen by heat treatment of wood charcoal. Journal of Wood Science. 48: 451–454.

Sharma, R.K.; Wooten, J.B.; Baliga, V.L.; Hajaligol, M.R. 2001. Characterization of chars from biomass derived materials: pectin chars. Fuel. 80: 1825–1836.

Sharma, R.K.; Wooten, J.B.; Baliga, V.L.; Lin, X.; Chan, W.G.; Hajaligol, M.R. 2004. Characterization of chars from pyrolysis of lignin. Fuel. 83: 1469–1482.

Wampler, T.P., ed. 2006. Applied pyrolysis handbook. 2nd ed. Boca Raton, FL: CRC Press.

An Investigation of Fabrication Thermal Insulation Wood-Based Composite Using Nanotechnology

Reza Zahedsheijani[1,*], Mohammad Layeghi[2], Hosein Yousefi[3], Mehdi Faezipour[4]

[1] MSc Student, Department of Wood and Paper Science & Technology, Faculty of Natural Resources, University of Tehran, Karaj, Iran, e-mail: reza.zahedsheijani@gmail.com & reza_zahed2009@ut.ac.ir

[2] Assistant Professor, Department of Wood and Paper Science & Technology, Faculty of Natural Resources, University of Tehran, Karaj, Iran, e-mail: mlayeghi@ut.ac.ir

[3] PhD Student, Department of Wood and Paper Science & Technology, Faculty of Natural Resources, University of Tehran, Karaj, Iran, e-mail: yousefi329@gmail.com

[4] Professor, Department of Wood and Paper Science & Technology, Faculty of Natural Resources, University of Tehran, Karaj, Iran, e-mail: mfaezi@ut.ac.ir

* Corresponding author:
Reza Zahedsheijani, Department of Wood and Paper Science & Technology, Faculty of Natural Resources, University of Tehran, Karaj, Iran, P.O.BOX: 31585-4314, Tel: (98) 261 222 30 44, Fax: (98) 261 222 30 44, e-mail: reza.zahedsheijani@gmail.com & reza_zahed2009@ut.ac.ir

Introduction

Medium density fiberboard (MDF) is widely used in cinema halls and conference halls. Nowadays with rising energy costs, optimization in the use of energy has been considered. Thus, many researchers study the new ways to increase the thermal insulation properties (reduction of thermal conductivity) in internal walls of houses and conference halls. Nanotechnology represents a major opportunity for the forest products industry to develop new products. The nanotechnology searches to develop materials and structures that significantly improved physical and chemical properties and functions due to their nanoscale size (Wegner et al. 2005; Wegner and Jones 2006). Lei et al. (2008) found that slight percentages of NaMMT nanoclay could improve the performance of thermosetting UF resin. It had an accelerating effect on the curing of UF resin that could lead to increase water resistance of plywood and internal bond of particleboard. Also, X-ray diffraction of NaMMT/UF resin composites indicated that after dispersion inside the resin, the NaMMT was completely exfoliated. Laoutid et al. (2009) in his review article on the clay/nanocomposites noted that the collection of clay on the surface of the material limits heat transfer within the material. Our study is aimed to evaluate the effects of Na^+ montmorillonite (NaMMT) nanoclay on the thermal insulation properties of MDF. For this purpose, we applied nanoclay/UF resin to produce the MDF. The effect of nanoclay was analyzed by means of thermal conductivity test and scanning electron microscopy (SEM).

Materials and methods

Materials

Urea formaldehyde (UF) resin was used at level of 10% based on the oven-dry weight of wood fibers. The commercial UF resin was purchased from Tiran Chemie Inc., Iran. The characteristics of the resin are given in Table 1. Ammonium chloride (NH_4CL) was added as a

hardener in UF resin at a level of 2% based on the oven-dry weight of resin. Na^+ montmorillonite (Na^+MMT) nanoclay with a cation exchange capacity (CEC) value of 92.6 mequiv/100 g was obtained from Southern Clay Products Inc., USA. The nanoclay was added to the resin at three levels of 0%, 2.5% and 5% based on the oven-dry weight of resin. The characteristics of Na^+MMT nanoclay are given in Table 2. The wood fibers of Hardwoods were kindly provided from the Arian Sina Inc., Mazandaran, Iran. The final moisture content of the fibers after drying was about 1–2%. The dry fibers were classified using the Sonic Sifter (VU100 type), Imal Inc., Italy. The average fiber length was 1.1 mm, and the amount of dust was close to 39.2%.

Table 1. The characteristics of UF resin based on laboratory tests.

Density (kg m^{-3})	1300
Gel time (s)	69
Viscosity (CP)	320
pH	7
Solid amount (%)	60

Table 2. The characteristics of Na^+MMT nanoclay based on Southern Clay Products Inc., USA.

Supplier designation	Cloisite® Na^+
Organic modifier	None
Density (kg m^{-3})	2860
Moisture (%)	4–9
Weight loss on ignition (%)	7

Preparation of composites

MDF composites measuring 0.4×0.4×0.016 m^3 with two densities of 650 and 750 kg m^{-3} were manufactured. The UF resin was mixed with the Na^+MMT nanoclay by mechanical stirring for 360 s at the room temperature to get a good dispersion and partly exfoliation of Na^+MMT in the UF resin (Lei et al. 2008). It seems the UF resin can also wet Na^+MMT and partly penetrates into the silicate layers during this time. Then, the UF resin containing well-dispersed nanoclay was

sprayed into the fibers by using a rotary blender. Mats were hand formed in a forming frame and then the fiber mats were manually pre-pressed. The fiber mats at 10% moisture content were exposed to the hot press. The hot press was applied at a pressure of 3.43×10^6 Pa at 175 °C for 360 s. Three replicate composites were made for each treatment. All composites were conditioned at 65±5% relative humidity and 20±1°C for about 2 weeks. The different prepared MDF trials are given in Table 3.

Table 3. Amount of Na^+MMT added and density of boards for the different MDFs

Code	Density of board (kg m^{-3})	Na^+MMT nanoclay (%)
A1		0
A2	650	2.5
A3		5
B1		0
B2	750	2.5
B3		5

Measurement of thermal conductivity

Thermal conductivity test was applied according to ASTM C177 specification. The guarded hot plate apparatus consists of heating and cooling units and edge insulation to prevent excessive edge losses. Thermal conductivity was calculated using the following equation:

$$K = \frac{W\,t}{A\,\Delta T} \tag{1}$$

where K is the thermal conductivity, W is the power in watts, t is the thickness of sample, A is the cross section of sample and ΔT is the steady-state temperature difference between the two plates where the sample is placed.

Field Emission Scanning Electron Microscopy (FE-SEM)

A vacuum dried thin layer of MDF containing Na^+MMT was coated with platinum by an ion sputter coater and was observed with a FE-SEM (JSM-6700F; JEOL Ltd., Tokyo, Japan) operating at 5000 V.

Results and discussion

The results of the thermal conductivity test are plotted in Fig. 1. The results show that all modified MDFs have less thermal conductivity values in comparison to control MDF, meaning a

suitable barrier property in the modified MDFs. The stabilization of nanoclay through the material acts as a protective layer that limits heat transfer in the material (Laoutid et al, 2009). The thermal conductivity value of control MDF (A1) is 0.125 W m^{-1} K^{-1}, while that of MDFs treated with 2.5% and 5% of NaMMT nanoclay (A2 and A3) is 0.113 W m^{-1} $K^{-1}$and 0.112 W m^{-1} K^{-1}, respectively. Similarly, in the case of denser MDFs, the thermal conductivity value for B1 specimen is 0.149 W m^{-1} K^{-1}, while the value for B2 and B3 specimens is 0.109 W m^{-1} K^{-1} and 0.103 W m^{-1} K^{-1}, respectively. The thermal conductivity values for A2 and A3 MDFs decreased by 10.6% and 11.6% of the corresponding value for control MDF, respectively. Similarly, the thermal conductivity values for B2 and B3 MDFs decreased by 36.7% and 44.7% of the corresponding value for control MDF, respectively. The barrier performance of NaMMT nanoclay improves by increasing of nanoclay loading. Qin et al. (2005) has been suggested that the principal thermal stability mechanism is due to the formation of the barrier effect of exfoliated layered silicates against heat and volatiles due to the movement of nanolayer to the material surface.

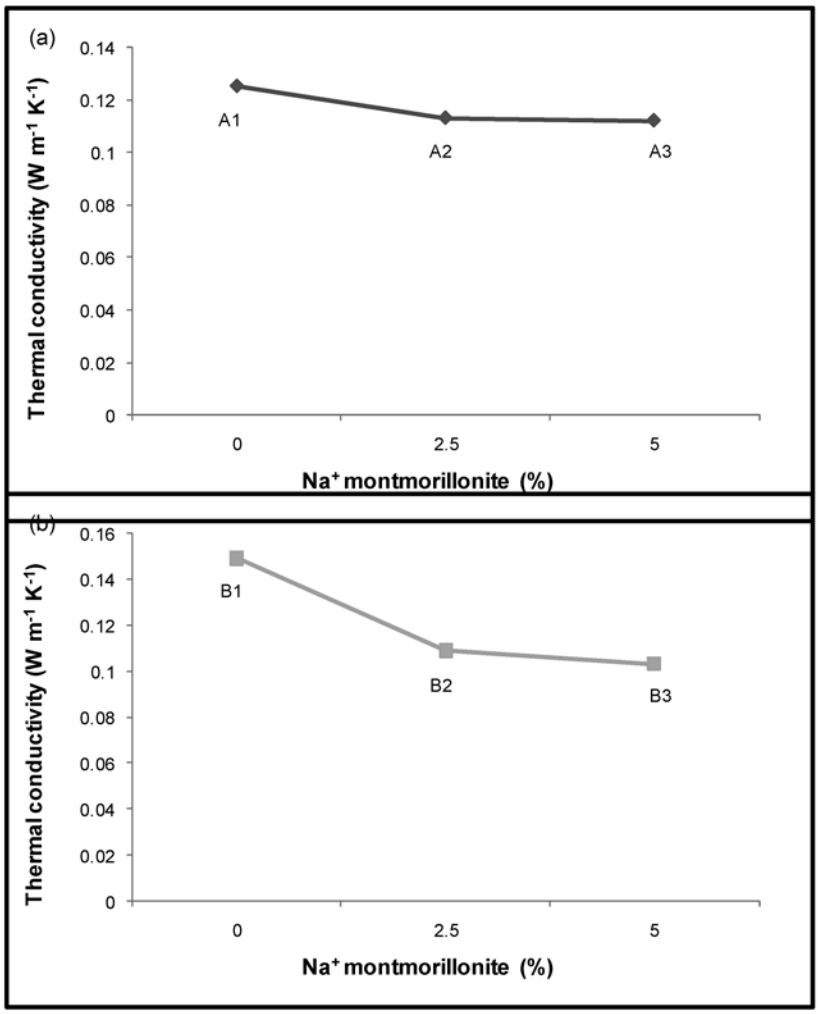

Fig. 1. The thermal conductivity chart for 6 groups of samples.

Fig. 2 shows the FE-SEM micrographs of MDF produced by adding of 5% Na^+MMT nanoclay in the UF resin. Based on Fig. 2, nanoclay with a bit agglomeration is observed in the MDF structure. The observations are similar to those for a previous study which evaluated the effects of nanoparticle and matrix interface on the nanocomposites properties (Miller 2008). The micrographs show distinct regions of clay while adjacent regions of the MDF contain little visible nanofiller which might be covered by the resin.

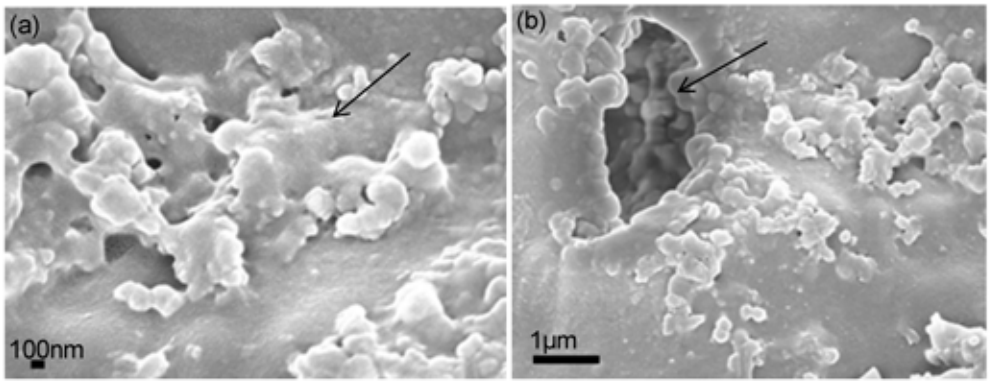

Fig. 2. SEM images of MDF produced with a Na^+MMT nanoclay-added UF resin. (a) The arrow shows the silicate layers covered by UF resin (30,000×) (b) A pit partially filled by UF resin and silicate layers (15,000×). The tiny particles of silicates can decrease the thermal conductivity.

Conclusion

Thermal conductivity property were determined for medium density fiberboard (MDF) reinforced with Na^+MMT nanoclay. The thermal conductivity through the reinforced MDF decreases by increasing the nanoclay particles. The incorporation of exfoliated nanoclay provides a tremendous improvement in thermal conductivity. In fact, slight percentages of Na^+ montmorillonite (NaMMT) nanoclay could improve the thermal insulation properties of MDF.

The dispersion and exfoliation phases of NaMMT nanoclay particles have a suitable effect on thermal conductivity of the MDFs. This means that the barrier effect of exfoliated layered silicates has a good cooperation on the reduction of thermal conductivity in MDF.

Acknowledgements

We would like to give a special thanks to Professor Takashi Nishino from Kobe University for FE-SEM studies. The authors are also thankful to Dr. Asghar Tarmian for their general help.

Literature Cited

Laoutid, F., Bonnaud, L., Alexandre, M., Lopez-Cuesta, J.M. and Dubois, Ph., 2009. New prospects in flame retardant polymer materials: From fundamentals to nanocomposites, Materials Science and Engineering 63:100-125.

Lei, H., Du, G., Pizzi, A. and Celzard, A., 2008. Influence of nanoclay on urea-formaldehyde resins for wood adhesives and its model, Journal of Applied Polymer Science 109:2442-2451.

Miller, S.G., 2008. Effects of nanoparticle and matrix interface on nanocmposite properties. PhD Thesis, Akron University, USA, 207 pages.

Qin, H., Zhang, S., Zhao, C., Hu, G. and Yang, M., 2005. Flame retardant mechanism of polymer/clay nanocomposites based on polypropylene, Polymer 46:8386-8395.

Wegner, T.H. and Jones, Ph.E., 2006. Advancing cellulose-based nanotechnology, Cellulose 13:115-118.

Wegner, T. H., Winandy, J. E. and Ritter, M. A., 2005. Nanotechnology opportunities in residential and non-residential construction. In: 2nd International Symposium on Nanotechnology in Construction, Spain, pp. 208-220.

Mechanical and Thermal Properties of Microcrystalline Cellulose/Nanoclay/Polypropylene

[1]Amir. Nourbakhsh*, [2]Alireza. Ashori

[1] Associate Professor, Department of Wood and Paper Science, Research Institute of Forests and Rangelands (RIFR), Tehran, Iran, [2] Assistant Professor, Department of Chemical Technologies, Iranian Research Organization for Science and Technology (IROST), *Tehran, Iran* , [3]
*(Tel: +98 21 9126766416, e-mail: nourbakhsh_amir@yahoo.com)

Abstract

Microcrystalline cellulose (MCC) / Polypropylene (PP) / composites were prepared containing polypropylene-graft-maleic anhydride (PP-*g*-MA) as compatibilizer. The weight ratio of the cellulosic materials to polymer matrix was 40:60 (w:w). The obtained results showed that tensile, flexural and impact strengths of the composites were significantly enhanced with addition of MCC, as compared with pure PP and composites without MCC. The effect of MCC on impact was minimal compared to the effects of PP-*g*-MA content. Scanning electron microscopy has shown that the composite, with compatibilizer, promotes better fiber–matrix interaction. In all cases, the degradation temperatures shifted to higher values after addition of PP-*g*-MA. The maximum improvement on the thermal stability of the composites was achieved when 5% PP-*g*-MA was used. However, the increase in MCC content substantially reduced the thermal stability. This work showed that MCC along with wood flour could be effectively used as reinforcing agent in thermoplastic matrix.

Keywords: Microcrystalline cellulose; Physical properties; mechanical testing; injection molding

1. Introduction

Many studies are ongoing to find ways to use cellulose-based fibers in place of synthetic fibers as reinforcements [1]. Therefore, plant fibers obtained from wood or non-wood have recently attracted the attention of researchers both from academia and industry. This trend has been prompted mainly due to various environmental, economic and performance issues.

These natural plant fibers provide several benefits over synthetic fibers. They are generally of lower density and exhibit high specific strength and stiffness that allow the production of low-density composites with higher filler concentration. Additionally, plant fibers have flexibility and are therefore less susceptible to fracture during processing [2,3]. One of the most common plant fibers used in the thermoplastics industry is wood flour, which is produced commercially from post-industrial sources such as planer shavings and sawdust. The scrap wood is sourced for species purity and then ground to specific particle size distributions [4].

Cellulose, the most abundant biopolymer on earth, is the main constituent of wood and non-wood. It is located predominantly in the secondary wall of the wood fiber. Approximately 45–50% of extractive-free dry substance in most plant species is cellulose, and it is the most single important component in the fiber cell wall in terms of its volume and effect on the characteristics of wood. Cellulose molecules consist of long linear chains of homo-polysaccharide, composed of

b-D-glucopyranose units, which are linked by (1–4)-glycosidic bonds [5]. Within the microfibrils in the cell wall, cellulose is arranged into regions that display both amorphous and crystalline. Cellulose of various plant origins (wood and non-wood) exhibits a wide range of crystallinity (20–90%). Crystalline cellulose is much stronger and stiffer than amorphous cellulose and cellulose itself, and is supposed to be a better reinforcing agent than cellulose. MCC is crystalline cellulose and is typically derived from the acid hydrolysis of cellulose. This is a low cost process for production of MCC. The acid hydrolysis preferentially removes the amorphous regions of cellulose [6,7]. A new class of cellulosic reinforcing agent is microcrystalline cellulose (MCC). MCC has been widely used especially in food, cosmetic and medical industries as a water-retainer, a suspension stabilizer, a flow characteristics controller in the systems used for final products. In addition, MCC is used in polymer composites as a reinforcing agent. When compared with glass fibers, silica and carbon black, MCC in composites has many advantages: low cost, low density, little abrasion to equipment, renewability, and biodegradability [7]. Enhancement of material properties achieved with MCC has stimulated active research in polymer composites
[2,8–10]. Although, there have been some studies on MCC in polymer composites in the past few years [11–14], little work has been done on the effects of using MCC as a reinforcing filler in wood plastic composites. The goal of present work is to prepare and characterize MCC/wood flour/polypropylene composites, through addition of PP-g- MA as a compatibilizing agent. The objectives are: (a) to characterize the mechanical properties, thermal stability and morphology of the resulting composites and (b) to evaluate the synergetic effects of the compatibilization and MCC on the mechanical behavior of the composites.

2. Experimental methods

2.1. Materials

The cellulosic reinforcing materials used in this work are MCC and wood flour. MCC (Pulver-40 micron), was supplied by Aldrich Chemical Company. The poplar sawdust from local mill was ground to obtain 60 mesh fractions.

The polypropylene (PP) was obtained from Bandar Imam Petrochemical Commercial Co., Iran, as polymer matrix. PP had a melt flow index of 7–10 g/10 min and density of 0.90 g/cm^3. Polypropylene-graft-maleic anhydride (PP-*g*-MA) was supplied by Eastman Chemical Company, with 16 mg KOH/g, melt flow index of 142 °C and molecular weight of 60,000.

2.2. Composite preparation

All the composites were made with cellulosic materials to PP mass ratio of 40/60 (w/w); this value amount was selected because it is typical of many industrial formulations and represents excellent balance between performances and cost. Formulations of the composites and their mass ratios used for the respective blends prepared are given in Table 1. In the first stage, the raw materials were premixed based on formulations before being fed into the extruder. The compounding of the blends was performed in a co-rotating twin screw extruder (Collin). The barrel temperatures of the extruder were controlled at 165, 175, 185 and 190 °C for zones 1, 2, 3 and 4, respectively, while the temperature of the die was held at 190 °C. The melt temperature was kept 190 °C to prevent wood degradation, and screw speed was set at 60 rpm. The extruded strand was passed through a water bath and granulated. In the second stage, the cooled extrudate in the form of strands were injection molded at 190 °C to produce standard ASTM specimens.

2.3. Mechanical testing

After conditioning (23 ± 2 °C, 50 ± 5% RH), all the specimens were tested following ASTM standard D638 for tensile properties, ASTM D790 for flexural properties and D256 for notched Izod impact strength. Tensile and bending tests were conducted using an Instron Universal Testing Machine (model 1186) at speeds of 1.5 and 2 mm/min, respectively. A pendulum impact tester (Zwick 1446) was used for the Izod impact test. For each treatment level, five replications were conducted.

2.4. Thermogravimetric analysis (TGA)

TGA was used to study the thermal stability characteristics of resultant composites. Samples of 8 mg were heated from room temperature to 600 °C under nitrogen atmosphere with a constant heating rate of 10 °C/min.

2.5 Morphological study

Studies on the morphology of the composites were carried out using a Philips XL 30 scanning electron microscope (SEM). The fracture surfaces of the specimens after tensile test were sputter-coated with gold before analysis in order to eliminate electron charging.

3. Results and discussion

3.1. Tensile properties

Fig. 1 shows the tensile strength of the composites made with various MCC and PP-*g*-MA contents. Maximum tensile strength ranges from 36 to 39 MPa for type C, while minimum tensile strength is approximately 28 MPa for pure PP. In other words, tensile strength of pure PP is enhanced at least 1.3-fold when PP-*g*-MA and MCC are used. The mechanical properties of the composites are determined by several factors, such as nature of the reinforcement fiber, fiber aspect ratio, fiber–matrix interfacial adhesion, and also the fiber orientation in the composites [15]. The improvement in tensile strength at the presence of cellulosic materials is expected as they are to be much stiffer than polymer matrix and as a result it adds stiffness to the composites [16].

In order to enhance the bonding strength between the cellulosic materials and the matrix polymer, compatibilizing agent was used. With the addition of PP-*g*-MA, tensile strength of the composites significantly improved up to the pure PP. In general, composites with high PP-*g*-MA content exhibited better tensile strength than the untreated ones. Most effective content of PP-*g*-MA is 5 wt.% as shown in Fig. 1. The increase in tensile strength is due to the improved chemical bond between the fibers and PP polymer chains. Results demonstrate that modifying the fibers surface enhances the compatibility of hydrophobic polymer and hydrophilic cellulosic fibers. Similar observations were reported for other lignocellulosic fibers based PP composites [17].

3.2. Flexural properties

The flexural proprieties of the composites vary significantly with PP-*g*-MA and MCC content. Composites made with MCC showed the highest strength of flexural, whereas pure PP and sample A1 composites exhibited the lowest properties, respectively (Fig. 1). The maximum flexural strengths were shown in C3 sample. It was found that composites made with 5 wt% compatibilizer provided significantly higher flexural strength, compared with untreated samples.

This increase was expected due to the improved adhesion between components in the composites. It is also observed that the flexural strength increases with increasing MCC as well as the PP-*g*-MA. For example, the flexural strength of the composite type A1 is 38.9 MPa, while the flexural strength of B1 and C1 is 48.3 and 50.2 MPa, respectively. Generally, all the compositions showed a flexural strength higher than the pure PP.

3.3. Impact strength

The notched specimens were tested shows the Izod impact strengths of the composites made with the different PP-*g*-MA and MCC contents. Like the tensile and flexural strengths, the Izod impact strength of composites increased with the increase in the compatibilizing agent content. Composites made with MCC (types B and C) had significant effect on the impact strength. In other words, the specimens made with 4 and 8 wt.% of MCC exhibited remarkably higher impact strength than the specimen made without MCC (type A). Cellulosic fiber is a kind of stiff organic agent, so adding fiber could decrease the impact strength of composite. With addition of PP-*g*-MA, the interfacial bonding between the fiber and the matrix polymer was improved, thus the crack was not initiated at the interface.

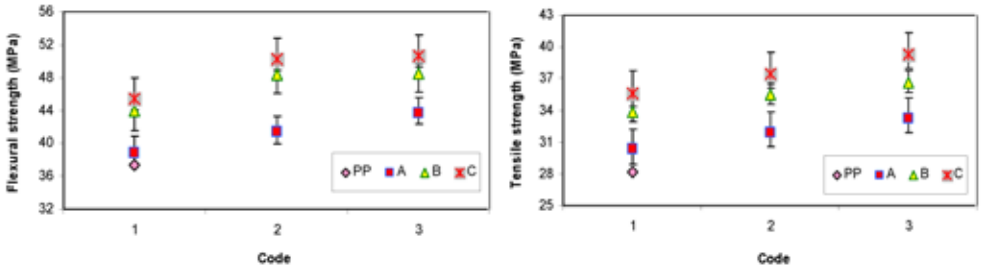

FIG. 1. Tensile and flexural strength of the composites as a function of the PP-*g*-MA and MCC.

3.4. Morphology characteristics

The effect of addition of PP-*g*-MA on the morphology of the composites was studied by SEM (Fig. 4). Non-coupled composites (samples A1 and B1) displayed a rough morphology with the presence of many voids and cavities resulting from fiber pullout. This indicates poor interfacial adhesion, thus revealing the low affinity between the polymer matrix and the wood flour filler. A few traces of filler particles, either pulled out or fractured filler particles, are to be seen in the micrographs of the composites containing compatibilizing agent (B2). The presence of the compatibilizing agent changed the morphology of the materials. Addition of PP-*g*-MA to the composites produced a more homogeneous surface with less voids and cavities (sample C3). This indicated that PP-*g*-MA had a positive effect on the interfacial adhesion between filler and matrix. The use of 5 wt.% PP-*g*-MA greatly improved the interfacial bonding between the wood flour filler and the PP matrix, as it can be observed through the surface photomicrograph in Fig. 4 (C3). This composite showed a more homogeneous and a smoother surface with very small voids and few cavities.

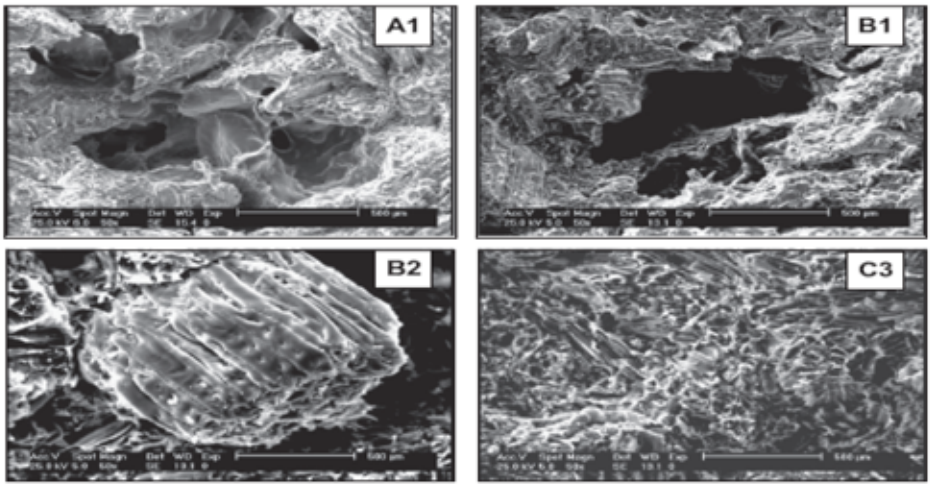

FIG. 4. SEM micrographs of fracture surfaces of the composites.

3.5. Thermal properties

The thermal stability of the composites is a very important parameter for the processing and usage of these materials. The manufacture of such composites requires the mixing of fibers and matrix at high temperatures, so the degradation of the cellulosic materials can produce undesirable effects on the properties. The TGA of pure PP showed a single-mass loss step with maximum degradation rate centered at 360 °C (Fig. 4). For the non-coupled composite (sample A1), it was verified that the maximum degradation rate was shifted to a higher temperature (around 400 °C) showing that the presence of the wood flour improved the thermal stability of the polymer compared with the pure PP. Another important feature observed was the higher degradation temperature of the polymer matrix in the composites containing the PP-*g*-MA. The temperature of degradation of the polymer matrix increased about 40 °C in comparison to the non-coupled composite, indicating that PP-*g*-MA improved the thermal stability of the polymer. This indicates that the compatibility and the interfacial bonding increased by mixing both components in the presence of the compatibilizing agent. These results illustrate that the thermal stability of the composites decreases after using MCC compared to the wood flour (sample A1). This could be explained by the low thermal stability of cellulose and hemicellulose compared to the lignin [18]. In an interesting research, Yildiz et al. [19] also reported that lignin is thermally the most stable component of wood.

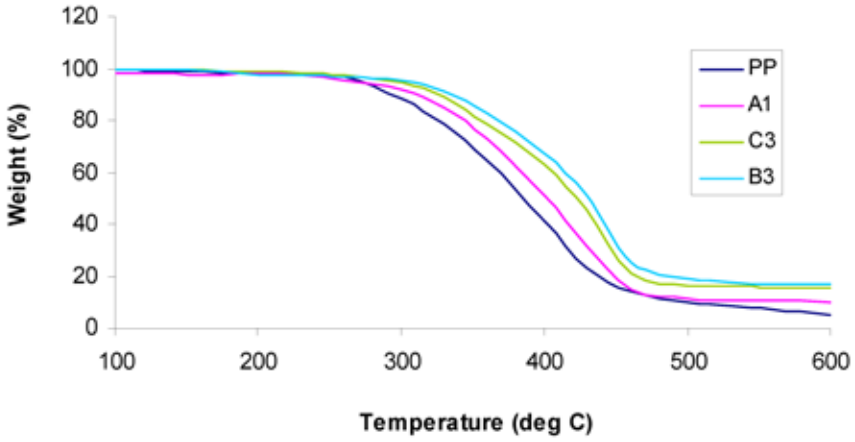

FIG. 4. TGA curves of the composites.

4. Conclusions

Based on the results of this study the following conclusions can be drawn:

1. Mechanical properties of the composites made with MCC and PP-*g*-MA were superior to those of untreated ones, due to the stronger interfacial bonding between the cellulosic fiber and the matrix polymer.
2. SEM study also shows that interfacial adhesion between the fiber and the matrix is improved with the addition of PP-*g*-MA.
3. The thermal stabilities of all composites were remarkably enhanced as compared to the pure PP. This was reflected by the fact that the onset temperature of thermal degradation increased with the incorporation of MAPP. It is to be noted that MCC could not improve the thermal stability.
4. The results showed that MCC along with wood flour could be effectively used as reinforcing agent in thermoplastic matrix.

References

[1] Yang H-S, Kim H-J, Son J, Park H-J, Lee B-J, Hwang T-S. Rice-husk flour filled polypropylene composites; mechanical and morphological study. Compos Struct 2004; 63(3-4):305–12.

[2] Li H, Sain MM. High stiffness natural fiber-reinforced hybrid polypropylene composites. Polym Plast Technol Eng 2003;42(5):853–62.

[3] Spoljaric S, Genovese A, Shanks RA. Polypropylene–microcrystalline cellulose composites with enhanced compatibility and properties. Composites Part A 2009; 40(6-7):791–9.

[4] Stark NM, Rowlands RE. Effects of wood fiber characteristics on mechanical properties of wood/polypropylene composites. Wood Fiber Sci 2003;35(2): 167–74.

[5] Sjöström E. Wood chemistry: Fundamentals and applications. 2nd ed. Academic: San Diego, USA, 1993.

[6] Lin Z, Renneckar S, Hindman DP. Nanocomposite-based lignocellulosic fibers 1. Thermal stability of modified fibers with clay-polyelectrolyte multilayers. Cellulose 2008; 15(2):333–46.

[7] Bai W, Li K. Partial replacement of silica with microcrystalline cellulose in rubber composites. Composites Part A 2009; 40(10):1597–1605.

[8] Kong Q, Hu Y, Lu H, Chen Z, Fan W. Synthesis and properties of polystyrene/Fe-montmorillonite nanocomposites using synthetic Fe-montmorillonite by bulk polymerization. J Mater Sci 2005; 40(17):4505–9.

[9] Mohan TP, Kumar MR, Velmurugan R. Thermal, mechanical and vibration characteristics of epoxy-clay nanocomposites. J Mater Sci 2006;41(18): 5915–25.

[10] Lei Y, Wu Q, Clemons C, Yao F, Xu Y. Preparation and properties of recycled HDPE/clay hybrids. J Appl Polym Sci 2007; 103 (5):3056–63.

[11] Edge S, Steele DF, Chen A, Tobyn MJ, Staniforth JN. The mechanical properties of compacts of microcrystalline cellulose and silicified microcrystalline cellulose. Inter J Pharmaceutics 2000; 200(1):67–72.

[12] Gindl W, Martinschitz KJ, Boesecke P, Keckes J. Structural changes during tensile testing of an all-cellulose composite by in situ synchrotron X-ray diffraction. Compos Sci Technol 2006; 66(15):2639–47.

[13] Petersson L, Oksman K. Biopolymer based nanocomposites: Comparing layered silicates and microcrystalline cellulose as nanoreinforcement. Compos Sci Technol 2006; 66(13):2187–2196.

[14] Ma X, Chang PR, Yu J. Properties of biodegradable thermoplastic pea starch/carboxymethyl cellulose and pea starch/microcrystalline cellulose composites. Carbohydrate Polym 2008;72(3): 369–75.

[15] Sameni JK, Ahmad SH, Zakaria S. Effects of processing parameters and graft-copoly(propylene/maleic anhydride) on mechanical properties of thermoplastic natural rubber composites reinforced with wood fibres. Plast Rubber Compos 2002; 31(4):162–6.

[16] Salemane MG, Luyt AS. Thermal and mechanical properties of polypropylene-wood powder composites. J Appl Polym Sci 2006;100(5):4173–80.

[17] Ashori A. Hybrid composites from waste materials. Polym Environ 2009 (DOI:10.1007/s10924-009-0155-6).

[18] Georgopoulos STh, Tarantili PA, Avgerinos E, Andreopoulos AG, Koukios EG. Thermoplastic polymers reinforced with fibrous agricultural residues. Polym Degrad Stabil 2005; 90(2):303–12.

[19] Yildiz S, Gezer ED, Yildiz UC. Mechanical and chemical behavior of spruce wood modified by heat. Build Environ 2006; 41(12):1762–6.